Hans Christian Karlsen

Statistics of wave induced nonlinear loads and responses

Thesis for the degree doktor ingeniør

Trondheim, September 2006

Norwegian University of Science and Technology
Faculty of Information Technology, Mathematics
and Electrical Engineering
Department of Mathematical Sciences

NTNU
Innovation and Creativity

NTNU
Norwegian University of Science and Technology

Thesis for the degree doktor ingeniør

Faculty of Natural Sciences and Technology
Department of Mathematical Sciences

© Hans Christian Karlsen

ISBN 82-471-8132-0 (printed version)
ISBN 82-471-8131-2 (electronic version)
ISSN 1503-8181

Doctoral theses at NTNU, 2006:180

Printed by NTNU-trykk

The basic law of the seaway is the apparent lack of any law.

Lord Rayleigh

Acknowledgement

During my work with this thesis, a variety of people have been influencal in one way or the other. I therefore wish to express special thanks both my advisor, professor Arvid Naess at the Department of Mathematics and Statistics, NTNU, and the third member of the team, Eirik Mo. Thanks to Arvid Naess for his helpful and patient guidance through my work with this thesis and thanks to Eirik Mo for always being positive and helpful, and for providing thoughts, ideas and solutions. Without these two scientists, this thesis would have turned out quite different.

Thanks also goes to: Dr. Christian Skaug, Consiglio Nazionale di Ricerca (CNR), Bari, and Professore Vincenzo Capasso, Dipartimento di Matematicá, Universita degli Studi di Milano, for all support in mathematical and practical matters during the time spent in Italy. Friends and colleagues at the department, for helpful discussions and for being social humans. My mother and father for always being a supporting team, providing me with hunger for knowledge and good manners in life. My two sisters and their families, for always being there for me.

And last, but not least, I would like to thank my lovely Randi for being a strong support during the last stages of the writing process. Also, a huge hug to little Syver for showing me what really matters in life. Together they enrich my life.

The research was financed by The Research Council of Norway under the BeMatA program, and was mainly carried out at the Department of Mathematical Sciences, Norwegian University of Science and Technology, Trondheim. The project manager, Dr. Vibeke Moe of Marintek a/s, is acknowledged for having provided data for the moored offshore platform model considered in this thesis.

Hans Christian Karlsen
Trondheim, August, 2006

Contents

General rules

- The transpose of a matrix or a vector is denoted by the superscript $\top$.
- The complex conjugate is denoted by the superscript *.
- Differentiation with respect to time is symbolised by a superscript dot, e.g. $\dot{x} = dx/dt$, $\ddot{x} = d^2x/dt^2$.
- Random variables and random vectors are represented by capital letters, and specific outcomes of these by small letters.
- Components of vector and matrices are denoted by subscript, e.g. ω_k, A_{mn}.
- Time dependency is often denoted by subscript, e.g. $W(t) = W_t$.

Abbreviations

CK	Chapman-Kolmogorov(equation)
CPU	Central Processing Unit
FORTRAN	Formula Translation, computer language
FP	Fokker-Planck (equation)
ISSC	International Ship Structures Congress
JONSWAP	Joint North Sea Wave Atmosphere Program
JPDF	Joint Probability Density Function
MARINTEK	Marine Technology Research Institute, Trondheim
MATLAB	Matrix Laboratory (Mathworks, Inc.), computer language
MDF	Moored Deep Floater
MDOF	Multi-Degree Of Freedom
PDF	Probability Density Function
PI	Path Integration (technique)
SDE	Stochastic Differential Equation
SP	Stochastic Process
TPD	Transition Probability Density

Mathematical operators

$\lvert \cdot \rvert$	Absolute value
$A \bigcap B$	Intersection between to events A and B
$A \bigcup B$	Union of to events A and B
$\det A$	Determinant of matrix A
dx/dy	Derivative of x with respect to y
E	Expectation
$\hat{F}$	Fourier transform
I_0	Modified Bessel function of first kind, of order 0
$\Im$	Complex value
$\mathrm{J}(\cdot)$	Jacobi determinant
ln	Natural logarithm
$\log_{10}$	Brigg's logarithm
$\min\{a, b\}$	Minimum value of a and b
$\max\{a, b\}$	Maximum value of a and b
$\mathcal{O}$	Order of magnitude symbol
$\Re$	Real value
Var	Variance

Vectors, scalars, sets and spaces

a	Positive constant
b_Φ	Inverse of roll inertia
B_i	Independent normal complex Gaussian variables with independent identically distributed real and imaginary parts
$B_{j,k,\mathbf{t}}$	The jth B-spline of order k for the knot sequence $\mathbf{t}$
$\mathbb{C}$	Complex plane
$c(t, s)$	Covariance function
C	Covariance matrix
C_D	Drag coefficient
C_m	Inertia coefficient
d	Pile diameter
$D(t)$	Damping term
$F(t)$	Surge force
$F_X(\cdot)$	Probability distribution function
$f_X(\cdot)$	Probability density function
$\bar{f}(x)$	Stationary density
$\mathcal{F}$	Family of subsets of Ω
g	Acceleration of gravity
G	Probability current
h	Hour

$h[\cdot]$	Non-linear restoring force
h_1	Impulse response function
h_2	Quadratic impulse response function
$\hat{H}_1$	Linear transfer function
$\hat{H}_2$	Quadratic transfer function
H_s	Significant wave height
i	Imaginary unit
$\hat{I}$	Numerical estimate of the integral I
k	Order of B-spline
$K_s(x)$	Intensity coefficients
$\hat{K}_2(\cdot,\cdot)$	Quadratic transfer function
m	Number of time histories
m_n	Simple moment
$m(X_t,t)$	Drift vector
M	Total mass
$M(t)$	Roll excitation moment
$M(\cdot,\cdot)$	Characteristic function
n	Number of grid points in the 1-D case
nx, ny, nz	Number of grid points in the 3-D case
n_2	Non-linear stiffness factor
$n^+(\cdot)$	Realization of $N^+(\cdot)$
$N(t) = N_t$	Gaussian white noise
$\bar{N}(t)$	Vector of Gaussian white noise
$N_Z^+(\zeta)$	Rate of up-crossing of the level ζ
$P(\cdot)$	Probability that an event occurs
P_F	Exceedance probability
p	Number of integration points
$p(x,t\|x',t')$	Transition probability density
$p_R(\cdot)$	Exact transition probability density
Q	Diffusion matrix
$\mathbb{R}$	Real number
$r(t,s)$	Correlation function
$R = R(t)$	Rayleigh process
R_s	Radius
s	Seconds
$\hat{s}(\cdot)$	Empirical standard deviation
$S_X(t)$	Spectral density
t	Time
$\mathbf{t}$	Knot sequence
T	Duration of time interval
T_e	Natural period
T_0	Slow drift period

T_1	Mean wave period
T_p	Spectral peak wave period
T_s	Spectral period
$u(\cdot,\cdot)$	Drift term
$U(t)$	Particle velocity
$v(\cdot,\cdot)$	Diffusion term
v_j	Orthonormal eigenvectors
$X(t)$	Random variable
$W(t)$	Wiener process
$\bar{W}(t)$	Real stationary normal Gaussian variables
$Z(t)$	Surge displacement
$Z(t)$	Response process
$Z_2(t)$	Slow-drift component
$\emptyset$	The empty set
α	B-spline coefficients
β	Linear damping factor
$\delta(\cdot)$	Dirac's delta function
ΔW_{ts}	$W(t) - W(s)$
ζ	Level of up-crossing
η	Mean damping parameter
η_t	Gaussian white noise
η_1	Quadratic damping factor
κ	Noise intensity
λ	Eigenvalue
μ	Force parameter
$\bar{\mu}$	Force parameter
μ_n	Central moment
$\nu_Z^+(\zeta)$	Mean upcrossing rate of level ζ
ξ	Damping ratio
ϖ_s	Saddle point
ρ	Density of water
ρ_3	Cubic stiffness factor
Σ	Covariance matrix
τ	Time increment
τ_c	Characteristic time
$\Phi_X(u)$	Characteristic function
$\Phi(t)$	Roll angle
ω	Circular frequency
ω_n	Undamped natural frequency in sway
ω_0	Natural frequency in sway
ω_p	Peak frequency
ω_q	Suitably chosen frequency
Ω	Set of all outcomes in a probability space

Chapter 1

Introduction

The challenge to calculate the response statistics of nonlinear, compliant offshore structures subjected to a random seaway is still substantial. The topic has been studied intensively for decades, and a substantial amount of work has been done to derive methods for efficient analysis of these processes for engineering applications. The main object in this thesis is calculating the mean level upcrossing rate of such response processes. Since the mean upcrossing rate is a key parameter for estimating the large and extreme responses, it is clearly of importance to develop methods for its calculation.

Chapter 2 is a collection of mathematical definitions and objects, providing the reader with some background in stochastic analysis and probability densities.

The focus on chapter 3 is the representation of the horizontal motions of a moored, large volume floating structure in random seas in terms of a second order stochastic Volterra series, and numerical methods for calculating the mean level upcrossing rate of such series. For one of these methods, no approximations are made. Hence, the only source of inaccuracy is in the numerical calculation, which can be controlled. It is demonstrated how the method of steepest descent can be applied to the numerical calculation of the mean crossing rate. In addition to the exact method, two approximate methods are also discussed.

In chapter 4 the reader is introduced to the Path Integral technique. This method used to evaluate solutions of the Fokker-Planck equation, corresponding to stochastic differential equations describing e.g. the motion of moored large volume structures in random sea.

The main part of this thesis is chapter 5. Here the results of a renewed effort to use the method of numerical path integration for this purpose presented. In particular, the goal is to calculate the response statistics of a nonlinearly moored large volume floater designed for use in oil production in deep waters. Specific emphasis has been placed on the modelling of nonlinear wave loads in addition to the nonlinear mooring characteristics. The calculated results for the response statistics are compared with the results obtained by Monte Carlo simulations, and the agreement is found to be very good.

Chapter 6 is an extension of chapter 5, estimating the response statistics of the system described earlier, by use of more powerful tools. Different approaches to handle the Rayleigh process are studied, some without success. The cause of numerical errors are discussed, as well as what difficulties one should expect using the Path Integration technique

on the Rayleigh process. Understanding the causes of these problems are important for further studies in this area of research.

Chapter 2

Theory of random variables and processes

Before entering the world of stochastic processes, it is necessary to define some mathematical objects. This to give some background theory for the proceeding chapters. For further details, consult e.g. Øksendal (1995), Cramer and Leadbetter (1968) or Williams (1991) .

2.1 σ-algebra

Definition 2.1 *If Ω is a given set, then a σ-algebra $\mathcal{F}$ in Ω is a family $\mathcal{F}$ of subsets of Ω with the following properties:*

1. $\Omega \in \mathcal{F}$
2. $F \in \mathcal{F} \Rightarrow F^C \in \mathcal{F}$, *where* $F^C = \Omega \setminus F$ *is the complement of* F *in* Ω
3. $A_1, A_2, \ldots \in \mathcal{F} \Rightarrow A := \bigcup_{i=1}^{\infty} A_i \in \mathcal{F}$.

Ω is called sample space. The pair $(\Omega, \mathcal{F})$ is called a *measurable space*.

Definition 2.2 *A probability measure P on a measurable space $(\Omega, \mathcal{F})$ is a function $P : \mathcal{F} \to [0, 1]$ such that*

1. $P(\emptyset) = 0$
2. $P(\Omega) = 1$
3. *If $A_1, A_2, \ldots \in \mathcal{F}$ and $\{A_i\}_{i=1}^{\infty}$ is disjoint (i.e. $A_i \cap A_j = \emptyset$ if $i \neq j$), then*

$$P(\bigcup_{i=1}^{\infty} A_i) = \sum_{i=1}^{\infty} P(A_i)$$

.

The triple $(\Omega, \mathcal{F}, P)$ is called a *probability space*.

Every subset $F \in \mathcal{F}$ is called $\mathcal{F}$-measurable. In a probability context these sets are called *events* and we use the interpretation

$P(F) =$ 'the probability that the event F occurs'.

In particular, if $P(F) = 1$ we say that "'F occurs with probability 1, or almost surely (a.s.)'

Definition 2.3 *Given two subsets $A, B \in \mathcal{F}$, and $P(A \cap B)$ is the probability that both A and B occur. The conditional probability of A, given that B has occurred, is given by*

$$P(A|B) = \frac{P(A \cap B)}{P(B)}, \quad P(B) \neq 0. \tag{2.1}$$

If the event A is unaffected by whether or not B has occurred, $P(A|B) = P(A)$, which together with equation (2.1) implies

$$P(A \cap B) = P(A) \cdot P(B).$$

In this case we say that the events A and B are *independent*.

2.2 Random variables and probability distributions

From now on, $(\Omega, \mathcal{F}, P)$ denote a given complete probability space.

Definition 2.4 *A random variable X is an $\mathcal{F}$-measurable function $X : \Omega \to \mathbb{R}^n$.*

Let $\mathcal{B}$ be the Borel σ-algebra on Ω, and the elements $B \in \mathcal{B}$ are the Borel sets. $\mathcal{B}$ contains all open sets, all closed sets, all countable unions of closed sets, all countable intersections of such countable unions etc.

Definition 2.5 *Every random variable induces a probability measure F_X on $\mathbb{R}^n$, where*

$$F_X(B) = P(X^{-1}(B)).$$

F_X is called the *probability distribution function* of the random variable $X(t)$, and has the following properties for $X : \Omega \to \mathbb{R}$;

1. $F_X \in [0, 1]$.
2. F_X is a nonnegative, continuous to the right, and nondecreasing function of the real variable x. In addition, $F_X(-\infty) = 0$ and $F_X(\infty) = 1$.
3. If a and b are two real numbers such that $a < b$, then

$$P(a < X < b) = F_X(b) - F_X(a).$$

Definition 2.6 *For a continuous random variable $X : \Omega \to \mathbb{R}$, the function*

$$f_X(x) = \frac{dF_X(x)}{dx} \tag{2.2}$$

exists for all x, and is called the probability density function (PDF) of $X(t)$.

The PDF of $X(t)$ has the following properties;

1. $f_X(x) \geq 0$
2. $F_X(x) = \int_{-\infty}^{x} f_X(y)dy$
3. $\int_{-\infty}^{\infty} f_X(x)dx = 1$
4. If a and b are two real numbers such that $a < b$, then

$$P(a < X < b) = \int_a^b f_X(x)dx.$$

The results above may easily be extended for $X(t) : \Omega \to \mathbb{R}^n$. Consider n random variables $X_1(t), \ldots, X_n(t)$. Their joint probability distribution function (JPDF) is defined by

$$F_{X_1 \ldots X_n}(x_1, \ldots, x_n) = F_X(x) = P(X_1 \leq x_1 \cap \ldots \cap X_n \leq x_n),$$

introducing a probability distribution in an n-dimensional Euclidean space, $X = (X_1, \ldots, X_n)$, $x = (x_1, \ldots, x_n)$. The corresponding joint density function is

$$f_X(x) = \frac{\partial^n F_X(x)}{\partial x}.$$

Various properties possessed by these function may be found in Papoulis (1984); Soong and Grigoriu (1993). If $n = 2$, they may be summarised as

$$\begin{aligned}
f_{X_1X_2}(x_1, x_2) &= \frac{\partial^2 F_{X_1X_2}(x_1, x_2)}{\partial x_1 \partial x_2}, \\
F_{X_1X_2}(x_1, x_2) = P\{X_1 \leq x_1 \cap X_2 \leq x_2\} &= \int_{-\infty}^{x_2}\int_{-\infty}^{x_1} f_{X_1X_2}(y_1, y_2)dy_1dy_2, \\
P\{x_{1a} \leq X_1 \leq x_{1b} \cap x_{2a} \leq X_2 \leq x_{2b}\} &= \int_{x_{1a}}^{x_{1b}}\int_{x_{2a}}^{x_{2b}} f_{X_1X_2}(x_1, x_2)dx_1dx_2, \\
\int_{-\infty}^{\infty}\int_{-\infty}^{\infty} f_{X_1X_2}(x_1, x_2)dx_1dx_2 &= 1, \\
\int_{-\infty}^{\infty} f_{X_1X_2}(x_1, x_2)dx_2 &= f_{X_1}(x_1), \qquad (2.3) \\
\int_{-\infty}^{\infty} f_{X_1X_2}(x_1, x_2)dx_1 &= f_{X_2}(x_2). \qquad (2.4)
\end{aligned}$$

The functions on r.h.s. in equation (2.3) and equation (2.4) are called the *marginal density functions* of X_1 and X_2, respectively.

2.3 Conditional distributions and densities

Assuming a two dimensional distribution function as in section 2.2, we may define a conditional distribution function.

Definition 2.7 *The conditional distribution function of a random variable $X_2(t)$, given that another random variable $X_1(t)$ has taken a value x_1 is*

$$F_{X_2|X_1}(x_2|x_1) = P(X_2 \leq x_2|X_1 = x_1).$$

Let $X_1(t), X_2(t)$ be continuous random variables. The *conditional density function* is

$$f_{X_2|X_1}(x_2|x_1) = \frac{dF_{X_2|X_1}(x_2|x_1)}{dx_2} = \frac{f_{X_2X_1}(x_2, x_1)}{f_{X_1}(x_1)}, \quad f_{X_1}(x_1) \neq 0. \tag{2.5}$$

Of course, when X_1 and X_2 are independent, equation (2.5) is simply

$$f_{X_2|X_1}(x_2|x_1) = f_{X_2}(x_2),$$

and

$$f_{X_2X_1}(x_2, x_1) = f_{X_2}(x_2)f_{X_1}(x_1).$$

For the case of n random variables $X = (X_1, \ldots, X_n)$, we can write

$$\begin{aligned} f_X(x) = {} & f_{X_n|X_{n-1},\ldots,X_1}(x_n|x_{n-1}, \ldots, x_1) \\ & \cdot f_{X_{n-1}|X_{n-1},\ldots,X_1}(x_{n-1}|x_{n-2}, \ldots, x_1) \cdot \ldots \cdot f_{X_2|X_1}(x_2|x_1)f_{X_1}(x_1), \end{aligned} \tag{2.6}$$

or

$$f_{X_n\ldots X_1}(x_n, \ldots, x_1) = f_{X_n}(x_n) \cdot \ldots \cdot f_{X_1}(x_1)$$

if the random variables are independent.

2.4 Expectation

Let $(\Omega, \mathcal{F}, P)$ be a probability space and let $X : \Omega \to \mathbb{R}^n$ be a continuous random variable. If $\int_\Omega |X(\omega)|dP(\omega) < \infty$, then the number

$$\mathrm{E}[X] := \int_\Omega X(\omega)\, dP(\omega) = \int_{\mathbb{R}^n} x\, dF_X(x)$$

is called the *expectation* of X (w.r.t. P). If $g : \Omega \to \mathbb{R}^n$ is Borel-measurable and $\int_\Omega |g(X(\omega))|dP(\omega) < \infty$, then

$$\mathrm{E}[g(X)] := \int_\Omega g(x(\omega))\, dP(\omega) = \int_{\mathbb{R}^n} g(x)\, dF_X(x). \tag{2.7}$$

2.5 Moments and the characteristic function

Let $(\Omega, \mathcal{F}, P)$ be a probability space and let $X : \Omega \to \mathbb{R}$ be a random variable. Besides the probability density $f_X(x)$ from equation (2.2), the characteristic function

$$\Theta_X(u) = \mathrm{E}[\exp(\mathrm{i}ux)] = \int \exp(\mathrm{i}ux)\, f_X(x)\, dx$$

completely characterises the random variable X[1]. $f_X(x)$ is just the Fourier transform of $\Theta_X(u)$,

$$f_X(x) = \frac{1}{2\pi} \int \exp(-\mathrm{i}ux)\, \Theta_X(u)\, du.$$

Choosing $g(x) = x^n$ in equation (2.7), the *simple moments*,

$$m_n = \mathrm{E}[X^n], \quad n = 1, 2, \ldots$$

of the random variable X can be obtained from the characteristic function by differentiation

$$m_n = \frac{1}{\mathrm{i}^n} \frac{d^n \Theta_X(u)}{du^n}\Big|_{u=0}.$$

We can also write $\Theta_X(u)$ as a Maclaurin series

$$\Theta_X(u) = 1 + \sum_{n=1}^{\infty} \frac{(\mathrm{i}u)^n}{n!} m_n. \tag{2.8}$$

Of course, we can only write equation (2.8) when the moments m_n are finite and do not grow to rapidly as the index n is increased.

Definition 2.8 *The n-th central moment of X, μ_n, are*

$$\mu_n = \mathrm{E}[(X - m)^n] = \int (x - m)^n f_X(x)\, dx \quad n > 1,$$

where $m = \mathrm{E}[X]$.

The central moment of a random variable X are moments of X with respect to its mean. The *variance* of X is the second central moment μ_2, commonly denoted by σ_X^2 or $\mathrm{Var}(X)$, -a measure of dispersion of a distribution of X about its mean. The relation between variance and simple moments is $\sigma_X^2 = m_2 - m_1^2$.

[1]When limits of integration are omitted, they will always be understood to be from $-\infty$ to ∞.

2.6 Stochastic processes

Definition 2.9 *A stochastic process (SP) is a parameterised collection of random variables* $\{X_t\}_{t\in T}$ *defined on a probability space* $(\Omega, \mathcal{F}, P)$*, and assuming values in* $\mathbb{R}^n$*.*

The parameter space T is usually the half-line $[0, \infty)$, but it may be an interval $[a, b]$, the non-negative integers and even subsets of $\mathbb{R}^n$ for $n \geq 1$. For each $t \in T$ fixed, we have a random variable $\omega \to X_t(\omega); \omega \in \Omega$. Fixing $\omega \in \Omega$, we can consider the function $t \to X_t(\omega); t \in T$, which is called a *path* of X_t. We usually think of t as 'time' and each ω as an individual 'particle'. $X_t(\omega)$ would represent the 'result' at time t of the particle ω. We may also regard the process as a function of two variables

$$(t, \omega) \to X(t, \omega)$$

from $T \times \Omega \to \mathbb{R}^n$.

A stochastic process is, in other words, a mathematical model of a dynamic process whose dependence on a parameter t is governed by probabilistic laws.

Practical examples of stochastic processes could be thermal noise in electrical circuits, wind or wave loads on structures, ground acceleration due to earthquakes, turbulence, or material imperfections.

2.7 Classification of stochastic processes

A stochastic process $X(t)$ can be characterised in several ways. Following Risken (1989), we may classify the processes based upon memory. Other ways may be found for example in Soong and Grigoriu (1993).

2.7.1 Purely random processes

The simplest stochastic process is one without memory. A SP $X(t), t \in T$, has *no memory* or is *completely stochastic*, when a random variable defined by $X(t)$ at a given t is independent of the random variables defined by $X(t)$ at all other t's. Since
$P(x_n, t_n | x_{n-1}, t_{n-1}; \ldots; x_1, t_1) = P(x_n, t_n)$, it follows that the n-th distribution function is given by

$$F_n(x_n, t_n; \ldots; x_1, t_1) = P(x_n, t_n) \cdot F_{n-1}(x_{n-1}, t_{n-1}; \cdots; x_1, t_1) = \prod_{j=1}^{n} P(x_j, t_j), \quad \forall\, n.$$

Thus the complete information of the process is contained in $P(x_1, t_1) = F_1(x_1, t_1)$. As Soong and Grigoriu (1993) points out, although mathematically simple, a continuous-parameter, completely stochastic process is not physically realizable because it implies absolute independence between its states at any two distinct time instants, no matter how closely they are spaced. On the other hand, discrete-parameter, completely stochastic processes are not uncommon, for example throwing a die.

2.7.2 The Markov process

The next in order of complexity are stochastic processes whose statistical information is completely contained in their second probability distribution functions. An important class of stochastic processes possessing this property, are called *Markov processes*, named after A. A. Markov, who in 1906 initiated the study of stochastic processes of this type. Books devoted entirely to Markov processes and their applications include Bharucha-Reid (1960); Stratonovich (1968). A Markov process is also called a process without aftereffect.

Definition 2.10 *A stochastic process $X(t), t \in T$, is called a Markov process if for every n and for $t_1 < \ldots < t_n$ in T we have*

$$F(x_n, t_n | x_{n-1}, t_{n-1}; \ldots; x_1, t_1) = F(x_n, t_n | x_{n-1}, t_{n-1}). \tag{2.9}$$

For a continuous-valued process, equation (2.9) is equivalent to

$$f(x_n, t_n | x_{n-1}, t_{n-1}; \ldots; x_1, t_1) = f(x_n, t_n | x_{n-1}, t_{n-1}), \tag{2.10}$$

provided the density function exist. We see that the conditional probability density function only depends on the value of the random variable at the latest time. Rewriting equation (2.6) and applying equation (2.10) and equation (2.5), gives, for $n \geq 2$ and $t_1 < \ldots < t_n$,

$$\begin{aligned} f(x_1, t_1; \ldots; x_n, t_n) &= f(x_1, t_1) \prod_{i=1}^{n-1} f(x_{i+1}, t_{i+1} | x_i, t_i; \ldots; x_1, t_1) \\ &= f(x_1, t_1) \prod_{i=1}^{n-1} f(x_{i+1}, t_{i+1} | x_i, t_i) \end{aligned}$$

A great number of physical situations are modelled or can be closely approximated by processes of this type. The Brownian motion in section 2.10 is Markovian, noise and signal processes in engineering systems, communication networks, and transport phenomena are also frequently modelled by Markov processes. And the Path Integral solution described in chapter 4, rely heavily on the Markov property.

2.7.3 General processes

Next, it is natural considering processes where the conditional probability density function depends only on the values of the random variable at the two latest times. However, according to Risken (1989), this further classification is not suitable to describe non-Markovian processes. Solutions to this includes several time-dependent variables or generalised Fokker-Planck equations which contains a memory function.

2.8 Second order statistics and stationary processes

Many of the most important properties of a stochastic process can be expressed as properties of their first and second order moments. Let $X(t)$ be a $\mathbb{R}^n$-valued process in $L_2(\Omega, \mathcal{F}, P)$, that is, the coordinates of $X(t)$ have finite second moments at all times. Then

$$\begin{aligned} \mu(t) &= \mathrm{E}[X(t)] \\ r(t,s) &= \mathrm{E}[X(t)X(s)^T] \\ c(t,s) &= \mathrm{E}[(X(t)-\mu(t))(X(s)-\mu(s))^T], \end{aligned}$$

where $\mu(t)$, $r(t,s)$, and $c(t,s)$ are called mean -, correlation -, and covariance function, respectively.

Definition 2.11 *A stochastic process $X(t)$ is said to be weakly stationary or stationary in the weak sense if*

1. *The mean function $\mu(t) = \mu$ is time invariant, and*
2. *The correlation and the covariance functions $r(t,s)$ and $c(t,s)$ depends on only the time lag $\tau = t - s$, that is, $r(t,s) = r(\tau)$ and $c(t,s) = c(\tau)$.*

Let $X_t : \Omega \to \mathbb{R}$ be a stationary process, and $\mathrm{E}[|X_t|^2] < \infty$, then

$$\begin{aligned} \mathrm{E}[X_t] &= \mu \\ c_X(t, t+\tau) &= \mathrm{E}[(X_t - \mu)(X_{t+\tau} - \mu)] = c_X(\tau). \end{aligned}$$

If $c_X(\tau) \to 0$ rapidly enough and $\int_{-\infty}^{\infty} |c_X(\tau)| < \infty$, we know from Fourier analysis (Grigoriu, 2002; Kreyszig, 1988) that the covariance $c_X(\tau)$ and the *spectral density* $S_X(\omega)$ constitute a Fourier transform pair;

$$\begin{aligned} c_X(\tau) &= \int_{-\infty}^{\infty} S_X(\omega) \exp(\mathrm{i}\omega\tau) d\omega, \\ S_X(\omega) &= \frac{1}{2\pi} \int_{-\infty}^{\infty} c_X(\tau) \exp(-\mathrm{i}\omega\tau) d\tau. \end{aligned} \tag{2.11}$$

Thus knowledge of the covariance function is sufficient to determine the energy spectral density exactly by equation (2.11), and vice versa.

An appealing property one often assumes, is that stochastic processes are ergodic.

Definition 2.12 *A stochastic process $X(t)$ is said to be ergodic if ensemble averages equal time averages, that is, if we have*

$$\mathrm{E}[g(X(t))] = \lim_{\tau \to \infty} \frac{1}{\tau} \int_{-\frac{\tau}{2}}^{\frac{\tau}{2}} g(X(s))\, ds$$

for any real-valued measurable function g such that $\mathrm{E}[g(X(t))] < \infty$.

By assuming that the stochastic process is ergodic, the expectation, variances and covariances may be calculated from a single time history.

Using equation (2.11) and equation (A.2), it's seen that the stochastic process $X(t) = N_t$, which has a constant spectral density $S_N(\omega) = S_0/2\pi$, has the covariance function

$$c_N(\tau) = \int_{-\infty}^{\infty} \frac{S_0}{2\pi} \exp(\mathrm{i}\omega\tau) d\omega = S_0\, \delta(\tau),$$

where $\delta(\tau)$ is the impulse function described in appendix A. Such a process N_t is (roughly speaking) called *Gaussian white noise* (see also section 2.10 or Schuss (1980)), although such a process exists only in mathematic theory and not in real life.

Also strictly stationary processes may be defined.

Definition 2.13 *A stochastic process X_t is called stationary (or strictly stationary) if $\{X_t\}$ has the same distribution as $\{X_{t+h}\}$ for any $h > 0$.*

Calculus like continuity, differentiation and integration, are well defined in Grigoriu (2002), emphasised at second order processes.

2.9 Normal random variables

Definition 2.14 *Let $(\Omega, \mathcal{F}, P)$ be a probability space. A random variable $X : \Omega \to \mathbb{R}$ is normal if the distribution of X has a density of the form*

$$f_X(x) = \frac{1}{\sigma\sqrt{2\pi}} \exp\left(-\frac{(x-m)^2}{2\sigma^2}\right)$$

where $\sigma > 0$ and m is constant.

Following definition 2.8, we find

$$\mathrm{E}[X] = \int_\Omega X dP = \int_{\mathbb{R}} x f_X(x) dx = m$$

and

$$\mathrm{Var}[X] = \mathrm{E}[(X-m)^2] = \int_{\mathbb{R}} (x-m)^2 f_X(x) dx = \sigma^2.$$

More generally, a random variable $X : \Omega \to \mathbb{R}^n$ is called multi-normal $\mathcal{N}(m, C)$ if the distribution of X has a density of the form

$$f_X(x_1, \cdots, x_n) = \frac{\sqrt{\det A}}{(2\pi)^{\frac{n}{2}}} \exp\left(-\frac{1}{2}\sum_{j,k}(x_j - m_j)a_{jk}(x_k - m_k)\right)$$

where $m = (m_1, \cdots, m_n) \in \mathbb{R}^n$ and $C^{-1} = A = [a_{jk}] \in \mathbb{R}^{n \times n}$ is a positive definite matrix, i.e. a symmetric matrix where the eigenvalues are strictly greater than zero. If this is the case then

$$\mathrm{E}[X] = m$$

and

$$A^{-1} = C = [c_{jk}]$$

is the covariance matrix of X, i.e.

$$c_{jk} = \mathrm{E}[(X_j - m_j)(X_k - m_k)].$$

There are good reasons why Gaussian processes are important. First of all, the central limit theorem states that for statistically independent samples, the probability distribution of the sample mean tends to become Gaussian as the number of statistically independent samples is increased without limit, regardless of the probability distribution of the random variable or process being sampled, as long as it has a finite mean and a finite variance. Since many real life random phenomena are a sum of a large number of independent fluctuations, one often expect that a Gaussian process will approximate well. Secondly, the response of constructions with a small damping coefficient will be more Gaussian than the loading is. And finally, Gaussian distributions provide us a significant analytical simplicity. An essential property is that this class of random variables is closed under linear operations; if a linear MDOF-system subjected to a Gaussian vector process excitation, then the response vector process will also be Gaussian.

2.10 Brownian motion and the Wiener process

An important class of stochastic processes are those with *independent increments*, that is for which the random variables $X(t_{j+1}) - X(t_j), j = 0, \ldots, n-1$ are independent for any finite set of time instants $t_0 < t_1 < \ldots < t_n$ in T. If t_0 is the smallest time instant in T, then the random variables $X(t_0)$ and $X(t_j) - X(t_0)$ for any other t_j in T are also required to be independent.

In 1828 the Scottish botanist Robert Brown observed that pollen grains suspended in liquid performed an irregular motion. The chaotic motion was later explained by the random collisions with the molecules of the surrounding liquid. The first explanation of the phenomenon of Brownian motion was given by Einstein in 1905. However, the preceding concise definition of this stochastic process underlying Brownian motion was given by Wiener in a series of papers originating in 1918.

An important example of a continuous time stochastic process with independent increments is the standard Wiener process, $W_t = W(t), t \geq 0$. The Wiener process is often called Brownian motion, but separate terminology is often used to distinguish between the mathematical and physical processes.

Einstein was able to show that, assuming

$$P\{W(0) = 0\} = 1,$$

the PDF of $\Delta W_{ts} = W(t) - W(s), t > s$ is Gaussian with

$$\begin{aligned} &\mathrm{E}(\Delta W_{ts}) = 0 \\ &\mathrm{E}(\Delta W_{ts}^2) = \mathrm{Var}(W(t) - W(s)) = 2D(t-s) = \Delta_{ts}, \end{aligned}$$

for all $0 \leq s < t$, and D is a physical constant. This process was proposed by Wiener as a mathematical description of Brownian Motion. A *standard Wiener process* is a Wiener process as described above, with $D = 1/2$. It is easy to show that the Wiener process $W(t), t > 0$ is a Gaussian process. Rewriting

$$W(t) = [W(t) - W(t_n)] + [W(t_n) - W(t_{n-1})] + \ldots + [W(t_1) - W(0)]$$

where $0 \leq t_1 < \ldots < t_n < t$, it's seen that the Wiener process is a linear sum of Gaussian random variables and is of course a Gaussian random variable itself.

The Wiener process has continuous samples with probability one, since for any $\epsilon > 0$,

$$\lim_{h\to 0} P\{|W(t+h) - W(t)| < \epsilon\} = \lim_{h\to 0} \left\{1 - 2\Phi\left(-\frac{\epsilon}{\sqrt{2Dh}}\right)\right\} = 1,$$

where

$$\Phi(x) = \frac{1}{\sqrt{2\pi}} \int_{-\infty}^{x} \exp\left(-\frac{1}{2}u^2\right) du$$

denotes the standard Gaussian random variable. However, since

$$\lim_{h\to 0} P\left\{\left|\frac{W(t+h) - W(t)}{h}\right| > \epsilon\right\} = \lim_{h\to 0} 2\Phi\left(-\frac{\epsilon h}{\sqrt{2Dh}}\right) = 1,$$

the Wiener process has non-differentiable samples with probability one. In Soong and Grigoriu (1993) it is shown that the Wiener process is not even differentiable in mean square. So any attempt to derive any results due to the derivative of a Wiener process is doomed to fail. However, we often talk about *Gaussian white noise*, a wide sense stationary process with constant nonzero spectral density $S(\omega) = S_0/2\pi$. The name white noise comes from the fact that its average power is uniformly distributed in frequency, which is characteristic of white light. Considering the process

$$X_h(t) = \frac{W(t+h) - W(t)}{h}, \quad t \geq 0,$$

as shown in Kloeden and Platen (1992), is a wide-sense stationary Gaussian process with zero means, covariances

$$c(t-s) = \frac{1}{h} \max\left\{0, 1 - \frac{1}{h}|t-s|\right\},$$

and a spectral density

$$S_h(\tau) = \frac{1}{h}\int_{-h}^{h}\left(1-\frac{|s|}{h}\right)\cos(2\pi\tau s)\,ds = \left(\frac{\sin(2\pi\tau h)}{\pi\tau h}\right)^2.$$

This density is very broad for small h, and converges to 1 for all $\tau \neq 0$ as $h \to 0$. This suggests that the process $X_h(t)$ converges to a Gaussian white noise process $N_t = \dot{W}$ as $h \to 0$, and that a Gaussian white noise process is the derivative of a Wiener process. However, a Gaussian white noise process cannot be a stochastic process in the usual sense, but must be interpreted in the sense of generalised functions like the Dirac delta function. It cannot be realized physically, but it can be approximated to any desired degree of accuracy by the conventional stochastic processes with broad banded spectra, such as $X_h(t)$, which is called *coloured white noise*.

2.11 Ito stochastic calculus

During the first decade of the 20th century, attempts were made to formulate dynamics caused by Brownian motion in terms of differential equations. The resulting equations were written in the form

$$dX_t = u(t, X_t)\,dt + v(t, X_t)\,dW_t, \tag{2.12}$$

which is a short-hand notation for

$$X_t(\omega) = X_{t_0}(\omega) + \int_{t_0}^{t} u(s, X_s(\omega))\,ds + \int_{t_0}^{t} v(s, X_s(\omega))\,dW_s(\omega)\,, \tag{2.13}$$

where $u(t, X_t)$ is a drift term and $v(t, X_t)\,dW_t$ is the noisy, diffusive term. Equation (2.12) and equation (2.13) are usually called *Ito stochastic differential equation* and *Ito stochastic integral*, respectively.

One problem is that a Wiener process is nowhere differentiable, so strictly speaking the process dW_t does not exist as a conventional function of t; -indeed a flat spectral density implies that its covariance function is a constant multiple of the Dirac delta function. Thus the integral in equation (2.13) cannot be an ordinary Riemann or Lebesgue integral. Worse still, the continuous sample path of a Wiener process are not of bounded variation on any bounded time interval, so the latter integral in equation (2.13) cannot even be interpreted as a Riemann-Stieltes integral for each sample path. For a constant $v(t, x) \equiv v$ one would expect the second integral in equation (2.13) to equal $v\,[W_t(\omega) - W_{t_0}(\omega)]$. This is the starting point for Ito's definition of a stochastic integral, as written in Kloeden and Platen (1992). The conclusion is that the first integral in equation (2.13) is made as a Lebesgue (or Riemann) integral for each sample path, and the second integral is an Ito integral. The second integral could optionally be done as a Stratonovic integral, as well explained in Kloeden and Platen (1992).

In general, the solutions of a stochastic differential equation (2.12) are diffusion processes with their TPDs (section 2.12) satisfying certain properties for the drift $u(t, X_t)$ and diffusion coefficient $v(t, X_t)$.

In the multidimensional case, the vector process $X_t = (X_1(t), \ldots, X_n(t))^\top$ will satisfy the stochastic differential equation

$$dX_t = m\,[t, X_t]\,dt + Q\,[t, X_t]\,dW_t, \tag{2.14}$$

where $m[\cdot] = (m_1(\cdot), \ldots, m_n(\cdot))^\top$, $dW_t = (dW_1(t), \ldots, dW_m(t))^\top$, and $Q = (Q_{ij})$ denotes an $n \times m$ matrix. $m[\cdot]$ is usually called a *drift vector*, and $Q\,Q^\top$ is called a *diffusion matrix*. dW_t is a vector of increments of independent Wiener processes.

2.12 Transition probability density

We limit our discussion to real one dimensional processes for simplicity. The extension to $\mathbb{R}^n$-valued processes is straight forward.

Let $X(t)$ be a real-valued random process, and $X(t_1), \ldots, X(t_n)$ be a set of values at the consecutive time instants $t_1 < \ldots < t_n$. The conditional probability density of the value of $X(t)$ at the most recent time t_n is

$$f_{X_n|X_{n-1}\ldots X_1}(x_n|x_{n-1}, \ldots, x_1) = \frac{f_{X_n X_{n-1}\ldots X_1}(x_n, x_{n-1}, \ldots, x_1)}{f_{X_{n-1}\ldots X_1}(x_{n-1}, \ldots, x_1)},$$

where $X(t_i) = X_i$, $i = 1, \ldots, n$. Hence for a Markov process (section 2.7.2), we may write

$$f_{X_n|X_{n-1}\ldots X_1}(x_n|x_{n-1}, \ldots, x_1) = f_{X_n|X_{n-1}}(x_n|x_{n-1}) = p(x_n, t_n|x_{n-1}, t_{n-1}) \quad (n \geq 2).$$

$p(x_n, t_n|x_{n-1}, t_{n-1})$ is called the *transition probability density*, denoted as TPD. Equation (2.6) may be rewritten as

$$f_X(x) = p(x_n, t_n|x_{n-1}, t_{n-1}) \cdot \ldots \cdot p(x_2, t_2|x_1, t_1) f_{X_1}(x_1). \tag{2.15}$$

If we know the one-dimensional probability distribution $f_{X_1}(x_1)$ and the transition probability $p(x_n, t_n|x_{n-1}, t_{n-1})$ of $X(t)$, we may find the probability distributions of $X(t)$, i.e., the two mentioned functions completely characterise a process without aftereffect. Naturally, the TPD has to satisfy the normalisation condition

$$\int p(x_n, t_n|x_{n-1}, t_{n-1})\,dx_n = 1.$$

An important equation for Markov processes,

$$\int p(x_3, t_3|x_2, t_2)\,p(x_2, t_2|x_1, t_1)dx_2 = p(x_3, t_3|x_1, t_1), \quad (t_3 > t_2 > t_1), \tag{2.16}$$

known as is known as the *Chapman-Kolmogorov equation*. Equation (2.16) essentially describes the flow or transition of probabilities associated with $X(t)$ from an instant t_1 to another instant t_3 via any intermediate instant t_2. The equation occupy a central role in the theory of Markov processes.

Studying the time dependence of the one-dimensional probability density, we may choose $n = 2$ in equation (2.15), integrating with respect to x_1, obtaining

$$f_{X_2}(x_2) = \int p(x_2, t_2|x_1, t_1)\, f_{X_1}(x_1)\, dx_1. \tag{2.17}$$

2.13 Intensity coefficients

One way of converting equation (2.17) into a differential equation, as done by Stratonovich (1963), is by choosing t_1 close to t_2. Denoting $t_1 = t'$, $t_2 = t$, $\tau = t_2 - t_1$, $X_1 = X'$, and $X_2 = X$, we may rewrite equation (2.17) into the simpler form

$$f_X(x) = \int p(x, t|x', t')\, f_{X'}(x')\, dx'. \tag{2.18}$$

Remembering the theory from section 2.5, we introduce a new characteristic function,

$$\Theta(u; x') = \mathrm{E}[\exp(\mathrm{i}u(x - x'))] = \int \exp(\mathrm{i}u(x - x'))\; p(x, t|x', t')\, dx \tag{2.19}$$

of the random increment $x - x'$ which occurs during the time interval $[t', t]$ given x'. Substituting its inverse transform

$$p(x, t|x', t') = \frac{1}{2\pi} \int \exp(-\mathrm{i}u(x - x'))\, \Theta(u; x')\, du$$

into equation (2.18), we find

$$f_X(x) = \frac{1}{2\pi} \int \int \exp(-\mathrm{i}u(x - x'))\, \Theta(u; x')\, du\, f_{X'}(x')\, dx'.$$

According to equation (2.8), the characteristic function in equation (2.19) equals

$$\Theta(u; x') = 1 + \sum_{s=1}^{\infty} \frac{(\mathrm{i}u)^s}{s!}\, m_s(x') \tag{2.20}$$

in terms of the moments

$$m_s(x') = \mathrm{E}[(X - X')^s]$$

of the increment $x - x'$. Now

$$f_X(x) = \sum_{s=0}^{\infty} \frac{1}{s!} \frac{1}{2\pi} \int \int \exp(-\mathrm{i}u(x - x'))\, (\mathrm{i}u)^s\, du\, m_s(x')\, f_{X'}(x')\, dx'$$

Since

$$\frac{1}{2\pi}\int \exp(-\mathrm{i}u(x-x'))\,(\mathrm{i}u)^s\,du = (-\frac{\partial}{\partial x})^s\frac{1}{2\pi}\int \exp(-\mathrm{i}u(x-x'))\,du$$
$$= (-\frac{\partial}{\partial x})^s\delta(x-x'),$$

where $\delta(\cdot)$ is defined in appendix A, we find

$$f_X(x) = f_{X'}(x') + \sum_{s=0}^{\infty}\frac{1}{s!}(-\frac{\partial}{\partial x})^s\,[m_s(x)\,f(x)].$$

where $f(x) = f_X(x)$. Dividing by τ, and passing to the limit $\tau \to 0$, we obtain

$$\frac{\partial f(x)}{\partial t} = \sum_{s=0}^{\infty}\frac{1}{s!}(-\frac{\partial}{\partial x})^s[K_s(x)f(x)], \tag{2.21}$$

and

$$K_s(x) = \lim_{\tau\to 0}\frac{m_s(x)}{\tau}, \tag{2.22}$$

provided that these limits exists. According to equation (2.22), the moments depend on τ in the following way:

$$m_s(x) = K_s(x)\,\tau + \mathcal{O}(\tau^2), \quad s = 1, 2, \ldots.$$

K_s is called the *intensity coefficients* of the derivative $dx(t)/dt$, $t > t'$.

Wong and Hajek (1985) and Kloeden and Platen (1992) provides optional ways in obtaining equation (2.21).

2.14 The one-dimensional Fokker-Planck equation

Definition 2.15 *A Markov process is said to be continuous if its higher-order intensity coefficients $K_3, K_4, \ldots$ in equation* (2.22) *equals zero.*

In this case, equation (2.21) takes the form

$$\frac{\partial f(x)}{\partial t} = -\frac{\partial}{\partial x}[K_1(x)\,f(x)] + \frac{1}{2}\frac{\partial^2}{\partial x^2}[K_2(x)\,f(x)], \tag{2.23}$$

and is called the *Fokker-Planck equation* (FP) (or the *diffusion equation*). The FP-equation deals with the fluctuations of systems which stem from many tiny disturbances, -each of which changes the variables of the system in an unpredictable, but small way. The FP-equation is just an equation of motion for the distribution function of fluctuating

macroscopic variables, and according to Risken (1989) was first used by Fokker and Planck early in the 20th century to describe the Brownian motion of particles (section 2.10).

Introducing the *probability current*

$$G(x) = K_1(x)\, f(x) - \frac{1}{2}\frac{\partial}{\partial x}[K_2(x)\, f(x)],$$

the Fokker-Planck equation may be written

$$\frac{\partial f}{\partial t} + \frac{\partial G}{\partial x} = 0, \tag{2.24}$$

which we may understand as the *equation of conservation of probability*.

In order to obtain solutions to the FP-equation, we have to add initial conditions and boundary conditions. If we use an arbitrary initial distribution $f(x, t_0) = f_0(x)$ at some initial time t_0, we can find the function $f(x, t), t > t_0$. Using $f_0(x) = \delta(x - x_0)$, it can be shown (Stratonovich, 1963) that the resulting probability density is just the TPD $p(x, t|x_0, t_0)$. Therefore, the transition probability can be found as the solution of the equation

$$\frac{\partial p(x, t|x_0, t_0)}{\partial t} = -\frac{\partial}{\partial x}[K_1(x)\, p(x, t|x_0, t_0)] + \frac{1}{2}\frac{\partial^2}{\partial x^2}[K_2(x)\, p(x, t|x_0, t_0)] \tag{2.25}$$

with initial condition

$$p(x, t_0|x_0, t_0) = \delta(x - x_0).$$

It can be shown (Bharucha-Reid, 1960) that regarded as a function of x_0 and t_0, the TPD $p(x, t_0|x_0, t_0)$ satisfies another differential equation

$$\frac{\partial p(x, t_0|x_0, t_0)}{\partial t_0} = -\frac{\partial p(x, t_0|x_0, t_0)}{\partial x_0} K_1(x_0) - \frac{1}{2}\frac{\partial^2 p(x, t_0|x_0, t_0)}{\partial x_0^2} K_2(x_0)$$

called the *Kolmogorov equation*. In the case of a stationary random process where $K_1(x)$ and $K_2(x)$ do not depend on t, the TPD $p(x, t|x', t')$ depends only on the timelag τ and not on t.

If the function $X(t)$ can take all possible values from $-\infty$ to ∞, the boundary conditions take the form of conditions there. Integrating equation (2.24) with respect to x from $-\infty$ to ∞, and remembering that the normalisation condition $\int f(x)\, dx = 1$ is satisfied for all t, the conditions are;

$$G(-\infty, t) = 0 = G(\infty, t)$$
$$f(-\infty, t) = 0 = f(\infty, t).$$

Considering the FP-equation in an interval $x_1 \leq x \leq x_2$, the boundary conditions take the form

$$G(x_1, t) = 0 = G(x_2, t).$$

There is a close connection between the FP-equation and SDE. According to Grigoriu (2002), given a one-dimensional stochastic differential equation

$$dX(t) = u(X(t), t)dt + v(X(t), t)dW(t), \quad t \geq t_0$$

starting at $X(t_0) = x_0$, the TPD $f = p(x, t|x_0, t_0)$ satisfies the FP-equation

$$\frac{\partial f}{\partial t} = -\frac{\partial}{\partial x}(u\, f) + \frac{1}{2}\frac{\partial^2}{\partial x^2}(v^2\, f). \tag{2.26}$$

Comparing the equations (2.23) and (2.26), the connection between intensity factors and the drift- and diffusion term are

$$K_1(X(t), t) = u(X(t), t)\,,$$
$$K_2(X(t), t) = v(X(t), t)^2\,.$$

2.14.1 Solutions to the Fokker-Planck equation

The PDF $f(x, t)$ satisfying the FP-equation (2.23) is uniquely determined by the prescribed initial and boundary equations. In a special case where $K_1(x)$ and $K_2(x)$ do not depend on time, the distribution $f(x, t)$ will, according to Kloeden and Platen (1992), usually approach a stationary distribution $\bar{f}(x)$.

The stationary distribution does not depend on the initial distribution $f(x_0, t)$ or on the time. Hence,

$$\frac{\partial}{\partial t}\bar{f}(x) = 0. \tag{2.27}$$

Combining equation (2.27) and equation (2.24), we find

$$\bar{G}(x) = \text{const.}$$

It may now be shown (Stratonovich, 1963) that the stationary distribution is

$$\bar{f}(x) \propto \frac{1}{K_2(x)} \exp\left\{2\int_{x_1}^{x} \frac{K_1(y)}{K_2(y)}dy\right\}. \tag{2.28}$$

However, investigation of *transient processes*, which involves calculation of the TPD by solving the non-stationary equation (2.23), is a much more difficult problem. In some instances, the non-stationary FP-equation can be solved by applying the method of separation of variables.

2.14.2 The Rayleigh process

One important example of a stochastic equation driven by white noise, is the Rayleigh equation, also called the Rayleigh process,

$$\dot{R} = -\frac{\epsilon}{2}\left(R - \frac{\kappa}{R}\right) + \sqrt{\epsilon}\,\eta_t. \tag{2.29}$$

Here η_t is Gaussian white noise with the following properties

$$\begin{aligned} \mathrm{E}[\eta_t] &= 0, \\ \mathrm{E}[\eta_t \eta_{t+\tau}] &= \kappa\delta(\tau)\,, \end{aligned}$$

and $R = R(t) > 0$ may be regarded as the amplitude of a narrow-banded process. κ is the noise intensity.

The theory from section 2.14 allow us to rewrite equation (2.29) as a FP-equation,

$$\frac{2}{\epsilon}\frac{\partial f}{\partial t} = \frac{\partial}{\partial R}\left[-\left(R - \frac{\kappa}{R}\right) f\right] + \kappa\frac{\partial^2 f}{\partial R^2}. \tag{2.30}$$

Combining equation (2.28) and equation (2.30), we find the stationary distribution

$$\bar{f}(R) = \frac{R}{\kappa}\exp\left(-\frac{R^2}{2\kappa}\right), \tag{2.31}$$

which is the well-known Rayleigh distribution.

As shown in chapter 5 and 6, the Rayleigh equation plays an important role in statistical response predictions for nonlinearly moored large volume structures in random seas.

2.14.3 The exact transition probability density for a Rayleigh process

Changes in R represent a Markov process, and the expression for the TPD $p(R,t|R',t') = p(R|R')$, where as usual $t = t' + \tau$, may now be found;

$$f(R,R') = p(R|R')f(R'). \tag{2.32}$$

It can be shown (Davenport and Root, 1987) that

$$f(R,R') = \frac{RR'}{\kappa^2(1-Q^2)} I_0\left(\frac{Q}{1-Q^2}\frac{RR'}{\kappa}\right)\exp\left(-\frac{R^2+R'^2}{2\kappa(1-Q^2)}\right), \tag{2.33}$$

where $Q = \exp(-\epsilon|\tau|/2)$ and $I_0(z) = J_0(\mathrm{i}z)$ is the modified Bessel Function of first kind, of order zero. Combining equations (2.31) to (2.33), the exact TPD

$$p(R|R') = \frac{R}{\kappa(1-Q^2)} I_0\left(\frac{Q}{1-Q^2}\frac{RR'}{\kappa}\right)\exp\left(-\frac{R^2+Q^2R'^2}{2\kappa(1-Q^2)}\right) \tag{2.34}$$

may be found.

2.15 The multidimensional Fokker-Planck equation

Considerations made in section 2.12 can be generalised to the case of a multidimensional Markov process, which consists of several random functions $X_1(t), \ldots, X_m(t)$. Such a process is described by a transition probability $p(x_1(t), \ldots, x_m(t)|x_1(t'), \ldots, x_m(t'))$, in terms of which we can write the multidimensional probability densities. This TPD is just the conditional probability density

$$p(x_1(t), \ldots, x_m(t)|x_1(t'), \ldots, x_m(t')) = \frac{f(x_1, \ldots, x_m|x'_1, \ldots, x'_m)}{f(x'_1, \ldots, x'_m)}$$

of the random variables $X_1(t) = X_1, \ldots, X_m(t) = X_m$ at the time t, given the fixed values $X_1(t') = X'_1, \ldots, X_m(t') = X'_m$ at a previous time t'. In the case of a continuous Markov process, the probability density $f(x_1(t), \ldots, x_m(t))$ satisfies the *multidimensional Fokker-Planck equation*

$$\begin{aligned}\frac{\partial f}{\partial t}(x_1, \ldots, x_m) = &-\sum_{\alpha=1}^{m} \frac{\partial}{\partial x_\alpha}[K_\alpha(x_1, \ldots, x_m) f(x_1, \ldots, x_m)] \\ &+ \frac{1}{2}\sum_{\alpha=1}^{m}\sum_{\beta=1}^{m} \frac{\partial^2}{\partial x_\alpha \partial x_\beta}[K_{\alpha\beta}(x_1, \ldots, x_m) f(x_1, \ldots, x_m)], \end{aligned} \tag{2.35}$$

where the intensity coefficients K_α and $K_{\alpha\beta}$ are defined by the formulas

$$\begin{aligned} K_\alpha &= \lim_{\tau \to 0} \frac{1}{\tau} \mathrm{E}[X_{\alpha\tau} - X_\alpha], \\ K_{\alpha\beta} &= \lim_{\tau \to 0} \frac{1}{\tau} \mathrm{E}[(X_{\alpha\tau} - X_\alpha)\,(X_{\beta\tau} - X_\beta)]. \end{aligned}$$

As in the one-dimensional case, there is also a close connection between the FP-equation and the SDE in the multi-dimensional case. Let $X : \Omega \to \mathbb{R}^m$ be a diffusion process described by the stochastic differential equation

$$dX(t) = u(X(t), t)dt + v(X(t), t)dW(t), \quad t \geq t_0,$$

where $u(X(t), t)$ and $v(X(t), t)$ is the drift- and diffusion term as described in section 2.11. Assume that u and $vv^\top$ satisfies certain boundary conditions, and that the process starts at $X(t_0) = x_0$. Then, according to Grigoriu (2002), the TPD $f = p(x, t|x_0, t_0)$ satisfies the FP-equation

$$\frac{\partial f}{\partial t} = -\sum_{i=1}^{m} \frac{\partial}{\partial x_i}(u\, f) + \frac{1}{2}\sum_{i=1}^{m}\sum_{j=1}^{m} \frac{\partial^2}{\partial x_i \partial x_j}\left(vv^\top f\right).$$

2.15.1 Solutions to the multidimensional Fokker-Planck equation

The FP-equation from equation (2.35) can be written in the form

$$\frac{\partial f}{\partial t} = -\sum_{\alpha=1}^{m} \frac{\partial G_\alpha}{\partial x_\alpha}$$

where

$$G_\alpha = K_\alpha f - \frac{1}{2}\sum_{\beta=1}^{m} \frac{\partial}{\partial x_\beta}[K_{\alpha\beta} f]$$

are the components of a probability current vector $G = (G_1, \ldots, G_m)$ in the m-dimensional space. Now the stationary PDF $\bar{f}$ satisfies the equation

$$\sum_{\alpha=1}^{m} \frac{\partial \bar{G}_\alpha}{\partial x_\alpha} = 0.$$

However, if $m > 1$, the probability current G does not have to vanish inside the region $\mathbf{R}$ under consideration, even if G satisfies zero boundary conditions

$$\bar{G}_\alpha(x) = 0$$

on the boundary of $\mathbf{R}$, since rotational probability flows can occur. The current G vanishes in the whole region $\mathbf{R}$, i.e.,

$$K_\alpha(x)\bar{f}(x) - \frac{1}{2}\sum_{\beta=1}^{m} \frac{\partial}{\partial x_\beta}[K_{\alpha\beta}(x)\bar{f}(x)] = 0 \tag{2.36}$$

only in a special case called the *potential case*. Substituting $\bar{f}(x) = \exp(-U)$ into equation (2.36), we obtain the equations

$$\frac{\partial U}{\partial x_\gamma} = \sum_{\alpha=1}^{m}\sum_{\beta=1}^{m} A_{\gamma\alpha}\frac{\partial K_{\alpha\beta}}{\partial \beta} - 2\sum_{\alpha=1}^{m} A_{\gamma\alpha}K_\alpha, \tag{2.37}$$

where $A_{\gamma\alpha}$ is the inverse of the matrix $K_{\alpha\beta}$ and $\gamma = 1, \ldots, m$. It follows from equation (2.37) that the potential conditions now take the form

$$\frac{\partial}{\partial x_\delta}\sum_{\alpha=1}^{m} A_{\gamma\alpha}\left(\sum_{\beta=1}^{m}\frac{\partial K_{\alpha\beta}}{\partial x_\beta} - 2K_\alpha\right) = \frac{\partial}{\partial x_\gamma}\sum_{\alpha=1}^{m} A_{\delta\alpha}\left(\sum_{\beta=1}^{m}\frac{\partial K_{\alpha\beta}}{\partial x_\beta} - 2K_\alpha\right), \tag{2.38}$$

where $\gamma, \delta = 1, \ldots, m$. If these conditions are met, and if there is no flow of probability through the boundary of the region $\mathbf{R}$, then the assumption that the probability current vanishes everywhere in $\mathbf{R}$ is justified, and we can find the stationary probability density by calculating the potential function U from equation (2.37). This, of course, implies that the matrix $K_{\alpha\beta}$ is nonsingular so that it has an inverse.

Special cases may simplify equation (2.38) and equation (2.37). For example when the matrix $K_{\alpha\beta}$ is isotropic, i.e., $K_{\alpha\beta} = \kappa\delta_{\alpha\beta}$, when $K_{\alpha\beta}$ is independent of the argument $x_1, \ldots, x_m$ and when $K_1, \ldots, K_m$ are linear functions of $x_1, \ldots, x_m$.

2.16 Approximate TPD

2.16.1 1D case

The discretized version of the continuous SDE in equation (2.12) may be written as

$$X(t) = X(t') + \tilde{u}(t', X(t'), \tau) + v(t', X(t'))\,\Delta W_{t'}, \tag{2.39}$$

where the finite positive increment $\tau = t - t'$. $\tilde{u}(t', X(t'), \tau)$ is the discretized version of the drift term $u(t', X(t'))\,dt$ in some manner at time t', and using e.g. the basic Euler approximation, $\tilde{u}(t', X(t'), \tau) = u(t', X(t'))\tau$. $v(t', X(t'))$ is diffusion term at time t', and $\Delta W_{t'} = W(t) - W(t')$. From equation (2.39) it follows that the conditional PDF of $X(t)$, given that $X(t') = x'$, is given as

$$p(x, t|x', t') = \frac{1}{\sqrt{2\pi v(t', x')\tau}} \exp\left(-\frac{[x - (x' + \tilde{u}(t', x', \tau))]^2}{2v(t', x')\tau}\right). \tag{2.40}$$

As mentioned in section 2.11, equation (2.12) is only a short hand notation for equation (2.13), so the exact expression for $X(t)$ is

$$X(t) = X(t') + \int_{t'}^{t} u(s, X(s))\,ds + \int_{t'}^{t} v(s, X(s))\,dW_s, \tag{2.41}$$

and the accuracy in the solution is determined by how one decides to represent the integrals. Often, when the diffusion term is a constant, the latter integral in equation (2.41) may be found using an Euler-Maruyama approximation, but this is not the case of the Rayleigh process. This topic is further discussed in section 4.6.5.

Other approaches in obtaining equation (2.40), may be found in e.g. Risken (1989).

2.16.2 Multidimensional case

Assume $X(t) = (X_1(t), \ldots, X_n(t))^\top$ is a real-valued vector process satisfying equation (2.14). Rewriting it as a discretized system, we find

$$X(t) = X(t') + \tilde{m}(t', X(t'), \tau) + Q(t', X(t'))\,\Delta W_{t'}, \tag{2.42}$$

where the finite positive increment $\tau = t - t'$. $\tilde{m}(t', X(t'), \tau)$ is the discretized version of the drift term $m(t', X(t'))\,dt$ in some manner at time t', $Q(t', X(t'))$ is diffusion term at time t', and $\Delta W_{t'} = W(t) - W(t')$. The diffusion matrix is

$$G(x) = (g_{ij}(x)) = Q(x)Q(x)^\top = \left(\sum_{k=1}^{n} q_{ik}\, q_{jk}\right)$$

and assuming the first $r < n$ rows of the matrix Q to be zero, i.e.

$$Q_{ij} = 0, \qquad i = 1, \ldots, r.$$

This implies that

$$G = \begin{bmatrix} 0 & 0 \\ 0 & \tilde{G} \end{bmatrix},$$

where 0 denotes zero-matrices and $\tilde{G}$ denotes a $(n-r) \times (n-r)$ matrix with elements $g_{ij}(\cdot)$, $i, j = r+1, \ldots, n$, and are called a reduced diffusion matrix, assumed to be positive definite.

Proceeding in a manner similar to the derivations in section 2.16.1, from equation (2.42) it follows that the conditional PDF of $X(t)$, given that $X(t') = x'$, is given as

$$\begin{aligned} p(x,t|x',t') = & \prod_{i=1}^{r} \delta\left\{x_i - (x_i + \tilde{m}_i(x',t',\tau))\right\} \cdot (2\pi\tau)^{\frac{r-n}{2}} \left[\det\tilde{G}(x')\right]^{-\frac{1}{2}} \\ & \cdot \exp\left\{-\frac{1}{2\tau}\sum_{i=r+1}^{n}\sum_{j=r+1}^{n}\left[x_i - (x'_i + \tilde{m}_i(x',t',\tau))\right]\right. \\ & \left.\times \left[\tilde{G}(x')^{-1}\right]_{i-r,j-r}\left[x_j - (x'_j + \tilde{m}_j(x',t',\tau))\right]\right\}, \end{aligned} \tag{2.43}$$

where the determinant assumed to be greater than zero, $\tilde{G}(x)^{-1}$ is the inverse of matrix $\tilde{G}$, and $\delta(\cdot)$ is the delta-function described in Appendix A.

As in the one-dimensional case, equation (2.14) is only an short-hand notation of

$$X(t) = X(t') + \int_{t'}^{t} m(s, X(s))\, ds + \int_{t'}^{t} Q(s, X(s))\, dW_s, \tag{2.44}$$

the accuracy of the solution again depends on how one decides to handle the integrals of equation (2.44).

Chapter 3

Structural response

This chapter is based on the articles Naess and Karlsen (2004) and Naess et al. (2006).

3.1 Introduction

Stationary vessels floating or submerged in irregular waves are subjected to large first order wave forces and moments which are linearly proportional to the wave height and contain the same frequencies as the waves. They are also subjected to small second-order mean and low frequency wave forces and moments which are proportional to the square of the wave height. The frequencies of the second order low frequency component are associated with the frequencies of the wave groups occurring in irregular waves.

The first order wave forces and moments are the cause of the well known first order motions with wave frequencies. Due to the importance of the first order wave forces and motions they have been subjected to investigation for several decades. As a result of these investigations, methods have evolved by means of which these may be predicted with a reasonable degree of accuracy for many different vessel shapes (Pinkster, 1980).

From the point of view of practical assessment of the response statistics of engineering structures subjected to stochastic load processes, a quantity of particular importance is the average rate of upcrossings of high levels by the response. This is the key to e.g. estimation of extreme values.

In this chapter the focus is on response processes that can be expressed as a second order stochastic Volterra series, that is, a stochastic Volterra series that has been truncated after the second order term. Even if the Volterra series model was formulated more than 30 years ago, it is not until quite recently that general numerical methods have become available that allows accurate calculation of the probability distribution, and perhaps more importantly, the mean upcrossing rate of the total response process. While the method is mathematically sound, initial efforts to carry out the requisite calculations have revealed that some care is needed in setting up the numerical algorithms.

A substantial amount of work has been done to derive methods for efficient analysis of this model for engineering applications, starting with the seminal paper by Kac and Siegert (1947). Later contributions toward applications in ocean and offshore engineering

have been made, among many others, by Neal (1974), Vinje (1983), Næss (1985), Donley and Spanos (1990) and Næss (1990).

3.2 The response process

The response process $Z(t)$ that is considered here is assumed to be represented as a second order stochastic Volterra series. This would apply to the state of the art representation of e.g. the surge response of a large volume, compliant offshore structure in random waves. This response would consist of a combination of the wave frequency component $Z_1(t)$ and the slow-drift component $Z_2(t)$, as described in Næss (1990),

$$Z(t) = Z_1(t) + Z_2(t), \tag{3.1}$$

where

$$Z_1(t) = \int_0^\infty h_1(\tau) X(t-\tau) d\tau \tag{3.2}$$

$$Z_2(t) = \int_0^\infty \int_0^\infty h_2(\tau_1, \tau_2) X(t-\tau) X(t-\tau) d\tau_1 d\tau_2. \tag{3.3}$$

Equation (3.1) describes the standard representation of the two response components leading to a second order Volterra series model for the total response. In equation (3.2) and (3.3), $X(t)$ denotes a stationary, real Gaussian process, representing a unidirectional random wave elevation process or a stochastic wind-velocity field. How to deal with the multidimensional case is also shown in Næss (1990). $h_1(\tau)$ and $h_2(\tau_1, \tau_2)$ are real, continuous functions characterising the physical system that is modelled.

$h_1(\tau)$ is an ordinary *impulse response function* defining a linear physical problem. $h_2(\tau_1, \tau_2)$ is by analogy called the *quadratic impulse response function*, but as opposed to the linear impulse response function $h_1(\tau)$, $h_2(\tau_1, \tau_2)$ does not have a simple physical interpretation. $h_2(\tau_1, \tau_2)$ characterises the second-order properties of the physical system. $h_1(\tau)$ and $h_2(\tau_1, \tau_2)$ are found by the equations

$$\begin{aligned} h_1(\tau) &= \frac{1}{2\pi} \int_0^\infty \hat{H}_1(\omega) \exp(-\mathrm{i}\,\omega\,\tau)\, d\omega \\ h_2(\tau_1, \tau_2) &= \frac{1}{4\pi^2} \int_0^\infty \int_0^\infty \hat{H}_2(\omega_1, \omega_2) \exp(-\mathrm{i}\,\omega_1\,\tau_1) \exp(-\mathrm{i}\,\omega_2\,\tau_2)\, d\omega_1 d\omega_2. \end{aligned}$$

$\hat{H}_1(\omega)$ and $\hat{H}_2(\omega_1, \omega_2)$ are called linear and quadratic transfer functions (QTF), respectively. The problem of estimating $\hat{H}_2(\omega_1, \omega_2)$ with particular reference to nonlinear ocean engineering problems has been treated extensively in literature (Faltinsen and Løken, 1979; Neal, 1974). The function $h_2(\tau_1, \tau_2)$ may without loss of generality be considered symmetrical (Neal, 1974). Writing

$$X(t) = \sum_{j=-N}^{N} \left[S_X(\omega_j)\Delta\omega\right]^{\frac{1}{2}} B_j e^{\mathrm{i}\omega_j t},$$

it is shown (Næss, 1990) that for practical numerical calculations the following relations can be worked out

$$Z_1(t) = \sum_{i=-N}^{N} q_i B_i e^{\mathrm{i}\omega_i t} \tag{3.4}$$

$$Z_2(t) = \sum_{i=-N}^{N} \sum_{j=-N}^{N} Q_{ij} B_i B_j^* e^{\mathrm{i}(\omega_i - \omega_j)t} \tag{3.5}$$

where

$$q_i = \hat{H}_1(\omega_i) \left[\frac{1}{2} S_X(|\omega_i|)\Delta\omega\right]^{\frac{1}{2}}$$

$$Q_{ij} = \frac{1}{2}\hat{H}_2(\omega_i, -\omega_j) \left[S_X(|\omega_i|)S_X(|\omega_j|)\right]^{\frac{1}{2}} \Delta\omega, \tag{3.6}$$

and $S_X(\omega)$ denotes the one-sided spectral density of $X(t)$. $\{B_i\}_{i=1}^N$ is a set of independent, complex Gaussian N$(0,1)$-variables with independent, identically distributed real and imaginary parts. These variables are assumed to satisfy the relation $B_{-i} = B_i^*$, where * signifies complex conjugation. Throughout this chapter, when the summation index runs from negative to positive values, it invariably omits zero. $0 < \omega_1 < \cdots < \omega_N$ is an equidistant discretization of the pertinent part of the positive frequency axis; $\omega_{-i} = -\omega_i$ and $\Delta\omega = \omega_{i+1} - \omega_i$. The assumption of an equidistant discretization is adopted for simplicity of presentation and is not necessary, in fact, often a non-equidistant version is used to avoid having too many frequencies, which is sometimes convenient. The formulas are easily adapted to cover the situation of non-equidistant discretization.

It is shown Næss (1985, 1990) that by solving the eigenvalue problem (assumed non-singular)

$$Qv_j = \lambda_j v_j \tag{3.7}$$

to find the eigenvalues λ_j and orthonormal eigenvectors v_j, $j = -N, \ldots, -1, 1, \ldots, N$, of the matrix $Q = (Q_{ij})$, the quadratic response can be represented as

$$Z_2(t) = \sum_{j=-N}^{N} \lambda_j \bar{W}_j(t)^2 \tag{3.8}$$

Here $\bar{W}_j(t)$, $j = -N, -1, 1, \ldots, N$ are real stationary Gaussian $N(0,1)$-processes which can be represented as follows

$$\bar{W}_j(t) = \sum_{k=-N}^{N} v_j(\omega_k) B_k e^{\mathrm{i}\omega_k t} \tag{3.9}$$

where $v_j(\omega_k)$ denotes the kth component of v_j, and it can be assumed that $v_j(\omega_{-k}) = v_j(\omega_k)^*$. For each fixed t, $\{\bar{W}_j(t)\}$ becomes a set of independent Gaussian variables.

Since slow-drift response of offshore structures often occurs at periods of the order of minutes, it is usually a very good approximation to neglect second-order effects at frequencies higher than wave frequencies. In such cases, what is known as the slow-drift approximation may be adopted. It corresponds to neglecting forces of oscillations occurring at frequencies corresponding to the sum of frequencies in the input spectral density. In mathematical terms this approximation applied to e.g. the second-order response amounts to putting the QTF

$$\hat{H}_2(\omega_i, \omega_j) = 0, \quad \omega_i \cdot \omega_j > 0,$$

implying that the kernel $Q_{ij} = 0$ in equation (3.5), when $\omega_i \cdot \omega_j < 0$. When the kernel has this property, the eigenvalue problem in equation (3.7) will generate exactly double eigenvalues (Næss, 1986). Rewriting equation (3.8), we are now able to write the slow drift response, still denoted $Z_2(t)$, like

$$Z_2(t) = \sum_{j=1}^{\infty} \lambda_j \left\{ \bar{W}_{2j-1}(t)^2 + \bar{W}_{2j}(t)^2 \right\} \tag{3.10}$$

Note that the second order theory is based on the assumption that the QTF

$$\hat{H}_2(\omega_i, -\omega_j) = \hat{H}(\omega_i - \omega_j)\, \hat{K}_2(\omega_i, -\omega_j),$$

where $\hat{K}_2(\cdot, \cdot)$ is a QTF characterising the slowly varying sway (or surge) forces on the vessel, and $\hat{H}(\cdot)$ is a linear transfer function characterising the sway (or surge) motion of the vessel, that is

$$\hat{H}(\omega) = \frac{1}{M\ [-\omega^2 + 2i\xi\omega_0\omega + \omega_0^2]},$$

where M is mass, ω_0 is the natural frequency, and ξ is the damping ratio of the system.

In the slow-drift case, the stochastic process $\{\bar{W}_j(t)\}$ may optionally be represented as follows

$$\bar{W}_{2j-1}(t) + \mathrm{i}\bar{W}_{2j}(t) = \sqrt{2} \sum_{k=1}^{N} v_j(\omega_k) B_k e^{\mathrm{i}\omega_k t}.$$

The representation can be arranged so that $\bar{W}_{2j}$ becomes the Hilbert transform of $\bar{W}_{2j-1}$, cf. Næss (1990).

Having achieved the desired representation of the quadratic response $Z_2(t)$, it can then be shown that the linear response can be expressed as

$$Z_1(t) = \sum_{j=-N}^{N} \beta_j \bar{W}_j(t) \tag{3.11}$$

The (real) parameters β_j are given by the relations

$$\beta_j = \sum_{k=-N}^{N} \hat{H}_1^*(\omega_k)\sqrt{S_X(\omega_k)\Delta\omega}\, v_j(\omega_k)$$

Based on the representations given by equations (3.8) and (3.11), Næss (1987) describes how to calculate the statistical moments of the response process $Z(t)$. However, for important prediction purposes the crucial quantity is the mean rate of level upcrossings by the response process.

3.3 The mean crossing rate

Let $(\Omega, \mathcal{F}, P)$ be a complete probability space as defined in section 2.1, and let $Z(t)$ be a real (strictly) stationary stochastic process with continuously differentiable sample paths (a.s.). It is assumed throughout that the distribution function of $Z(0)$, denoted by $F_Z(z) = P(Z(0) \leq z)$ is absolutely continuous. For every fixed level $\zeta \in \mathbb{R}$, let $N_Z^+(\zeta)$ denote the rate of upcrossings of the level ζ by $Z(t)$, cf. Leadbetter et al. (1983), and let

$$\nu_Z^+(\zeta) = \mathrm{E}[N_Z^+(\zeta)].$$

Under the assumed conditions on $Z(t)$, it can be proved (Zähle, 1984) that if $\mathrm{E}[|Z(0)|] < \infty$, then

$$\nu_Z^+(\zeta) = \mathrm{E}\left[\dot{Z}^+ | Z = \zeta\right]\, f_Z(\zeta),$$

where the equality holds a.s. (Lebesgue) with respect to ζ, and $z^+ = \max(z, 0)$.

Assuming that the distribution of $(\dot{Z}|Z = \zeta)$ is absolutely continuous with a probability density function (PDF) $f_{\dot{Z}|Z}(s|\zeta)$, it follows that for a.e. ζ

$$\begin{aligned}\nu_Z^+(\zeta) &= \int_0^\infty s\, f_{\dot{Z}|Z}(s|\zeta)\, ds\; f_Z(\zeta) \\ &= \int_0^\infty s\, f_{Z\dot{Z}}(\zeta, s)\, ds \end{aligned} \tag{3.12}$$

where $f_{Z\dot{Z}}(\cdot,\cdot)$ denotes the joint PDF of $Z(0)$ and $\dot{Z}(0) = dZ(t)/dt|_{t=0}$. Equation (3.12) is often referred to as the Rice formula (Rice, 1954). $\nu_Z^+(\zeta)$ is assumed throughout to be finite, and it is referred to as the mean upcrossing rate of the level ζ. With additional assumptions on the joint densities of $Z(0), \dot{Z}(0)$ and $Z(0), h^{-1}\big(Z(h) - Z(0)\big)$ for small values of h, it can be shown that equation (3.12) is valid for every ζ, cf. Marcus (1977) or Leadbetter et al. (1983). However, the required conditions to ensure equality in equation (3.12) for every value of ζ are not easy to verify, but most importantly, the stronger version is rarely needed. In reliability applications the critical levels for which the crossing rate is required can in general only be given with finite accuracy. This means that the crossing rate needs

to be known for values of ζ belonging to small intervals who's length is determined by the level of the accuracy. Hence, the a.s. result is sufficient under such circumstances.

To calculate the mean crossing rate of a stochastic process represented as a second order stochastic Volterra series directly from equation (3.12) has turned out to be difficult due to the difficulties of calculating the joint PDF $f_{Z\dot{Z}}(\cdot,\cdot)$ (see chapter 4). However, the situation can be improved by invoking the concept of characteristic function.

Denote the characteristic function of the joint variable $(Z,\dot{Z})$ by $M_{Z\dot{Z}}(\cdot,\cdot)$, or, for simplicity of notation, by $M(\cdot,\cdot)$. Then

$$M(u,v) = M_{Z\dot{Z}}(u,v) = \mathrm{E}\left[\exp\left(\mathrm{i}uZ + \mathrm{i}v\dot{Z}\right)\right]$$

Assuming that $M(\cdot,\cdot)$ is an integrable function, that is, $M(\cdot,\cdot) \in L^1(\mathbb{R}^2)$, it follows that (a.s.)

$$f_{Z\dot{Z}}(z,s) = \frac{1}{(2\,\pi)^2}\int_{-\infty}^{\infty}\int_{-\infty}^{\infty} M(u,v)\,\exp\left(-\,\mathrm{i}uz - \mathrm{i}vs\right)\,du\,dv \tag{3.13}$$

By substituting from equation (3.13) back into equation (3.12), the mean crossing rate is formally expressed in terms of the characteristic function, but this is not a very practical expression.

The solution to this is obtained by considering the characteristic function as a function of two complex variables. It can then often be shown that this new function becomes holomorphic in suitable regions of $\mathbb{C}^2$, where $\mathbb{C}$ denotes the complex plane. As shown in detail in Næss (2002), under suitable conditions, the use of complex function theory allows the derivation of the following two alternative expressions for the crossing rate, which hold true for a.e. ζ,

$$\nu_Z^+(\zeta) = -\,\frac{1}{(2\,\pi)^2}\int_{-\infty-\mathrm{i}a}^{\infty-\mathrm{i}a}\int_{-\infty-\mathrm{i}b}^{\infty-\mathrm{i}b}\frac{1}{v^2}\,M(u,v)\,e^{-\,\mathrm{i}u\zeta}\,du\,dv\,, \tag{3.14}$$

where $0 < a < a_1$ for some positive constant a_1, and $b_0 < b < b_1$ for some constants $b_0 < 0$ and $b_1 > 0$. As pointed out by Næss (2001), in the case of a stationary process,

$$\nu_Z^+(\zeta) = -\,\frac{1}{(2\,\pi)^2}\int_{-\infty}^{\infty}\left(⨍_{-\infty}^{\infty}\frac{1}{v^2}\,M(u,v)\,dv\right)\,e^{-\,\mathrm{i}u\zeta}\,du, \tag{3.15}$$

where the inner integral wrt v is interpreted as a principal value integral in the following sense:

$$⨍_{-\infty}^{\infty} = \lim_{\epsilon\to 0^+}\left\{\int_{-\infty}^{-\,\epsilon} + \int_{\epsilon}^{\infty}\right\}.$$

The upcrossing frequency may optionally be evaluated with the formula

$$\nu_Z^+(\zeta) = -\,\frac{1}{(2\,\pi)^2}\int_{-\infty}^{\infty}\left(⨍_{-\infty}^{\infty}\frac{1}{v}\,\frac{\partial M(u,v)}{\partial v}\,dv\right)\,e^{-\,\mathrm{i}u\zeta}\,du, \tag{3.16}$$

as done in Machado (2002), but equation (3.15) is faster to evaluate, numerically. Equation (3.16) has some value though, been used to check the results from equation (3.15).

To actually carry out the calculations, the joint characteristic function need to be known. It has been shown (Næss, 2001) that for the second order stochastic Volterra series, it can be given in closed form. To this end, consider the multidimensional Gaussian vectors $\bar{W} = (\bar{W}_{-N}, \ldots, \bar{W}_N)^\top$ and $\dot{\bar{W}} = (\dot{\bar{W}}_{-N}, \ldots, \dot{\bar{W}}_N)^\top$. It is obtained that the covariance matrix of $(\bar{W}^\top, \dot{\bar{W}}^\top)^\top$ is given by

$$\Sigma = \begin{pmatrix} \Sigma_{11} & \Sigma_{12} \\ \Sigma_{21} & \Sigma_{22} \end{pmatrix}$$

where

$$\begin{aligned}
\Sigma_{11} &= I = \text{the } 2N \times 2N \text{ identity matrix,} \\
\Sigma_{12} &= (r_{ij}) = (\mathrm{E}[\bar{W}_i \dot{\bar{W}}_j]), \\
\Sigma_{21} &= (\mathrm{E}[\dot{\bar{W}}_i \bar{W}_j]), \\
\Sigma_{22} &= (s_{ij}) = (\mathrm{E}[\dot{\bar{W}}_i \dot{\bar{W}}_j]),
\end{aligned}$$

for $i, j = -N, \ldots, -1, 1, \ldots, N$. The identities $r_{ij} = -\,r_{ji}$ and $\Sigma_{12} = \Sigma_{21}^\top$ may also be shown. It follows from equation (3.9), that the entries of the covariance matrix Σ can be expressed in terms of the eigenvectors v_j, cf. Næss (1985). Let

$$\begin{aligned}
R_{ij} &= \sum_{k=1}^{N} -\mathrm{i}\omega_k v_i(\omega_k) v_j(\omega_k)^* \\
S_{ij} &= \sum_{k=1}^{N} \omega_k^2 v_i(\omega_k) v_j(\omega_k)^*.
\end{aligned}$$

Then

$$\begin{aligned}
r_{2i-1,2j-1} &= r_{2i,2j} = \Re\,(R_{ij}) \\
r_{2i-1,2j} &= -r_{2i,2j-1} = \Im\,(R_{ij}) \\
s_{2i-1,2j-1} &= s_{2i,2j} = \Re\,(S_{ij}) \\
s_{2i-1,2j} &= -s_{2i,2j-1} = -\Im\,(S_{ij})\,.
\end{aligned}$$

Let $\Lambda = \mathrm{diag}(\lambda_{-N}, \ldots, \lambda_N)$ be the diagonal matrix with the parameters λ_j on the diagonal, and let $\beta = (\beta_{-N}, \ldots, \beta_N)^\top$. It can now be shown (Næss, 2001) that

$$M_{Z\dot{Z}}(u, v) = \exp\left\{ -\frac{1}{2}\,\ln(\det(A)) - \frac{1}{2}\,v^2\,\beta^\top V\,\beta\, + \frac{1}{2}\,\alpha^\top A^{-1}\,\alpha \right\} \tag{3.17}$$

where

$$\begin{aligned}
A &= I - 2\mathrm{i}u\Lambda\, - 2\,\mathrm{i}\,v\,\left(\Lambda\,\Sigma_{21} + \Sigma_{12}\,\Lambda\right) + 4\,v^2 \Lambda\, V\,\Lambda, \\
V &= \Sigma_{22} - \,\Sigma_{21}\,\Sigma_{12}, \\
\alpha &= \left(\mathrm{i}u\,I + \mathrm{i}\,v\,\Sigma_{12} - 2v^2\,\Lambda\,V\,\right)\beta.
\end{aligned}$$

3.4 Numerical calculation

Previous efforts to carry out numerical calculation of the mean crossing rate using equation (3.15) has been reported in Naess and Machado (2000) and Næss (2001). These initial investigations indicated that the method had the potential to provide very accurate numerical results. In this chapter, the focus will be on the alternative expression given by equation (3.14), which is rewritten as

$$\nu_Z^+(\zeta) = -\frac{1}{(2\,\pi)^2}\int_{-\infty-\mathrm{i}a}^{\infty-\mathrm{i}a}\frac{1}{w^2}\,I(\zeta,w)\,dw \tag{3.18}$$

where

$$\begin{aligned} I = I(\zeta,w) &= \int_{-\infty-\mathrm{i}b}^{\infty-\mathrm{i}b} M(\varpi,w)\,e^{-\,\mathrm{i}\varpi\zeta}\,d\varpi \\ &= \int_{-\infty-\mathrm{i}b}^{\infty-\mathrm{i}b} \exp\{-\,\mathrm{i}\varpi\zeta + \ln M(\varpi,w)\}\,d\varpi. \end{aligned} \tag{3.19}$$

A numerical calculation of the mean crossing rate can start by calculating the function $I(\zeta,w)$ for specified values of ζ and w. However, a direct numerical integration of equation (3.19) is made difficult by the oscillatory term $\exp\{-\mathrm{i}\,\Re(\varpi)\,\zeta\}$, where $\Re(\varpi)$ denotes the real part of ϖ. This problem can be avoided by invoking the method of steepest descent, also called the saddle point method. For this purpose, we write

$$\begin{aligned} g(\varpi) &= -\,\mathrm{i}\varpi\zeta + \ln M(\varpi,w) \\ &= \phi(x,y) + \mathrm{i}\,\psi(x,y) \end{aligned} \tag{3.20}$$

where $\varpi = x + \mathrm{i}y$. $\phi(x,y)$ and $\psi(x,y)$ become real harmonic functions when $g(\varpi)$ is holomorphic. The idea is to identify the saddle point of the surface $(x,y) \to \phi(x,y)$ closest to the integration line from $-\infty - ib$ to $\infty - ib$. By shifting this integration line to a new integration contour that passes through the saddle point, and then following the path of steepest descent away from the saddle point, it can be shown that the function $\psi(x,y)$ stays constant, and therefore the oscillatory term in the integral degenerates to a constant. This is a main advantage of the method of steepest descent for numerical calculations. It can be shown that the integral does not change its value as long as the function $g(\varpi)$ is a holomorphic function in the region bounded by the two integration contours and if the integrals vanish along the contour segments required to close the region.

If ϖ_s denotes the identified saddle point, where $g'(\varpi_s) = 0$, the steepest descent path away from the saddle point will follow the direction given by $-\,\overline{g'(\varpi)}$, for $\varpi \neq \varpi_s$, where $\overline{z}$ denotes the complex conjugate of z, cf. Henrici (1977). Typically, the singular points of the function g will be around the imaginary axis, which indicates that the direction of the paths of steepest descent emanating from the saddle point will typically not deviate substantially from a direction orthogonal to the imaginary axis. This provides a guide for setting up a numerical integration procedure based on the path of steepest descent. First

the saddle point ϖ_s is identified. Then the path of steepest descent starting at ϖ_s and going 'right', is approximated by the sequence of points $\{\varpi_j\}_{j=0}^{\infty}$ calculated as follows:

$$\varpi_0 = \varpi_s \qquad \varpi_1 = \varpi_s + h \tag{3.21}$$

$$\Delta\varpi_j = -\frac{\overline{g'(\varpi_j)}}{|g'(\varpi_j)|}\, h, \quad j = 1, 2, \ldots$$

$$\varpi_{j+1} = \varpi_j + \Delta\varpi_j, \quad j = 1, 2, \ldots$$

where h is a small positive constant.

Similarly, the path of steepest descent going 'left' is approximated by the sequence $\{\varpi_j\}_{j=0}^{-\infty}$ calculated by

$$\varpi_{-1} = \varpi_s - h$$

$$\Delta\varpi_j = -\frac{\overline{g'(\varpi_j)}}{|g'(\varpi_j)|}\, h, \quad j = -1, -2, \ldots$$

$$\varpi_{j-1} = \varpi_j + \Delta\varpi_j, \quad j = -1, -2, \ldots$$

A numerical estimate $\hat{I}$ of I can be obtained as follows.

$$\hat{I} = \hat{I}^+ + \hat{I}^- \tag{3.22}$$

where

$$\hat{I}^+ = \Re\left(\frac{h}{2}\,\exp\{g(\varpi_s)\} + \sum_{j=1}^{K} \Delta\varpi_j\,\exp\{g(\varpi_j)\}\right)$$

and

$$\hat{I}^- = \Re\left(\frac{h}{2}\,\exp\{g(\varpi_s)\} - \sum_{j=-1}^{-K} \Delta\varpi_j\,\exp\{g(\varpi_j)\}\right)$$

for a suitable large integer K.

An example of how the method works may be found in Figure 3.1. Along the path of steepest descent, we see how quickly $\phi(x, y)$ from equation (3.20) descends to a number small enough to give a sufficient approximation of the integral $\hat{I}$ in equation (3.22). $\psi(x, y)$ is zero at the saddle point ϖ_s, and stays close to zero all along the path, with a maximum deviation of $4.8 \cdot 10^{-3}$.

A numerical estimate $\hat{\nu}_Z^+(\zeta)$ of the mean crossing rate can now be obtained by the sum

$$\hat{\nu}_Z^+(\zeta) = -\frac{1}{(2\,\pi)^2} \sum_{j=-L}^{L} \frac{1}{w_j^2}\,\hat{I}(\zeta, w_j)\,\Delta w_j \tag{3.23}$$

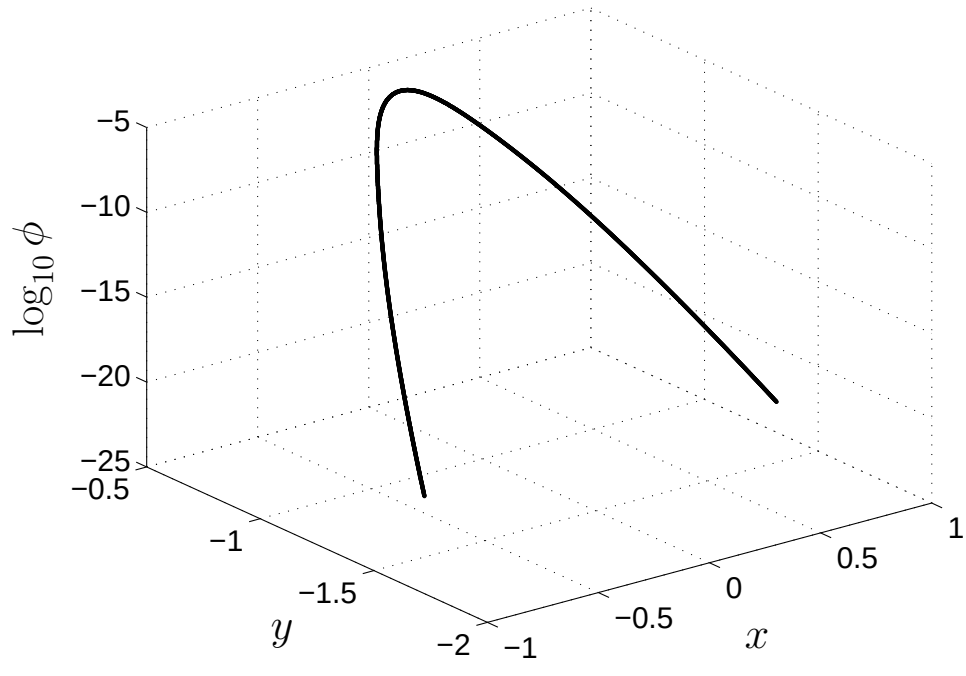

Figure 3.1: Logarithmic plot of $\phi(x, y)$ along the path of steepest decent.

where $w_j = v_j - ia$, $\{v_j\}_{j=-L}^{L}$ denotes a discretization of a suitable part of the real line, and Δw_j are consistently chosen increments to approximate the integral in equation (3.18). Actually, a closer scrutiny of this integral shows that the points w_j in equation (3.23) can be chosen to follow the negative real axis from a suitably large negative number up to a point at $-r$, where $0 < r \leq a$, then follow a semi-circle in the lower half plane to r on the positive real axis, and finally follow this axis to a suitably large positive number.

3.5 Numerical example

The performance of the proposed method for numerical calculation of the mean level up-crossing rate of $Z(t)$ is illustrated by invoking an example that was used previously for the same purpose, cf. Næss (1986). It concerns the slowly varying forces and motions of a moored half submerged long circular cylinder (2D problem) in random unidirectional beam sea waves. The cylinder is assumed to have radius $R_s = 10$ m, and total mass (including added mass) $M = 3.21 \cdot 10^5$ kg/m. The damping ratio is set equal to $\xi = 0.06$, and the natural frequency in sway is $\omega_0 = 0.1$ rad/s. This is, according to Standing et al. (1990), suitable values. The QTF $\hat{H}_2(\omega_i, -\omega_j)$ used here is then the same as in Næss (1986).

The random stationary sea state is specified by an ISSC spectrum, which is given as

follows

$$S_X(\omega) = \frac{173H_s^2}{T_1^4\omega^5}\exp\left(-\frac{691}{T_1^4\omega^4}\right),$$

where H_s = significant wave height and T_1 = mean wave period. For the subsequent calculations, $H_s = 2.0$ m and $T_1 = 5.5$ s. The natural frequency in sway is 0.1 rad/s, which is well below the range where the waves have noticeable energy. This is why the second, nonlinear term in the Volterra expansion is needed to capture the resonant motions in sway of the moored cylinder.

The upcrossing rate is known in closed form for the case of only one slow-drift component. In particular, for the reduced slow-drift response process

$$Y_2(t) = \lambda_1\left(\bar{W}_1(t)^2 + \bar{W}_{-1}(t)^2\right)$$

the upcrossing rate $\nu^+_{Y_2}(y)$ is given by the relation (Næss, 1985)

$$\nu^+_{Y_2}(y) = \frac{\hat{\sigma}_1}{\sqrt{2\pi}}\exp\left(-\frac{y}{2\lambda_1} + \frac{1}{2}\ln\left(\frac{y}{\lambda_1}\right)\right)$$

where $\hat{\sigma}_1 = \sqrt{s_{1,1} - (r_{1,-1})^2}$. The corresponding expressions for the reduced slowly varying sway forces $F_2(t)$ are entirely similar. This special case provides a suitable test for the accuracy of the numerical method.

For the specific example considered here it was found that the first four eigenvalues (as per decreasing absolute value) for the sway forces were $\mu_1 = 0.4963$ (kN/m), $\mu_2 = -0.0513$, $\mu_3 = 0.0280$, $\mu_4 = 0.0168$. For the sway response, the eigenvalues were $\lambda_1 = 0.2937$ (m), $\lambda_2 = 0.2580$, $\lambda_3 = 0.2277$, $\lambda_4 = 0.2070$. Note that the eigenvalues for the forces decrease rapidly with one dominant eigenvalue, while the eigenvalues for the sway response decrease much more slowly.

Let $\tilde{\nu}^+_{Y_2}(y)$ (resp. $\tilde{\nu}^+_{F_2}(s)$) denote the mean upcrossing rate of $Y_2(t)$ (resp. $F_2(t)$) calculated by the numerical method. Table 3.1 compares the analytical with the numerical upcrossing rate of the forces for different levels, while Table 3.2 gives the corresponding results for the response. It is seen that the agreement is remarkably good in both cases.

ζ	$\nu^+_{F_2}(\eta)$	$\tilde{\nu}^+_{F_2}(\eta)$
1.0	$3.0508 \cdot 10^{-2}$	$3.0506 \cdot 10^{-2}$
2.0	$1.5753 \cdot 10^{-2}$	$1.5752 \cdot 10^{-2}$
4.0	$2.9702 \cdot 10^{-3}$	$2.9696 \cdot 10^{-3}$
7.0	$1.9128 \cdot 10^{-4}$	$1.9121 \cdot 10^{-4}$
9.0	$2.8916 \cdot 10^{-5}$	$2.8902 \cdot 10^{-5}$
10.0	$1.1129 \cdot 10^{-5}$	$1.1123 \cdot 10^{-5}$

Table 3.1: Comparison of analytical and numerical upcrossing rate ($\eta = s/\mu_1$).

ζ	$\nu^+_{Y_2}(\zeta)$	$\tilde{\nu}^+_{Y_2}(\zeta)$
1.0	$6.1402 \cdot 10^{-3}$	$6.1397 \cdot 10^{-3}$
2.0	$1.5822 \cdot 10^{-3}$	$1.5822 \cdot 10^{-3}$
4.0	$7.4287 \cdot 10^{-5}$	$7.4271 \cdot 10^{-5}$
7.0	$5.9447 \cdot 10^{-7}$	$5.9424 \cdot 10^{-7}$
9.0	$2.2378 \cdot 10^{-8}$	$2.2367 \cdot 10^{-8}$
10.0	$4.2981 \cdot 10^{-9}$	$4.2954 \cdot 10^{-9}$

Table 3.2: Comparison of analytical and numerical upcrossing rate $(\zeta = y/\lambda_1)$.

The upcrossing rate may be approximated if we use more than one slow-drift component. Writing the slow-drift component as a sum

$$Y_2(t) = \sum_{i=1}^{k} \lambda_i \left(\bar{W}_i(t)^2 + \bar{W}_{-i}(t)^2 \right)$$

and the eigenvalues $\lambda_1 > |\lambda_2| > \ldots > |\lambda_k|$ in descending order, the upcrossing rate $\hat{\nu}^+_{Y_2}(y)$ is given by the relation (Næss, 1985)

$$\hat{\nu}^+_{Y_2}(y) \approx \frac{\hat{n}_1}{\sqrt{2\pi}} \exp\left(-\frac{y}{2\lambda_1} + \frac{1}{2} \ln\left(\frac{y}{\lambda_1} \right) \right), \tag{3.24}$$

where $\hat{n}_1 = \tilde{\sigma}_1 \prod_{j=2}^{k} k_j^{-1}$, $\tilde{\sigma}_1 = \sqrt{s_{1,1} - (r_{1,-1})^2}$, and $k_j = 1 - \lambda_j/\lambda_1$. The corresponding expressions for the sway forces $F_2(t)$ are entirely analogous.

Table 3.3 compares the approximated with the numerical upcrossing rate of $F_2(t)$ for different levels for $k = 4$. It is seen that the agreement is still very good. The reason for the good agreement is that the approximation in equation (3.24) is valid if $\mu_1 >> |\mu_j|,\ j \geq 2$. Clearly, this condition is satisfied to good approximation in this case.

ζ	$\hat{\nu}^+_{F_2}(\eta)$	$\tilde{\nu}^+_{F_2}(\eta)$
1.0	$3.0333 \cdot 10^{-2}$	$3.0387 \cdot 10^{-2}$
2.0	$1.5663 \cdot 10^{-2}$	$1.5835 \cdot 10^{-2}$
4.0	$2.8530 \cdot 10^{-3}$	$2.9581 \cdot 10^{-3}$
7.0	$1.9018 \cdot 10^{-4}$	$1.8740 \cdot 10^{-4}$
9.0	$2.8750 \cdot 10^{-5}$	$2.8161 \cdot 10^{-5}$
10.0	$1.1066 \cdot 10^{-5}$	$1.0792 \cdot 10^{-5}$

Table 3.3: Comparison of approximate and numerical upcrossing rate using $k = 4$ $(\eta = s/\mu_1)$.

The corresponding results for the sway response are presented in Table 3.4. The agreement between the numerical and the approximate calculations are not very good for this case. The reason is the violation of the validity condition $\lambda_1 \gg |\lambda_j|,\ j \geq 2$.

ζ	$\hat{\nu}^+_{Y_2}(\zeta)$	$\tilde{\nu}^+_{Y_2}(\zeta)$
1.0	$1.67 \cdot 10^{-2}$	$2.99 \cdot 10^{-3}$
2.0	$4.30 \cdot 10^{-3}$	$1.01 \cdot 10^{-3}$
4.0	$2.02 \cdot 10^{-4}$	$6.40 \cdot 10^{-5}$
7.0	$1.62 \cdot 10^{-6}$	$6.26 \cdot 10^{-7}$
9.0	$6.09 \cdot 10^{-8}$	$2.51 \cdot 10^{-8}$
10.0	$1.17 \cdot 10^{-8}$	$4.92 \cdot 10^{-9}$

Table 3.4: Comparison of approximate and numerical upcrossing rate using $k = 4$ ($\zeta = y/\lambda_1$).

3.6 Numerical considerations and difficulties

The path of steepest decent is a powerful technique, allowing us to calculate the integral of equation (3.15). However, some numerical problems arrive. Equation (3.15) is a double integral, an finding a stopping criteria in both directions is crucial. And how should one integrate?

Clearly, integrating with ϖ as a variable, the midpoint approach was chosen, as seen in equation (3.23). The stopping criteria was chosen so the integration along the path of steepest decent in one direction ended when the additional contribution was at order 10^{-9} of the total, which seems sufficient. As seen in Figure 3.1, the main contribution to the integral is close to the imaginary axis, so an accurate calculation there should give a good numerical result. This calls for a small h in equation (3.21), giving a precise numerical result and allowing us to stay on the path of steepest decent, -or as close to it as possible. However, choosing a too small h may not throw us off the saddle point, and choosing a too large one throws us off the path. Since h does not have to be a constant, the solution is to first choose a fairly large h, and afterwards using a smaller h. Since the contribution to the integral diminish as ϖ grows, the h was chosen large in the end, speeding up the program.

Finding an integration path in the w-direction was described in the end of section 3.4. The main part is to avoid $w = (0, 0)$ (complex notation), and the remedy was to integrate along a semi-circle in the lower plane. The integral from equation (3.18) was first parted into 3,

$$\begin{aligned}\nu^+_Z(\zeta) &= -\frac{1}{(2\,\pi)^2}\int_{-\infty-\mathrm{i}a}^{\infty-\mathrm{i}a}\frac{1}{w^2}\,I(\zeta,w)\,dw \\ &= -\frac{1}{(2\,\pi)^2}\left[I_1(\zeta)+I_r(\zeta)+I_2(\zeta)\right],\end{aligned}$$

where

$$
\begin{aligned}
I_1(\zeta) &= \int_{-\infty-\mathrm{i}a}^{-r-\mathrm{i}a} \frac{1}{w^2}\, I(\zeta, w)\, dw, \\
I_r(\zeta) &= \int_{-r-\mathrm{i}a}^{r-\mathrm{i}a} \frac{1}{w^2}\, I(\zeta, w)\, dw, \\
I_2(\zeta) &= \int_{r-\mathrm{i}a}^{\infty-\mathrm{i}a} \frac{1}{w^2}\, I(\zeta, w)\, dw.
\end{aligned}
\tag{3.25}
$$

a was chosen to be zero. Other integrating patterns, like rectangles and triangles, were used testing the program. The radius r of the semi-circle had to be tested, because of large oscillations of the integrating function close to zero. A radius of 0.4 seemed to work fine. The semi-axe was divided into smaller parts, each part calculated using a variable transformation,

$$w = r \exp(\mathrm{i}\,\theta),$$

allowing us to rewrite equation (3.25) as

$$
\begin{aligned}
I_r(\zeta) &= \int_{-r}^{r} \frac{1}{w^2}\, I(\zeta, w)\, dw \\
&= \mathrm{i} \int_{-\pi}^{0} \frac{1}{r} I(\zeta, r\exp(\mathrm{i}\,\theta)) \exp(-\mathrm{i}\,\theta) d\theta \\
&= \mathrm{i} \sum_{i=1}^{N-1} \int_{\alpha_i}^{\alpha_{i+1}} \frac{1}{r} I(\zeta, r\exp(\mathrm{i}\,\theta)) \exp(-\mathrm{i}\,\theta) d\theta,
\end{aligned}
$$

where $-\pi = \alpha_1 < \alpha_2 < \ldots < \alpha_N = 0$. The number N was chosen to be 10, giving a good approximation of the integral. Both $I_1(\cdot)$ and $I_2(\cdot)$ was found by dividing the integral in smaller pieces, e.g.

$$I_2(\zeta) = \int_{r}^{\infty} \frac{1}{w^2}\, I(\zeta, w)\, dw \approx \sum_{i=1}^{M} \int_{s_i}^{s_{i+1}} \frac{1}{w^2}\, I(\zeta, w)\, dw,$$

where $r = s_1$ and $s_{i+1} = s_i + 1$. A similar stopping criterion as in the case with ϖ, was used finding $I_1(\cdot)$ and $I_2(\cdot)$. Each integral was evaluated using a gauss-quadrature, found for example in Abramowitz and Stegun (1972), usually using 8 or 10 points, giving an accurate approximation.

A problem giving a lot of headache, was a numerical type. It occurred evaluating the function $M_{Z\dot{Z}}(u, v)$ from equation (3.17). Since the vector $\beta = 0$,

$$M_{Z\dot{Z}}(u, v) = \frac{1}{\sqrt{\det A}},$$

and evaluating this square root gives 2 answers. The program usually pick the right one, but occasionally the wrong one. This is done by both FORTAN and MATLAB. The remedy is to force the solution to be of the same type as the previous one, since M is assumed continuous.

3.7 Approximations

In general, the CPU time required to carry out the computations in equation (3.23) can be quite long, depending on the number N of eigenvalues. It is therefore tempting to look for approximations. The first approximation considered is the Laplace approximation for the inner integral over the saddle point (Henrici, 1977). The simplest version of this approximation, adapted to the situation at hand, leads to the result

$$I = I(\zeta, w) \approx \sqrt{\frac{2\pi}{-\frac{\partial^2 g(\varpi_s; w)}{\partial x^2}}}\, \exp\{\, g(\varpi_s; w)\} \tag{3.26}$$

which can be substituted directly into equation (3.23), leading to an approximation of $\nu_Z^+(\zeta)$, which is denoted by $\tilde{\nu}_Z^+(\zeta)$.

This approximation can be exploited in the following way:

1. The full method is used for an inner interval of w-values, which contribute significantly to the integral in equation (3.18).

2. A Laplace approximation is then used in an outer interval of w-values where the contribution is less than significant. Of course, the level of significance is chosen according to some suitable criterion. By this procedure, the CPU time was reduced by factor of about 3. This method will be referred to as the hybrid method, and the corresponding approximation of $\nu_Z^+(\zeta)$ is denoted by $\check{\nu}_Z^+(\zeta)$.

A simple approximation proposed in Teigen and Naess (1999a,b) is worth a closer scrutiny. It is based on the widely adopted simplifying assumption that the displacement process is independent of the velocity process. This leads to a further approximation of $\nu_Z^+(\zeta)$, which we shall denote by $\overline{\nu}_Z^+(\zeta)$. It is given by the formula

$$\overline{\nu}_Z^+(\zeta) = \nu_Z^+(\zeta_{\text{ref}}) \frac{f_Z(\zeta)}{f_Z(\zeta_{\text{ref}})} \tag{3.27}$$

where f_Z denotes the marginal PDF of the surge (horizontal translation) response, and ζ_{ref} denotes a suitable reference level, typically the mean response. Here, ζ_{ref} has been chosen as the point where f_Z assumes its maximum, which corresponds well with the mean response level. A general approximation for $\nu_Z^+(\zeta_{\text{ref}})$ is given in Teigen and Naess (1999a). If only slow-drift response is considered, a good approximation is obtained by putting $\nu_Z^+(\zeta_{\text{ref}}) \approx 1/T_0$, where $T_0 = 2\pi/\omega_0$ is the slow-drift period. The advantage of equation (3.27) is that the rhs is much faster to calculate than the exact formula.

An approximation developed by Langley and McWilliam (1993) expresses the joint PDF of $Z(t)$ and $\dot{Z}(t)$ as a series in the following way,

$$f_{Z\dot{Z}}(z, \dot{z}) = f_Z(z) f_{\dot{Z}}(\dot{z}) + \sum_{n=1}^{\infty} \sum_{m=1}^{\infty} (-1)^{n+m} A_{nm} f_Z^{(n)}(z) f_{\dot{Z}}^{(m)}(\dot{z}), \tag{3.28}$$

where $f_Z^{(n)}(z)$ is the nth derivative of $f_Z(z)$ and $f_{\dot{Z}}^{(m)}(\dot{z})$ is the mth derivative of $f_{\dot{Z}}(\dot{z})$. Both $f_Z(z)$ and $f_{\dot{Z}}(\dot{z})$ are given by infinite series expressions, which are truncated in practice, cf. Grime and Langley (2003); Langley and McWilliam (1993). The coefficients A_{mn} are defined in terms of comulants for the displacement and velocity. Expressions for calculating the mean crossing rate are provided in McWilliam and Langley (1993). Since explicit expressions are given, the computational burden incurred by adopting this approximation is practically negligible. For an example structure studied in Grime and Langley (2003), it is shown that the approximation expressed in equation (3.28) gives results very similar to equation (3.27).

3.8 Distribution of extreme response

To provide estimates of the extreme values of the response process, it is necessary to know the probability law of the extreme value of $Z(t)$ over a specified period of time T, that is, $M_Z(T) = \max\{Z(t); 0 \leq t \leq T\}$. An exact expression for this probability law is in general unknown, but a good approximation is usually obtained by assuming that upcrossings of high response levels are statistically independent events. Under this assumption, the probability distribution of $M_Z(T)$ can be written as

$$\mathrm{P}\left(M_Z(T) \leq \zeta\right) = \exp\{-\nu_Z^+(\zeta)\, T\}, \tag{3.29}$$

which clearly displays the crucial role of the mean upcrossing rate $\nu_Z^+(\zeta)$ in determining the extreme value distribution.

As already pointed out, equation (3.29) is only an approximation to the true extreme value distribution. If this is so, why is it of practical significance to be able to perform an accurate calculation of the upcrossing rate? It is a well known fact that the exact extreme value distribution is not completely determined by the upcrossing rate alone. That would be true only when the upcrossing events of the high response levels can be assumed to be statistically independent. Usually that is a good approximation except when the total damping is small. For such cases, Naess (1999) has developed an effective method to account for the effect of low damping on the extreme value distribution, and the key to an accurate estimation of the extreme value distribution is good estimates of the mean upcrossing rate at high response levels.

So far the analysis has been limited to a short-term sea state characterised by a wave spectrum. This means that the extreme value distribution of equation (3.29) applies to the response values within this short-term sea state. In the context of a design situation, this would imply that the sea state has to be chosen as a design sea state. In practice this would usually mean that the spectral parameters would be chosen along a sea state contour having a prescribed return period.

An alternative approach is to use a long-term analysis. Let us assume that a short-term sea state is characterised by significant wave height H_s and a spectral period T_s, which have a joint PDF $f_{H_sT_s}(h_s, t_s)$. Then, for each set of values $H_s = h_s$ and $T_s = t_s$, the mean upcrossing rate can be calculated as we have described above. Let it be denoted by

$\nu_Z^+(\zeta \,|\, h_s, t_s)$. As shown by Næss (1984), the distribution of the long-term extreme value over the time period T is given as follows

$$\mathrm{P}\left(M_Z(T) \leq \zeta\right) = \exp\left\{-T \int_0^\infty \int_0^\infty \nu_Z^+(\zeta|h_s,t_s) f_{H_sT_s}(h_s,t_s) dh_s dt_s\right\}.$$

Haver and Nyhus (1986) have proposed a model for the joint PDF $f_{H_sT_s}(h_s, t_s)$.

3.9 Numerical example II

We shall illustrate the developments above by carrying numerical calculations for a specific example structure. It is a moored deep floater (MDF) with main particulars as detailed in Table 3.5. Figure 3.2 shows the submerged part of the floater in the form of a computer

Table 3.5: Main particulars of the MDF

Draught (m)	80.0
Column diameter (m)	10.0
Natural period surge/sway (s)	133.5
Natural period yaw (s)	121

mesh, which is used for calculating the hydrodynamic transfer functions. The total mass (including added mass) of the MDF is $M = 12.5 \cdot 10^6$ kg. The damping ratio is set equal to $\xi = 0.06$, and the natural frequency in sway is $\omega_0 = 0.047$ rad/s. The random stationary sea state is specified by a JONSWAP spectrum, which is given as follows

$$S_X(\omega) = \frac{\alpha g^2}{\omega^5} \exp\left\{-\frac{5}{4}\left(\frac{\omega_p}{\omega}\right)^4\right\} \cdot \gamma^{\exp\left[-\frac{1}{2\sigma^2}\left(\frac{\omega}{\omega_p}-1\right)^2\right]},$$

where

$$g = 9.81 \ (\mathrm{m}/s^2),$$
$$\sigma = \begin{cases} 0.07 & \omega \leq \omega_p \\ 0.09 & \omega > \omega_p \end{cases}$$

ω_p denotes the peak frequency in rad/s, and α, γ and σ are parameters related to the spectral shape. The parameter γ is chosen to be equal to 3.0. The parameter α is determined from the following empirical relationship

$$\alpha = 5.06 \left(\frac{H_s}{T_p^2}\right)^2 (1 - 0.287 \ln \gamma).$$

H_s = significant wave height and $T_p = 2\pi/\omega_p$ = spectral peak wave period. For the subsequent calculations, $H_s = 10.0$ m and $T_p = 12$ s. The natural frequency in surge is

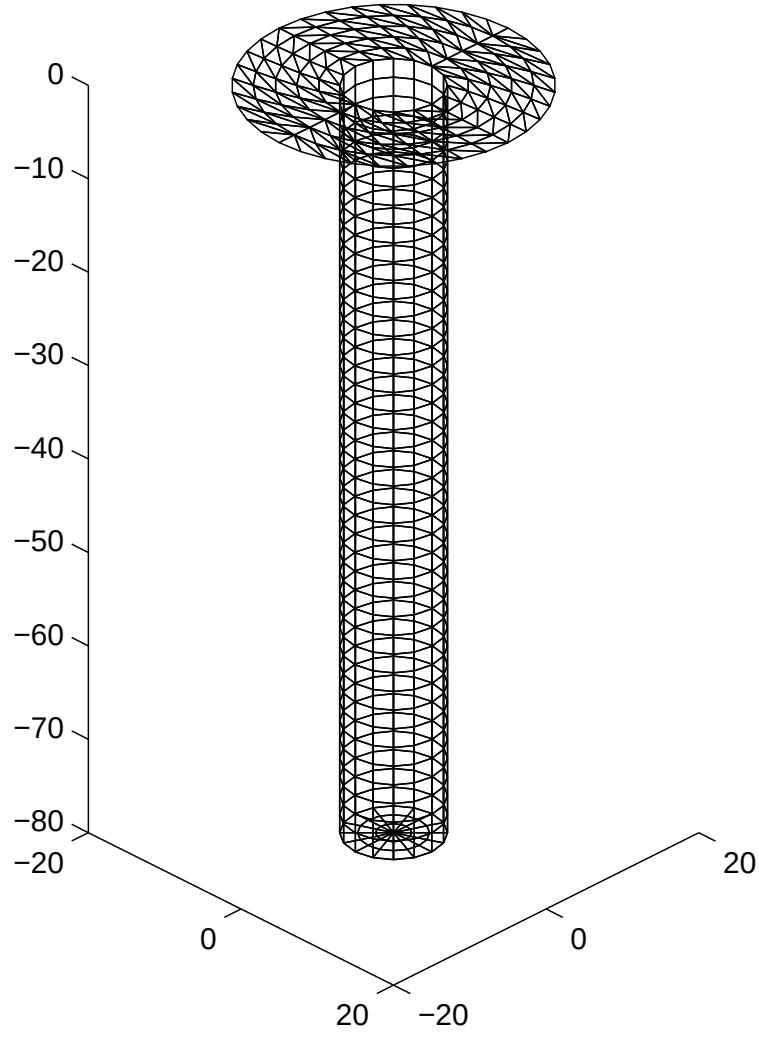

Figure 3.2: Computer mesh of the submerged part of the moored deep floater.

0.047 rad/s, which is well below the range where the waves have noticeable energy. This is why the second order, nonlinear term in the Volterra expansion is needed to capture the resonant motions in surge of the MDF.

To get an accurate representation of the response process, there is a specific requirement that must be observed. Since the damping ratio is only 6%, the resonance peak of the linear transfer function for the dynamics is quite narrow. Hence, to capture the dynamics correctly, the frequency resolution must secure a sufficient number of frequency values over the resonance peak. This usually leads to an eigenvalue problem (equation (3.7)) with the Q-matrix of size of the order of magnitude 100×100. Using the full representation of this size in calculating the mean crossing rate by the general method described here, would

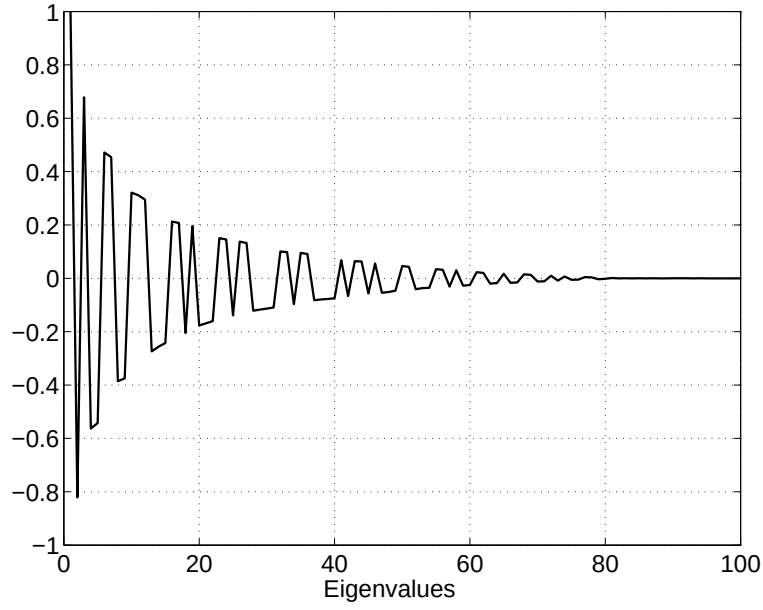

Figure 3.3: The 100 normalized eigenvalues λ_j/λ_1.

lead to very heavy calculations. In order to reduce this, we have investigated the effect of restricting the calculations by retaining only some of the terms in equation (3.10).

For the specific example considered here, where we have used exactly 100 (positive) frequencies, the values of the obtained eigenvalues λ_j have been plotted in Figure 3.3. It is seen that a substantial portion of the response variance, which is equal to $\mathrm{Var}[Z_2(t)] = 4\sum_{j=1}^{N}\lambda_j^2$, would be lost if only 10 or 20 eigenvalues were retained. This is also a factor to consider when deciding on the number of terms to retain.

As previous in this chapter, we have focused on the slow-drift response. Hence, only results for $Z_2(t)$ will be presented. In the tables, $\hat{\nu}^+_{Z_2}(\zeta)$, $\check{\nu}^+_{Z_2}(\zeta)$, $\tilde{\nu}^+_{Z_2}(\zeta)$, and $\overline{\nu}^+_{Z_2}(\zeta)$) denote the mean upcrossing rate of $Z_2(t)$ calculated by the full numerical method, the hybrid method, the Laplace approximation, and the simplified method of equation (3.27), respectively.

To highlight the effect of the increment parameter h, Table 3.6 compares the results obtained by the full numerical method for two values of h for 10 eigenvalues, that is, for a response representation retaining the first 10 terms. The CPU time differs by a factor of roughly 10 between the two choices of a value for h. Since the differences between the calculated crossing rates are fairly small, we have chosen to use the larger value to save CPU time.

In Tables 3.7 - 3.10 we have written down the results obtained for 10, 20, 30 and 50 eigenvalues, respectively. It is apparent that there is some variability of the calculated upcrossing rates depending on the number of eigenvalues included in the analysis. Ideally, it would therefore be desirable to carry out the calculations with at least 50 eigenvalues. However, our present implementation of the exact method is too expensive computationally

$\eta = \zeta/\lambda_1$	$h = 1.0 \cdot 10^{-3}$	$h = 1.0 \cdot 10^{-2}$
2.0	$8.38 \cdot 10^{-3}$	$8.38 \cdot 10^{-3}$
5.0	$3.93 \cdot 10^{-3}$	$3.93 \cdot 10^{-3}$
10.0	$5.53 \cdot 10^{-4}$	$5.50 \cdot 10^{-4}$
15.0	$5.70 \cdot 10^{-5}$	$5.65 \cdot 10^{-5}$
20.0	$5.34 \cdot 10^{-6}$	$5.26 \cdot 10^{-6}$
25.0	$4.81 \cdot 10^{-7}$	$4.71 \cdot 10^{-7}$

Table 3.6: Comparison of calculated upcrossing rate $\hat{\nu}^+_{Z_2}(\eta)$ for different step lengths.

to allow for more than about 50 eigenvalues. Even if this can be improved significantly, like for the hybrid method, it would still be a method requiring heavy computations.

To get a more detailed picture of how the crossing rate varies with the number of eigenvalues retained, the mean upcrossing rate was calculated for the level $\eta = 20$ as a function of the number of eigenvalues. The result is shown in Figure 3.4. It was also decided to investigate the effect of updating the truncated response representation so that it had the correct variance. This was achieved by multiplying the retained eigenvalues by a suitable factor. The effect of this updating on the calculated upcrossing rate is also shown in Figure 3.4. The figure indicates a couple of interesting conclusions. Updating for variance can lead to inaccurate results for the crossing rate for small to moderate number of eigenvalues retained. Comparing Figures 3.3 and 3.4 it is seen that surprisingly accurate results are obtained for even a small number of retained eigenvalues when the truncation is done exactly where negative eigenvalues are followed by positive eigenvalues. This seems to provide the right balance between the terms in the response representation, and it indicates a useful criterion for truncating the response representation for crossing rate calculations. It is also of great interest to observe that the simple Laplace approxi-

$\eta = \zeta/\lambda_1$	$\hat{\nu}^+_{Z_2}(\eta)$	$\check{\nu}^+_{Z_2}(\eta)$	$\tilde{\nu}^+_{Z_2}(\eta)$
2.0	$8.38 \cdot 10^{-3}$	$8.38 \cdot 10^{-3}$	$7.41 \cdot 10^{-3}$
5.0	$3.93 \cdot 10^{-3}$	$3.93 \cdot 10^{-3}$	$3.59 \cdot 10^{-3}$
10.0	$5.50 \cdot 10^{-4}$	$5.50 \cdot 10^{-4}$	$5.23 \cdot 10^{-4}$
15.0	$5.65 \cdot 10^{-5}$	$5.65 \cdot 10^{-5}$	$5.59 \cdot 10^{-5}$
20.0	$5.26 \cdot 10^{-6}$	$5.26 \cdot 10^{-6}$	$5.36 \cdot 10^{-6}$
25.0	$4.71 \cdot 10^{-7}$	$4.71 \cdot 10^{-7}$	$4.92 \cdot 10^{-7}$

Table 3.7: Calculated upcrossing rates for 10 eigenvalues

mation in fact provides quite accurate estimates of the mean upcrossing rates, and for this method the number of eigenvalues has practically no effect on the computational burden. Hence, from a practical point of view, this is an extremely appealing method. In Table 3.11 we have listed the results obtained by the hybrid method, the Laplace approximation and also the simple approximation of equation (3.27) for 100 eigenvalues. It is seen that while there is excellent agreement between the hybrid method and the Laplace approximation,

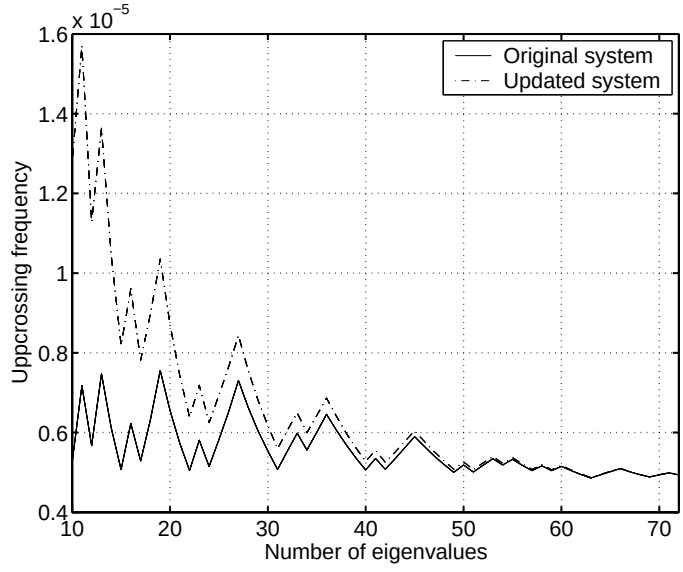

Figure 3.4: The crossing rate as a function of the number of retained eigenvalues. (−): Simple truncation. (− ·): Truncation and updating for correct variance.

$\eta = \zeta/\lambda_1$	$\hat{\nu}^+_{Z_2}(\eta)$	$\check{\nu}^+_{Z_2}(\eta)$	$\tilde{\nu}^+_{Z_2}(\eta)$
2.0	$8.09 \cdot 10^{-3}$	$8.10 \cdot 10^{-3}$	$7.27 \cdot 10^{-3}$
5.0	$4.19 \cdot 10^{-3}$	$4.19 \cdot 10^{-3}$	$3.82 \cdot 10^{-3}$
10.0	$6.51 \cdot 10^{-4}$	$6.51 \cdot 10^{-4}$	$6.06 \cdot 10^{-4}$
15.0	$6.95 \cdot 10^{-5}$	$6.95 \cdot 10^{-5}$	$6.74 \cdot 10^{-5}$
20.0	$6.56 \cdot 10^{-6}$	$6.56 \cdot 10^{-6}$	$6.58 \cdot 10^{-6}$
25.0	$5.91 \cdot 10^{-7}$	$5.91 \cdot 10^{-7}$	$6.11 \cdot 10^{-7}$

Table 3.8: Calculated upcrossing rates for 20 eigenvalues

$\eta = \zeta/\lambda_1$	$\hat{\nu}^+_{Z_2}(\eta)$	$\check{\nu}^+_{Z_2}(\eta)$	$\tilde{\nu}^+_{Z_2}(\eta)$
2.0	$7.21 \cdot 10^{-3}$	$7.21 \cdot 10^{-3}$	$6.51 \cdot 10^{-3}$
5.0	$3.58 \cdot 10^{-3}$	$3.58 \cdot 10^{-3}$	$3.27 \cdot 10^{-3}$
10.0	$5.48 \cdot 10^{-4}$	$5.48 \cdot 10^{-4}$	$5.11 \cdot 10^{-4}$
15.0	$5.85 \cdot 10^{-5}$	$5.85 \cdot 10^{-5}$	$5.67 \cdot 10^{-5}$
20.0	$5.54 \cdot 10^{-6}$	$5.54 \cdot 10^{-6}$	$5.55 \cdot 10^{-6}$
25.0	$5.00 \cdot 10^{-7}$	$5.00 \cdot 10^{-7}$	$5.17 \cdot 10^{-7}$

Table 3.9: Calculated upcrossing rates for 30 eigenvalues

the simple approximation leads to significantly lower values. In terms of extreme value predictions, for the example structure at hand the Laplace approximation is within about 1% of the hybrid method, while the simple approximations would lead to an underestimation of typically 5-10% compared with the two more accurate methods. While the results obtained by the simple approximation is somewhat lower than those obtained by the more

$\eta = \zeta/\lambda_1$	$\hat{\nu}^+_{Z_2}(\eta)$	$\check{\nu}^+_{Z_2}(\eta)$	$\tilde{\nu}^+_{Z_2}(\eta)$
2.0	$6.55 \cdot 10^{-3}$	$6.55 \cdot 10^{-3}$	$5.93 \cdot 10^{-3}$
5.0	$3.25 \cdot 10^{-3}$	$3.25 \cdot 10^{-3}$	$2.98 \cdot 10^{-3}$
10.0	$5.04 \cdot 10^{-4}$	$5.04 \cdot 10^{-4}$	$4.70 \cdot 10^{-4}$
15.0	$5.44 \cdot 10^{-5}$	$5.44 \cdot 10^{-5}$	$5.28 \cdot 10^{-5}$
20.0	$5.19 \cdot 10^{-6}$	$5.19 \cdot 10^{-6}$	$5.20 \cdot 10^{-6}$
25.0	$4.71 \cdot 10^{-7}$	$4.71 \cdot 10^{-7}$	$4.86 \cdot 10^{-7}$

Table 3.10: Calculated upcrossing rates for 50 eigenvalues

$\eta = \zeta/\lambda_1$	$\check{\nu}^+_{Z_2}(\eta)$	$\tilde{\nu}^+_{Z_2}(\eta)$	$\bar{\nu}^+_{Z_2}(\eta)$
2.0	$6.17 \cdot 10^{-3}$	$5.59 \cdot 10^{-3}$	$6.03 \cdot 10^{-3}$
5.0	$3.03 \cdot 10^{-3}$	$2.78 \cdot 10^{-3}$	$2.74 \cdot 10^{-3}$
10.0	$4.71 \cdot 10^{-4}$	$4.40 \cdot 10^{-4}$	$3.65 \cdot 10^{-4}$
15.0	$5.11 \cdot 10^{-5}$	$4.96 \cdot 10^{-5}$	$3.44 \cdot 10^{-5}$
20.0	$4.88 \cdot 10^{-6}$	$4.90 \cdot 10^{-6}$	$2.93 \cdot 10^{-6}$
25.0	$4.44 \cdot 10^{-7}$	$4.63 \cdot 10^{-7}$	$2.44 \cdot 10^{-7}$

Table 3.11: Calculated upcrossing rates for 100 eigenvalues

accurate methods, for some applications an accuracy within 5-10% would be considered quite satisfactory. However, the discrepancy needs to be checked for each specific case at hand. The results for the extreme value distributions are summarized in Figures 3.5 and 3.6, which show the exceedance probability

$$\mathrm{P}_F(\eta; T) = 1 - \mathrm{P}\left(M_Z(T) \leq \lambda_1 \, \eta\right) \tag{3.30}$$

for the various cases.

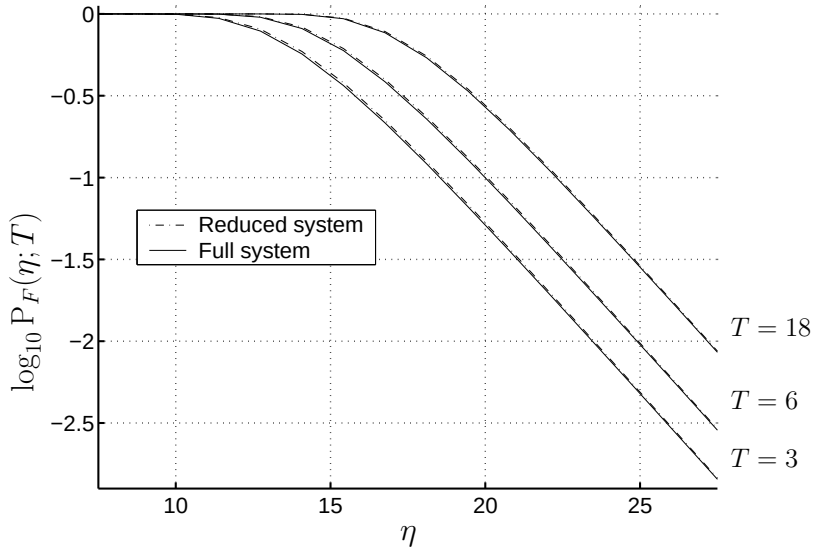

Figure 3.5: The exceedance probability $\mathrm{P}_F(\eta;T)$ as function of $\eta = \zeta/\lambda_1$ for $T = 3, 6, 18$ hours for 22 and 100 eigenvalues.

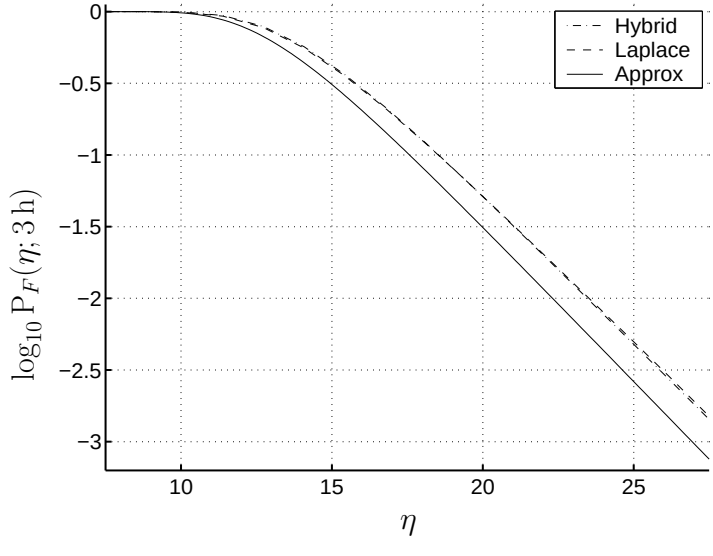

Figure 3.6: The exceedance probability $\mathrm{P}_F(\eta;T)$ as function of $\eta = \zeta/\lambda_1$ for $T = 3$ hours and 100 eigenvalues for the hybrid, Laplace and simple approximations.

3.10 Robustness of the upcrossing frequency

How much does the exceedance probability $\mathrm{P}_F(\eta;T)$ depend on $\nu_Z^+(\zeta)$? Assuming that the upcrossings are independent, the exact exceedance probability is found using equations (3.29) and (3.30), we write the exact and the approximate exceedance probability

$$p_f = 1 - \exp\left(-\nu T\right),$$
$$p_{f;\epsilon} = 1 - \exp\left(-\nu_\epsilon T\right),$$

where $p_f = \mathrm{P}_F(\eta;T)$, $\nu = \nu_Z^+(\eta\lambda_1)$ and $\nu_\epsilon = \nu\epsilon$, and $0 < \epsilon$. Assuming the relative difference between p_f and $p_{f;\epsilon}$ is less than a certain positive number α, we get the equation

$$\left|\frac{p_f - p_{f;\epsilon}}{p_f}\right| = \left|\frac{\exp(-\nu\epsilon T) - \exp\left(-\nu T\right)}{1 - \exp\left(-\nu T\right)}\right| \leq \alpha, \tag{3.31}$$

where $0 \leq \alpha \leq 1$, but preferably small. Equation (3.31) provides us with a condition on ϵ,

$$\frac{\ln[A + \alpha(1-A)]}{-\nu T} \leq \epsilon \leq \beta \tag{3.32}$$

where $A = \exp(-\nu T)$, and

$$\beta = \begin{cases} \infty & \text{if} \quad \nu T \geq \log\left(1 + \frac{1}{\alpha}\right) \\ -\frac{1}{\nu T}\ln[A - \alpha(1-A)] & \text{otherwise} \end{cases}$$

Assume α small. For the case that $\beta = \infty$, νT has to be large. This is not physically a very interesting incident, since the exceedance probability will be close to unity. νT is small in most cases we are interested in.

Assume νT small, so $1 - \exp\left(-\nu T\right) \approx \nu T$. A corresponding condition on ϵ is simply

$$1 - \alpha \leq \epsilon \leq 1 + \alpha. \tag{3.33}$$

As an example, using $\alpha = 0.05$, $T = 3\mathrm{h}$, $\eta = 15; \nu = 5.11 \cdot 10^{-5} s^{-1}$, we have from equation (3.32) that

$$0.934 \leq \epsilon \leq 1.068,$$

or from the simplified version of equation (3.33)

$$0.95 \leq \epsilon \leq 1.05,$$

allowing us to calculate the upcrossing frequency with a small error, but still have a reasonable result.

3.11 Improvement

As shown in Appendix B, equation (3.23) may be found in an even easier way, by using equation (B.6),

$$\nu_Z^+(\zeta) = -\frac{1}{2\,\pi^2}\Re\left\{\lim_{\epsilon\to 0+}\int_\epsilon^\infty \frac{1}{v^2}\int_0^\infty \left[M(u,v)+M(u,-v)\right]\,e^{-\,\mathrm{i}u\zeta}\,du\,dv\right\},$$

which is supposed to be approximately 4 times faster than the original one. Unfortunately, this was discovered after the articles Naess and Karlsen (2004); Naess et al. (2006) was written. The new and simpler equation for finding the upcrossing frequency has afterwards been tested numerically with good agreement to previous calculations.

Chapter 4

The path integration technique

4.1 Introduction

The theory of predicting structural response statistics of moored large volume structures subjected to random waves in chapter 3 has its limitations; -the equation of motion has to be linear and time-invariant. Unfortunately (and luckily!), the real world is **not** linear and time-invariant. The challenge of estimating response statistics of non-linear, time-dependent dynamic systems subjected to random forcing processes, has been a demanding challenge for several decades.

An early method of studying stochastic equations, was the methods of *stochastic linearization* (Caughey, 1963; Roberts and Spanos, 1990). The idea was to replace the non-linear equations with linear ones, -the difference between the sets being minimised in some appropriate sense, often the mean square. Its main value lies in the fact that, -unlike other methods, it can readily be used to deal with complex systems having many degrees of freedom, and with complex types of excitation. Since linear systems are easier analysed, the linear equations were studied intensively. Stochastic linearization is perhaps the most frequently used analytical method for analysing the response of many nonlinear systems, as it provides reasonable estimates for the mean square response. However, the method is not, in general, well suited for estimating the power spectra of stationary responses of randomly excited nonlinear systems. Donley and Spanos (1990) shows that the response spectral densities obtained using equations with non-linearities, exhibit significant resonance responses which can not be accounted for by linearization because they occur at frequencies outside the range of excitation frequencies. And for a Gaussian excitation, the linearized solution leads to a Gaussian probability distribution, whereas the true response is non-Gaussian.

Due to the rapid growth of computer power, Monte-Carlo techniques for calculating the response statistics of offshore and marine systems subjected to random seas are attractive, in the sense that non-linearities and time-dependence can be easily dealt with (Rubinstein, 1981). However, for some applications it can still be computationally very heavy, if not prohibitive. One such application is the estimation of the extreme slow drift response of moored offshore structures.

The method of Path Integration (PI) is a way to calculate a stationary PDF as a

solution to the Fokker-Planck equation of a corresponding Stochastic Differential Equation (SDE). PI may in addition to relatively short Monte-Carlo simulations be used with great success calculating upcrossing frequencies, even when the SDE has both non-linear and time-dependent terms.

4.2 Theory

The transition probabilities in section 2.16 and subsection 2.14.3 are needed to obtain the Path Integral (PI) solutions. They are derived by repeatedly applying the Chapman-Kolmogorov equation (2.16).

Assume $X(t)$ is a stochastic Markov process, having a known TPD $p(x_n, t_n|x_{n-1}, t_{n-1})$ and a distribution $f_0(x_0)$ as a *starting probability*. Now

$$p(x_N, t_N|x_0, t_0) = \int \dots \int \prod_{i=1}^{N} p(x_i, t_i|x_{i-1}, t_{i-1}) f_0(x_0) dx_{N-1} \dots dx_1$$

may be found directly, but in practice we first use equation (2.16) finding

$$p(x_2, t_2|x_0, t_0) = \int p(x_2, t_2|x_1, t_1)\, p(x_1, t_1|x_0, t_0) dx_1,$$

which is used iteratively finding

$$p(x_N, t_N|x_0, t_0) = \int p(x_N, t_N|x_{N-1}, t_{N-1})\, p(x_{N-1}, t_{N-1}|x_0, t_0) dx_{N-1} \quad N \geq 3. \tag{4.1}$$

Comparing equation (2.23) and equation (2.25) it's seen that finding the solution $f_X(x,t)$ to the FP-equation is the same as finding $p(x_N, t_N|x_0, t_0)$. Assuming that the system has a stationary solution, we find

$$\bar{f}(x) = \lim_{t\to\infty} f_X(x,t) = \lim_{N\to\infty} p(x_N, t_N|x_0, t_0).$$

4.3 System

From now on, the system we are interested in is

$$\dot{x} = m(x,t) + Q(x,t)N_t \tag{4.2}$$

where x is a n-dimensional vector, t is time, $m(x,t)$ is the drift term, $Q(x,t)$ is the diffusion term, and N_t is Gaussian random noise. In general Q is a diffusion matrix and N_t is a vector of Gaussian random noise input. By choosing the nth equation of equation (4.2) to

be a Rayleigh process, equation (4.2) may be written as

$$\begin{aligned} \dot{x}_i &= m_i(x,t) \qquad i = 1,\ldots,n-1 \\ \dot{x}_n &= m_n(x_n) + q\,N_t \\ m_n(x_n) &= a\left(\frac{1}{x_n} - x_n\right) \\ q &= \sqrt{2a}, \end{aligned} \tag{4.3}$$

where N_t is Gaussian white noise.

4.4 TPD

Now, a conditional PDF of $X(t)$ given that $X(t') = x'$ has to be found. Assuming the system in equation (4.2) to be autonomous and $r = n-1$ in equation (2.43), the approximate TPD will take the shape

$$\begin{aligned} p(x,t|x',t') = &\prod_{i=1}^{n-1} \delta\left(x_i - (x_i' + m_i(x')\tau)\right) \\ &\times \frac{1}{\sqrt{4\pi a\tau}} \exp\left(-\frac{[x_n - (x_n' + m_n(x')\tau)]^2}{4a\tau}\right). \end{aligned} \tag{4.4}$$

The exact TPD of the system of equations (4.3) may also be found,

$$p(x,t|x',t') = \prod_{i=1}^{n-1} \delta\left(x_i - (x_i' + m_i(x')\tau)\right)\, p_R(x_n,t|x_n',t'), \tag{4.5}$$

where

$$p_R(x,t|x',t') = \frac{x}{1-\exp(-2a\tau)} I_0\left(\frac{\exp(-a\tau)}{1-\exp(-2a\tau)} xx'\right) \exp\left(-\frac{x^2 + \exp(-2a\tau)x'^2}{2(1-\exp(-2a\tau))}\right). \tag{4.6}$$

As before, the $\delta(\cdot)$ denotes the Dirac delta function and $I_0(\cdot)$ denotes the modified Bessel function of first kind. Equation (4.6) is of course similar to equation (2.34). The TPD in equation (4.4) and equation (4.6) are describing the same movement of probability, and given the same problem, they should give the same stationary PDF as a solution to the corresponding Fokker-Planck equation.

4.5 Integration

In some way, the integration in equation (4.1) has to be done. By inserting equation (4.5) in equation (4.1) we get

$$\begin{aligned} p(x,t|x_0,t_0) &= \int p(x,t|x',t')\, p(x',t'|x_0,t_0)dx' \\ &= \int \prod_{i=1}^{n-1} \delta\left(x_i - (x'_i + m_i(x')\tau)\right) \\ &\quad \times \frac{1}{\sqrt{4\pi a\tau}} \exp\left(-\frac{[x_n - (x'_n + m_n(x')\tau)]^2}{4a\tau}\right) p(x',t'|x_0,t_0)\, dx' \,, \end{aligned} \tag{4.7}$$

where $p(x,t|x_0,t_0) = p(x_N,t_N|x_0,t_0)$, $p(x,t|x',t') = p(x_N,t_N|x_{N-1},t_{N-1})$, $p(x',t'|x_0,t_0) = p(x_{N-1},t_{N-1}|x_0,t_0)$, and $x = [x_1,\ldots,x_n]^\top$. This integral is actually an integral over n variables, but because of the form of the TPD, and the fact that integrating a delta function is easy (see appendix A), equation (4.7) reduces to a one-dimensional integral,

$$p(x,t|x_0,t_0) = \int |\mathrm{J}(x')|\, p(x_n,t|x'_n,t')\, p(x',t'|x_0,t_0)\, dx'_n, \tag{4.8}$$

where

$$p(x_n,t|x'_n,t') = \frac{1}{\sqrt{4\pi a\tau}} \exp\left(-\frac{[x_n - (x'_n + m_n(x')\tau)]^2}{4a\tau}\right), \tag{4.9}$$

and $\mathrm{J}(x)$ is a Jacobi determinant, due to integrating the delta functions. This is shown in appendix A for one dimension. This correction term has not been mention in any previous papers, except from Iourtchenko et al. (2006). Integration of exact TPD may be found in a similar way,

$$p(x,t|x_0,t_0) = \int |\mathrm{J}(x')| p_R(x_n,t|x'_n,t')\, p(x',t'|x_0,t_0)\, dx'_n, \tag{4.10}$$

where $p_R(x,t|x',t')$ is as described in equation (4.6).

4.6 Numerical interpretation

4.6.1 Time-stepping

Choosing a parameter τ for the time stepping procedure of the TPD in equations (4.8) and (4.10) is not an easy task. Johnsen (1992) uses the criterion

$$\tau_c = \min(f_{\tau_c}(x)), x \in \left\{x : p(x) \geq 10^{-6}\right\}$$

as a characteristic time when using an approximate TPD. Here,

$$f_{\tau_c}(x) = \frac{Q_n(x)}{m_n(x)^2},$$

where $m(\cdot)$ and $Q(\cdot)$ are as defined in section 4.3 As the author points out, the criterion works well in most cases. But it is not suitable when dealing with the Rayleigh process, where $\tau_c = 10^{-9}$ is a number far too low for any practical use.

Depending on whether or not we are using an approximate or an exact TPD, different τ has been chosen. In the latter case, as described in section 5.3, τ has to be quite large (≥ 0.40). An approximate TPD demands a small τ, often of the order 10^{-2}.

4.6.2 Interpolation

In equation (4.1), integration over the variable x_{N-1} has to be done. Although the PDF $p(x_{N-1}, t_{N-1}|x_0, t_0)$ is known, it is only known for some points, and the integrating procedure in equation (4.1) often requires the value of the PDF in a large number of points. Hence, an interpolation procedure has to be chosen.

One uses polynomials for approximation because they can be evaluated, differentiated, and integrated easily and in finitely many steps using the basic arithmetic operations of addition, subtraction, and multiplication. The limitation of polynomials is that global dependence on local properties may give poor approximations everywhere. This may be avoided using *piecewise polynomials* (pp).

Broken lines, i.e. piecewise linear approximation, are neither smooth nor efficient approximators. The use of piecewise linear interpolation for problems larger than 1-D, was in Skaug (2000) shown to be insufficient. As pointed out in Johnsen (1992), in order to maintain the flexibility of piecewise polynomials while at the same time achieving some degree of global smoothness, *B-splines* (basis splines) have to be chosen, relying heavily on the theory given by de Boor (2001). The most popular choice is a cubic approximating function, and will be discussed later. However, because we want our probability density functions to stay positive *everywhere*, it is sometimes necessary to use e.g. linear approximations in certain troublesome areas, often found in the boundary of the PDFs. This may be due to large local oscillations, similar to what one observes using global polynomials as described above.

Parabolic splines have also been investigated, and although faster evaluated than cubic splines, they didn't provide results as good as results using cubic splines in the inner area of the PDF. Another nice property we may exploit using cubic splines, is the not-a-knot condition, described in section 4.6.3.

4.6.3 B-splines

A procedure for piecewise B-spline interpolation will here be given.

Definition 4.1 *Let* $\mathbf{t} = (t_j)$ *be a finite, nondecreasing sequence. The jth B-spline of order* k *for the knot sequence* $\mathbf{t}$ *is denoted by* $B_{j,k,\mathbf{t}}$*, and is defined by the rule*

$$B_{j,k,\mathbf{t}}(x) = (t_{j+k} - t_j)[t_j, \ldots, t_{j+k}](\cdot - x)_+^{k-1} \quad \forall\, x \in \mathbb{R}.$$

Here $(\cdot - x)_+ = (t - x)_+ := \max[t - x, 0]$,

$$[t_i, \ldots, t_{i+r}]g = \frac{[t_{i+1}, \ldots, t_{i+r}]g - [t_i, \ldots, t_{i+r-1}]g}{t_{i+r} - t_i},$$

and

$$[t_i, t_{i+1}]g = \frac{g(t_i) - g(t_{i+1})}{t_i - t_{i+1}}.$$

Often $B_{j,k,\mathbf{t}}(x)$ is written $B_{j,k}(x)$, assuming a given knot sequence $\mathbf{t}$. A spline function of order k with knot sequence $\mathbf{t}$ is any linear combination of B-splines of order k for the knot sequence $\mathbf{t}$.

The B-splines may be found using a recursive algorithm, found in the books mentioned above. An example of a cubic B-spline is shown in figure 4.1, with knots at integer values of x.

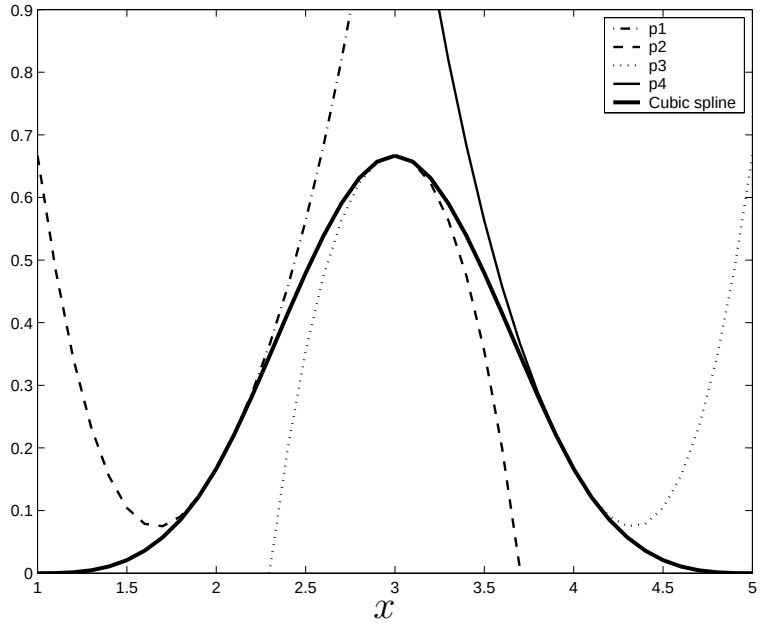

Figure 4.1: Four cubic polynomials $p_1, \ldots, p_4$ build a basis cubic B-spline

Some nice properties of the B-spline includes

1. B_i has local support, i.e. $B_i(x) = 0$ for $x \neq [t_i, t_{i+k}]$.

2. The B-splines forms a partition of unity, that is $\sum_i B_i(x) = \sum_{i=j-k+1}^{s-1} B_i(x) = 1$ for all $t_j < x < t_s$.

3. B_i is positive on its support, i.e. $B_i(x) > 0$ for all $t_i < x < t_{i+k}$.

4. $f(x)$ may be written in a unique way,

$$f(x) = \sum_{i=1}^{n} \alpha_i B_i(x).$$

The numbers $\{\alpha_i\}$ are called B-spline coefficients. In particular, if $t_j \leq x \leq t_{j+1}$ for some $j \in \{k, \ldots, n\}$ then property 1 and property 4 gives

$$f(x) = \sum_{i=j-k+1}^{j} \alpha_i B_i(x). \tag{4.11}$$

This means that the value at a site depends only on k of the coefficients, which is a huge advantage when setting up a numerical scheme.

Given the data $g(t_1), \ldots, g(t_n)$ with $a = t_1 < \ldots < t_n = b$, where $\mathbf{t} = [t_1, \ldots, t_n]$ are knot points, we construct an interpolant f to g as follows. On each interval $[t_i, t_{i+1}]$, f will agree with some polynomial P_i of order k,

$$f(x) = p_i(x), \qquad t_i \leq x \leq t_{i+1}, \quad i = 1, \ldots, n-1\,. \tag{4.12}$$

Each polynomial p_i has a degree of $k-1$, and the spline is $k-2$ times continuously differentiable in the knot points and infinite differentiable elsewhere.

To produce a spline representation, the number of unknowns necessarily have to match the number of conditions. We now assume that a cubic spline representation is to be found, i.e. $k = 4$. Having L polynomial functions, and each function has 4 unknown coefficients, the total number of unknown coefficients are $4\,L$. For each interior point, there are 3 continuity conditions over each knot, providing us with $3\,(L-1)$ equations. In addition we know the value in each knot, providing us with $L+1$ conditions. This leaves us short with 2 conditions. In order of getting a solvable system of equations with one solution, we need to add two conditions. The two most common ways of obtaining these conditions, are the *not-a-knot condition* and the *natural end condition*.

The natural end condition is to assume that the function in some way goes to zero outside the interpolated area, often assuming the $f'' = 0$. This is suitable for many PDFs.

When nothing is known about the end point derivatives, the not-a-knot condition is reasonable. Here one chooses $P_1 = P_2$ and $P_{n-2} = P_{n-1}$ from equation (4.12), -the first and the last interior knots are not active. This is the same as assuming $t_2 = t_1$ and $t_{n-1} = t_n$, reducing the number of polynomial functions by 2.

A third way to handle the two missing equations, and applied here in section 4.6.4, is to assume that the PDF is zero outside the chosen interval, putting the spline coefficients for basis functions with support outside the interval, to zero.

Many of the simple algebraic properties of ordinary polynomial splines in one dimension can be carried over and easily generalised to multivariate approximating problems by tensor product methods. The theory may be found e.g. in Johnsen (1992) and Schumaker (1981), and is not repeated here.

4.6.4 Fast numerical procedure

This is a procedure made by Eirik Mo, which is a *fast* numerical procedure for interpolation when using uniform grid and the third method of handling missing equations, as described in the previous section.

We divide the interval x into n points x_i, and use a knot sequence t where $t_i = x_i, 1 \leq i \leq n$. The value in each point x_i is $g(x_i)$, and α is the B-spline coefficients of f. Assuming a cubic B-spline interpolation, each spline is a translation of the previous one, allowing us to write for $x \in \mathbf{t}$,

$$g(x) = A\,\alpha, \tag{4.13}$$

where

$$A = \frac{1}{6}\begin{bmatrix} 4 & 1 & 0 & \dots & 0 & 0 \\ 1 & 4 & 1 & \dots & 0 & 0 \\ 0 & 1 & 4 & & 0 & 0 \\ & & & \ddots & & \\ 0 & 0 & 0 & \dots & 4 & 1 \\ 0 & 0 & 0 & \dots & 1 & 4 \end{bmatrix}.$$

Now, the spline coefficients α of equation (4.13) have to be found. Since A has its special form, the LU factorisation may be done analytically. This is an advantage, providing us with a numerical procedure finding α. But the benefit by constructing A in this way, is that the $B_i(x)$ from equation (4.11) may now easily be found quickly, speeding up the program.

However, when using general grid and a not-a-knot condition, A loses its nice form. This is no practical problem, but we may not find $B_i(x)$ so fast.

4.6.5 Taylor approximations

We shall use truncated stochastic Taylor expansions to derive time discrete approximations appropriate for the weak convergence criterion. This may be found in e.g. Kloeden and Platen (1992), which is highly recommended for readers interested in different numerical schemes.

We consider a Ito process $X = \{X_t, t_0 \leq t \leq T\}$ satisfying the SDE

$$dX_t = u(X_t, t)\,dt + v(X_t, t)\,dW_t \tag{4.14}$$

on $t_0 \leq t \leq T$ with the initial value $X_{t_0} = X_0$, and a time discretization

$$t_0 = \tau_0 < \tau_1 < \ldots < \tau_N = T.$$

on the time interval $[\tau_0, T]$. The simplest time discrete approximation is the stochastic generalisation of the Euler approximation, which sometimes is called the *Euler-Maruyama approximation*, but often just *Euler approximation*. For the SDE in equation (4.14), the Euler approximation is a continuous time stochastic process $Y = \{Y(t), t_0 \leq t \leq T\}$ satisfying the iterative scheme

$$Y_{n+1} = Y_n + u\,\Delta_n + v\,\Delta W_n, \tag{4.15}$$

for $n = 0, 1, \ldots, N-1$ with initial value $Y_0 = x_0$. $\Delta_n = \tau_{n+1} - \tau_n$ is the length of the time discretization subinterval $[\tau_n, \tau_{n+1}]$, $\Delta W_n = W_{\tau_{n+1}} - W_{\tau_n}$ is the $N(0, \Delta_n)$ increment of the Wiener process W_t on $[\tau_n, \tau_{n+1}]$, $u = u(Y_n, \tau_n)$ and $v = v(Y_n, \tau_n)$. The maximum time step δ is defined as the largest of all Δ_n. Usually we use a equidistant time discretization, $\tau_n = t_0 + n\delta$, with $\delta = \Delta_n = (T - t_0)/N$ for some N large enough so that $\delta \in (0, 1)$.

The following definition is a criterion for the closeness of the sample paths of the Ito process X and the approximation Y at a time T.

Definition 4.2 *An approximating process Y converges in the strong sense with order $\gamma \in (0, \infty)$ if there exists a finite constant K and a positive δ_0 such that*

$$\mathrm{E}(|X_T - Y_T|) \leq K\delta^\gamma$$

for any time discretization with maximum step size $\delta \in (0, \delta_0)$.

However, in many practical situations it is not necessary to have a close pathwise approximation of an Ito process. Often one is only interested in some function of the value of the Ito process at a given final time T, such as the expectation $\mathrm{E}(g(X_T))$ for some function g. The objective may be to have a good approximation of the PDF of the random variable X_T rather than a close approximation of sample paths. This type of approximation required then is much weaker than that provided by the strong convergence criterion.

Definition 4.3 *An approximating process Y converges in the weak sense with order $\beta \in (0, \infty)$ if for any polynomial g there exists a finite constant K and a positive δ_0 such that*

$$|\mathrm{E}(g(X_T)) - \mathrm{E}(g(Y_T))| \leq K\delta^\beta$$

for any time discretization with maximum step size $\delta \in (0, \delta_0)$.

Equation (4.15) represents the simplest strong Taylor approximation and generally attains the order of strong convergence $\gamma = 0.5$. The simplest useful weak Taylor approximation is the weak Euler scheme

$$Y_{n+1} = Y_n + u\,\Delta_n + v\,\Delta\hat{W}_n, \tag{4.16}$$

for $n = 0, 1, \ldots, N-1$. The random increments ΔW_n of the Wiener process from the strong case may in the weak case be replaced by other and more convenient approximations $\Delta\hat{W}_n$ which have similar moment properties to the ΔW_n. It can be shown that equation (4.16) has a weak order $\beta = 1.0$ if the coefficients a and b are four times continuously differentiable with these derivatives satisfying a growth bound. This contrasts the order $\gamma = 0.5$ of the strong Euler scheme.

Assuming u to be autonomous and v is a constant, -as in the Rayleigh equation (2.29), the weak Taylor approximation of order $\beta = 2.0$ has the form

$$Y_{n+1} = Y_n + u\,\Delta_n + v\,\Delta\hat{W}_n + \frac{1}{2}\,u'\,v\,\Delta\hat{W}_n\,\Delta_n + \frac{1}{2}\,u\,u'\,\Delta_n^2, \tag{4.17}$$

under certain conditions for u and v. Numerical schemes for multi-dimensional cases may for example be found in Kloeden and Platen (1992).

4.6.6 Discretized system

For the numerical solution Y of equation (4.2), a discretization procedure has to be implemented. For a finite time increment τ, the basic version is the Euler-Maruyama approximation, which can be expressed as

$$Y_{n+1} = Y_n + m[Y_n]\tau + q\,\Delta\hat{W}, \tag{4.18}$$

as described in section 4.6.5. As discussed by Naess and Moe (2000), to achieve higher numerical accuracy it is advantageous to replace the Euler-Maruyama approximation with the Runge-Kutta-Maruyama approximation. Considering only the deterministic part of the SDE (4.2), equation (4.18) reduces to the Euler approximation $Y_{n+1} = Y_n + m[Y_n]\tau$. As is well known, this approximation is only accurate to order $\mathcal{O}(\tau^2)$. To improve the accuracy of the discretization process in following the evolution in time of the deterministic part of the system, a 4th order Runge-Kutta approximation is implemented, which is accurate to order $\mathcal{O}(\tau^5)$. This amounts to replacing the function $m[Y_n]\tau$ by the corresponding Runge-Kutta approximation, $r[Y_n] = (r_1[Y_n], r_2[Y_n], r_3[Y_n])^T$ say. The explicit expression for $r[Y_n]$ will not be given here since the procedure to obtain it is described in any elementary book on numerical methods, e.g. Abramowitz and Stegun (1972). Equation (4.15) will therefore be replaced by what will be referred to as the Runge-Kutta-Maruyama (RKM) approximation

$$Y_{n+1} = Y_n + r[Y_n] + v\,\Delta\hat{W}_n. \tag{4.19}$$

The corresponding TPD for the RKM approximation in equation (4.19), will now become

$$p(x_n, t|x'_n, t') = \frac{1}{\sqrt{4\pi a\tau}}\exp\left(-\frac{[x_n - (x'_n + r(x'))]^2}{4a\tau}\right). \tag{4.20}$$

instead of the TPD found in equation (4.9).

The weak Taylor approximation of order $\beta = 2.0$ in equation (4.17) may equally be modified,

$$\begin{aligned} Y_{n+1} &= Y_n + u\,\Delta_n + v\,\Delta\hat{W}_n + \frac{1}{2}\,u'\,v\,\Delta\hat{W}_n\,\Delta_n + \frac{1}{2}\,u\,u'\,\Delta_n^2 \\ &= Y_n + r[Y_n] + \hat{v}\,\Delta\hat{W}_n, \end{aligned} \tag{4.21}$$

where

$$\hat{v} = v + \frac{1}{2}\,u'\,v\,\tau$$

is the updated noise term. The corresponding TPD for the weak Taylor approximation of order $\beta = 2.0$ found in equation (4.21) is

$$p(x_n, t|x'_n, t') = \frac{1}{\sqrt{2\pi\hat{v}^2}} \exp\left(-\frac{[x_n - (x'_n + r(x'))]^2}{2\hat{v}^2}\right), \tag{4.22}$$

and will be used in chapter 6.

4.6.7 The back-stepping procedure

The integral of equation (4.8) and equation (4.10) is supposed to be over $\mathbb{R}^+ = [0, \infty\rangle$. Since this numerically is not possible, we have to integrate a certain part $\Gamma \in \mathbb{R}^+$. In this thesis two different integration schemes have been developed, depending on whether or not an exact or an approximate TPD was used. Since the integral is to be found in the previous time-step, the first problem is to find *where* to integrate. Secondly, x' has to be found.

$x'_i, i = 1, \ldots, n$ are found using a back-stepping procedure. Using an Euler-Maruyama approximation for the discretized system, we find the first $n-1$ unknown solving the equations

$$x_i - (x'_i + m_i(x')\tau) = 0, \quad i = 1, \ldots, n-1. \tag{4.23}$$

For a more accurate calculation of $x'_i, i = 1, \ldots, n$, it is possible, -as discussed in section 4.6.6, to replace the equations (4.23) by a 4th order Runge-Kutta scheme,

$$x_i - r(x'_i, \tau) = 0, \quad i = 1, \ldots, n-1,$$

giving precise values of $x'_i, i = 1, \ldots, n-1$. In addition, the last variable x'_n has to be found.

Using an exact TPD, it is seen from equation (4.10), that x_n has to be chosen for all positive x'_n. Hence, the integration area is $\Gamma = [0, s]$, where s is a suitable large number.

The integral in equation (4.8) is build up by multiplying the known TPD $p(x', t'|x_0, t_0)$ with a Gaussian TPD, $p(x, t|x', t')$. Since most of the probability mass of the latter TPD is centred around its mean value, we assume that the product of these two TPDs is small

outside a certain range r, say six times the standard deviation. We choose an interval around x_n, $[x_n - r, x_n + r] = [x_{n1}, x_{n2}]$. Now the back-stepping procedure using a 4th order backward Runge-Kutta scheme on x_{n1} and x_{n2} provide us with two points at the previous time, x'_{n1} and x'_{n2}. Hence, the integral area is $\Gamma = [x'_{n1}, x'_{n2}]$.

In order for the backward RK4 scheme to work properly, singularities giving large derivatives throwing x'_i far away from x_i have to be avoided. The Rayleigh process in equation (2.29) has a singularity at $R = 0$. Hence, calculation of RK4 steps close to $R = 0$ has to be done with great care. This can be done in different ways, but in this thesis two different approaches have been chosen. The first approach is using a uniform grid for x_n, and adapting the τ to the back-stepping. The advantage is that a uniform grid may be applied, but τ is now dependent on how many grid points you use. More grid points implies smaller τ. The second approach is using a general grid, making sure the x_{n1} may withstand a backward RK4. This allows a much larger τ, but may give bad interpolation values because the first and the second grid point is not as close as they should.

4.6.8 Numerical integration

Given an integral area $\Gamma = [x'_A, x'_B]$, one may choose an integrating technique which suits best to evaluate the integral in equations (4.8) and (4.10). Popular choices includes *Simpson's approximation*, the *Trapezodial approximation* and *Gauss quadrature*. Using e.g. a Simpson's approximation, $p(x, t|x', t')$ from equation (4.8) may be approximated

$$\begin{aligned} p(x, t|x_0, t_0) &= \int_\Gamma F(x')\, dx'_n \\ &= \frac{\Delta x_n}{3} \sum_{i=0}^{p} \gamma F(x'_{i;n}), \end{aligned} \tag{4.24}$$

where

$$\gamma = \begin{cases} 1 & , \quad i \in \{0, p\} \\ 4 & , \quad \mathrm{mod}\ (i, 2) = 1 \\ 2 & , \quad \mathrm{mod}\ (i, 2) = 0 \end{cases}$$

$$\Delta x'_n = \frac{x'_B - x'_A}{p}$$

$$x'_{i;n} = x'_A + i \cdot \Delta x'_n$$

and p is an even number.

4.6.9 Number of iterations

In practice, finding $p(x_N, t_N|x_0, t_0)$ in equation (4.1) is done repeatedly until the difference between two following TPDs are less than or equal to a certain number. (Johnsen, 1992) uses the criterion

$$\left| \frac{p(x_{m+1}, t_{m+1}|x_0, t_0) - p(x_m, t_m|x_0, t_0)}{p(x_m, t_m|x_0, t_0)} \cdot \tau \right| \approx 0.01 - 0.03, \tag{4.25}$$

where τ is the time increment, but warns that although the criterion gives a solution that normally is close to the stationary solution, it is not always the situation. Our experience of a *stopping time*, is that it depends heavily on the damping factor of each system, and that it is not as easy finding a suitable stopping time as the criterion in equation (4.25) suggests. A visual inspection in addition of the PDF or a marginal PDF, has been proven effective. By visual inspection, either in a normal or a logarithmic scale (or both), it is easily seen when the system *settles down*, approaching the stationary solution.

Chapter 5

Statistical response predictions

This chapter is based on the article Karlsen and Næss (2005), and deals with statistical response prediction for a nonlinearly moored large volume structure in random seas.

5.1 Introduction

For the design of floating structures to be used in the production of oil or gas offshore, it is mandatory to carry out a statistical response analysis to verify compliance with the design code provisions applicable to the location in question. Final design verification is very often accomplished by model testing. However, computational methods based on numerical models are now commonly applied during the first phases of the design process. Monte Carlo simulation methods is for example widely used for systems with significant nonlinearities. Its wide spread use has been facilitated by the rapid growth in computing power over the last decade. Nevertheless, for some applications it can still be computationally very heavy, if not prohibitive. One such application is the estimation of the extreme slow drift response of moored offshore structures. In this case a significant nonlinear element in the analysis is the slowly varying wave drift forces, which is due to the presence of a nonlinear transfer mechanism between the waves and the wave forces on the structure. The modelling of the resulting nonlinear wave forces is carried out to include second order effects. This means that the wave forces on the structure will include components at the difference frequency and the sum frequency of every pair of wave components at frequencies in the wave spectrum. This implies that the wave forces on the structure contain slowly varying and rapidly varying components in addition to linear force terms at the wave frequencies. This provides the force mechanism necessary to excite the slow drift motions of a moored large volume structure, which typically has a natural period in e.g. surge of 1-2 minutes. Clearly, there is no wave energy at these periods. Hence, according to linear theory there is no structural response. Since such response is observed, it points to the presence of nonlinear force mechanisms.

For structural response that can be modelled as linear, the calculation of the response statistics of moored large volume structures subjected to random waves has been described by Næss (1990), Naess and Ness (1992), Grime and Langley (2003) and Naess and Karlsen

(2004), to mention but a few. These papers contain extensive references to previously published work on this topic.

For nonlinear structures the paper by Naess and Johnsen (1993) describes the use of numerical path integration (PI) to calculate the response statistics. Lin and Yim (2004) also deals with stochastic characteristics of the surge response of a nonlinear singe-degree-of-freedom moored structure subjected to random wave exitations using PI. The results were good, although the forces were modelled differently than in this thesis. PI is based on the theory of Markov diffusion processes. The application of the theory of Markov processes to estimate the response statistics of offshore structures was pioneered by Roberts (1981). He used this theory to investigate the slowly varying motions of nonlinearly moored floating vessels subjected to random waves. The problem was formulated in terms of a three-dimensional Markov vector process. The joint PDF of this vector process satisfies a Fokker-Planck equation, but no attempt was made to solve this equation. Instead, the problem was simplified by assuming that the slow drift forces could be approximated by a Gaussian white noise process for small damping. As shown by Naess and Johnsen (1993), this assumption cannot be justified in general, especially if large or extreme responses are to be estimated. Early efforts to solve the Fokker-Planck equation associated with a three-dimensional Markov process similar to the one formulated by Roberts (1981) using a Galerkin technique may be noted, cf. Marthinsen (1987). However, the obtained results were rather of an indicative nature since it was very hard to assess their accuracy.

In this chapter we shall apply the PI method to study the response statistics of the slow drift motions of a moored large volume structure intended for oil production in deep waters. So in determining the response of the system due to a randomly applied force, we shall obviously not expect to know it in any greater detail than in which we can describe the excitation. Our aim in determining the response of a system due to random loading, is therefore to be able to specify the probability density of the response, when the corresponding properties of the excitation are known, i.e. the wave spectrum.

5.2 The dynamic model

A typical equation of motion may be written as

$$M\ddot{Z}(t) + g\left[D(t), \dot{Z}(t)\right] + h\left[Z(t)\right] = F(t), \tag{5.1}$$

where $Z(t)$ denotes the surge displacement, M is the mass of the structure and may include added mass, $g[\cdot]$ denotes a nonlinear, time-variant damping term, $F(t)$ is the wave-drift excitation force, e.g. in surge, and $h[\cdot]$ is a nonlinear restoring force of the mooring system.

5.2.1 Wave drift excitation

A significant nonlinear element in the analysis is the slowly varying wave drift forces, which is due to the presence of a nonlinear transfer mechanism between the waves and the wave forces on the structure. An example, the Morison's equation (Donley and Spanos, 1990; Roberts and Spanos, 1990; Vinje, 1980),

$$F(t) = \frac{C_M \rho \pi d^2}{4} \frac{dU(t)}{dt} + \frac{C_D \rho D}{2} U(t)|U(t)|, \tag{5.2}$$

was introduced by Morison *et.al.* in 1950, and show a non-linear expression of the hydrodynamic forces on a circular cylinder in regular waves. Here C_M and C_D denotes the inertia and drag coefficients, ρ is the density of water, d is the pile diameter, and $U(t)$ is the particle velocity in the direction of the wave travel.

Assume that the ocean surface elevation can be modelled as a zero-mean, stationary Gaussian process. On the basis of this assumption it has been shown (Næss, 1990) that the commonly accepted model for the wave drift excitation force in long-crested or short-crested random seas can be expressed as follows. Let $F(t)$ denote the wave drift force in a given direction, e.g. surge, on a given large volume structure subjected to a random seaway. Then $F(t)$ can be represented by the relation

$$F(t) = \sum_{j=1}^{N} \lambda_j \left\{ \bar{W}_{2j-1}(t)^2 + \bar{W}_{2j}(t)^2 \right\}, \tag{5.3}$$

where the λ_j are the eigenvalues of a matrix G, which for the long-crested seas case is given in terms of the (one-sided) wave elevation spectrum $S_X(\omega)$, and the so-called quadratic transfer function $\hat{K}_2(\omega, \omega')$, which characterises the wave drift force. Specifically, for the (equidistant) discretization $0 < \omega_1 < \ldots < \omega_N$ of the frequency axis ($\Delta\omega = \omega_j - \omega_{j-1}$):

$$G = (G_{jk}) = \left(\frac{1}{2} \sqrt{S_X(\omega_j)\, S_X(\omega_k)}\, \Delta\omega\, \hat{K}_2(\omega_j, -\omega_k) \right) \tag{5.4}$$

Each $\bar{W}_j(t)$ is a stationary Gaussian N(0,1)-process determined by the corresponding eigenvector $v_j = (v_j(\omega_1), \ldots, v_j(\omega_N))^\top$ of the same matrix. In particular, the spectral density $S_j(\omega)$ of $\bar{W}_j(t)$ is given as $S_{2j-1}(\omega_k) = S_{2j}(\omega_k) = |v_j(\omega_k)|^2$. The processes $\bar{W}_j(t)$ are constructed in such a way that $\bar{W}_{2j-1}(t)$ and $\bar{W}_{2j}(t)$ are Hilbert transform pairs for each j, as described in section 3.2. Thus, $F(t)$ can be expressed as

$$F(t) = \sum_{j=1}^{N} \lambda_j\, R_j(t)^2,$$

where $R_j(t) = \{\bar{W}_{2j-1}(t)^2 + \bar{W}_{2j}(t)^2\}^{1/2}$ is a Rayleigh process. For more information on these points, the reader is referred to Næss (1990).

For many structures, it turns out that a good approximation to $F(t)$ is obtained by retaining only the first term on the rhs of equation (5.3), and this is also the case for the

example structure studied in this chapter. It has been assumed here that the eigenvalues have been ordered so that $\lambda_1 > |\lambda_2| > \ldots$. Hence, we shall adopt the approximation

$$F(t) = \overline{\mu} + \mu\, R(t)^2\,, \tag{5.5}$$

where $R(t) = R_1(t)$ and where we have introduced the two parameters $\overline{\mu}$ and μ in order to obtain correct mean value and variance. It can be shown (Næss, 1985) that

$$\mathrm{E}[F(t)] = 2\sum_{j=1}^{N} \lambda_j\,,$$
$$\mathrm{Var}[F(t)] = 4\sum_{j=1}^{N} \lambda_j^2\,,$$

which leads to the requirement

$$\overline{\mu} + 2\mu = 2\sum_{j=1}^{N} \lambda_j\,,$$
$$\mu^2 = \sum_{j=1}^{N} \lambda_j^2\,.$$

According to Stratonovich (1963) the Rayleigh process $R(t)$ can be described by an Itô stochastic differential equation (SDE), that is, $R(t)$ is a Markovian Rayleigh process if

$$S_1(\omega) = S_2(\omega) = \frac{a}{\pi}\left(\frac{1}{(\omega-\omega_q)^2} + \frac{1}{(\omega+\omega_q)^2}\right) \tag{5.6}$$

where a is a positive constant, and ω_q is a suitably chosen frequency. In the section on numerical results it will be shown that this equation is satisfied to a fair degree. By adopting equation (5.6), $R(t)$ satisfies the following SDE

$$dR(t) = -a\left(R(t) - \frac{1}{R(t)}\right)\,dt + \sqrt{2a}\,dW(t) \tag{5.7}$$

where $W(t)$ is a Wiener process, cf. Wong and Hajek (1985). Remembering that the derivative of a Wiener process is a mathematically construction (section 2.10), we in all simplicity write equation (5.7) in the following manner

$$\frac{dR(t)}{dt} = a\left(\frac{1}{R(t)} - R(t)\right) + \sqrt{2a}\,N(t), \tag{5.8}$$

where

$$N(t) = \frac{dW}{dt}$$

is understood as Gaussian white noise.

5.2.2 Damping term

Damping forces are modelled in different ways. The easiest way is stochastic linearization, as done in chapter 3, assuming that the damping is proportional to the speed of the structure, i.e.

$$g\left[D(t), \dot{Z}(t)\right] = D\dot{Z}(t), \tag{5.9}$$

where D is a constant. However, this might be a crude simplification of the *true* behaviour. In the Morison's equation (5.2) for example, the damping force is quadratic. Another equation of motion

$$\ddot{\Phi} + \left(\beta + n_1|\dot{\Phi}|\right)\dot{\Phi} + \left(\omega_n^2 + n_2\Phi^2\right)\Phi = b_\Phi M(t), \tag{5.10}$$

also describes how the damping term is non-linear. Here Φ is a roll angle for a ship rolling in irregular beam waves for small to moderate angle of roll ($|\Phi| \leq 35°$), $M(t)$ is the roll excitation moment, β and n_1 are the linear and quadratic damping factors, respectively, ω_n denotes the undamped natural frequency of roll, n_2 is a non-linear stiffness factor, and b_Φ is the inverse of a total, effective roll inertia of the ship. Assuming a linear damping term, as discussed in Roberts and Spanos (1990), may not always be a good description of the motion.

Due to strong coupling between the mean wave-drift force and mean-drift damping coefficient in surge (Aanesland et al., 1990), an approximation of the damping is assumed

$$g\left[D(t), \dot{Z}(t)\right] = c_1 + c_2 F(t),$$

where c_1, c_2 are constants chosen to obtain the correct mean value and standard deviation of the wave drift damping, and $F(t)$ is the wave-drift force. In Naess and Johnsen (1993), $c_1 = 0$ is assumed, making a further simplification.

As mentioned in Naess and Johnsen (1993), due to strong similarity between $D(t)$ and $F(t)$, one may assume that the damping term D in equation (5.9) is

$$D(t) = \eta S^2(t). \tag{5.11}$$

Here $S(t)$ is a Markov-Rayleigh process and η is a mean damping parameter. To provide coupling between the force and the damping, the SDE for $S(t)$ is written

$$S(t) = b\left\{\frac{1}{S(t)} - S(t)\right\} + \sqrt{2b}\left\{\beta N(t) + \sqrt{1-\beta^2}\tilde{N}(t)\right\} \tag{5.12}$$

where $\tilde{N}(t)$ are standard Gaussian noise, $N(t)$ is the same Gaussian white noise process as in equation (5.8), b is some positive constant, and $0 \leq \beta \leq 1$. Varying degree of statistical dependence between damping and force result as β increases from 0 to 1. For $\beta = 0$, $D(t)$ and $F(t)$ are statistically independent.

In the main model, described in section 5.5, the damping is assumed linear, in lack of more precise measurements.

5.2.3 Restoring force

The restoring force is usually described as a polynomial,

$$h[Z(t)] = \sum_{i=1}^{N} a_i Z(t)^i, \tag{5.13}$$

where a_i are constants. A constant term in equation (5.13), $a_0 \neq 0$, assuming a restoring force subjected when the system is at a point of equilibrium, would not be physically correct. Although, when $N = 1$, approximating the restoring force with a linear function, one usually need a constant term not equal to zero. A restriction, $h[-Z(t)] = -h[Z(t)]$, due to the direction of the force, is usually added.

There are a number of applications where the restoring force is assumed to be linear, i.e. simple spring examples with small excursions. Examples of non-linear restoring forces are for example seen in equation (5.10) and also for the Duffing oscillators described in Roberts (1983),

$$\ddot{y} + 2\xi\omega_0\dot{y} + \omega_0^2 y(1 + \rho_3 y^2) = f(t).$$

Here $y(t)$ is the displacement, ξ is a non-dimensional linear damping parameter, ω_0 is the natural frequency of the system, ρ_3 is a cubic stiffness factor, and $f(t)$ is some force driving the system.

In the main model described in section 5.5, the restoring force assumes both linear and quadratic terms.

5.3 A numerical solution to the Rayleigh process

The Rayleigh process from equation (5.8) is discussed theoretically in section 2.14.2 and section 2.14.3. An effort to achieve a stationary PDF using the PI-technique and an approximate TPD found in equation (4.20), has to be done carefully. The presence of numerical errors in the PDF was noted in Johnsen (1992), and the reason is that equation (5.8) has a singularity for $R = 0$. If measures not are taken, the error in both the approximate and the exact TPD near zero becomes large, and spreads into the numerical solution when propagating forward in time.

Equation (5.8) has a corresponding Fokker-Planck, and 4 stationary solutions are presented in Figure 5.1; the theoretical solution from equation (2.31), the solution found using a Monte Carlo simulation, the solution using the PI technique and the exact TPD from equation (4.6), and the solution using the PI technique and the approximate TPD using a Runge-Kutta-Maruyama approximation from equation (4.20).

As illustrated, the PI technique works superb when using an exact TPD, even with few grid points ($n = 51$) in the R-variable and few integrating points ($p = 41$). We can hardly distinguish it from the exact one, -even in the logarithmic plot of Figure 5.2. Increasing n and p, the two graphs can be shown to be almost identical. Comparing the exact solution

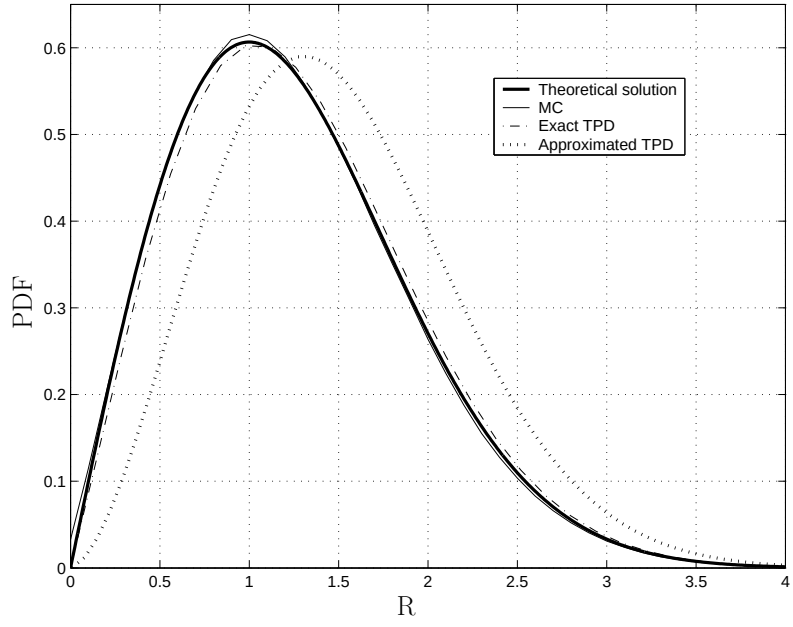

Figure 5.1: Stationary solutions of the Rayleigh process .

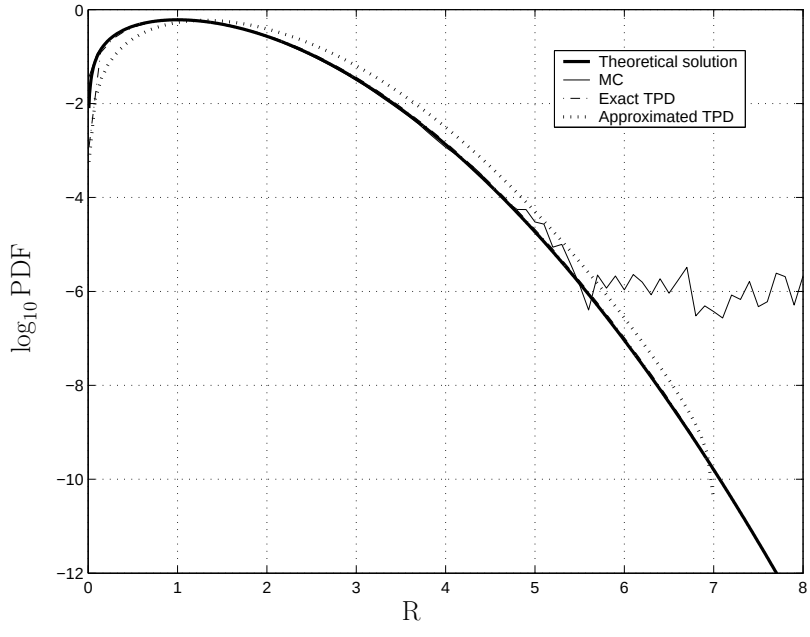

Figure 5.2: Stationary solutions of the Rayleigh process, logarithmic scale.

with the Monte Carlo simulation, two differences is spotted. In Figure 5.1 we see that the MC solution overestimates the PDF close to $R = 1$. Secondly, as seen in Figure 5.2, the MC simulation has problems achieving good results for low probabilities. PI provides good estimates also of the tails of the PDF. That is a quality we might use calculating upcrossing frequencies. The PI technique using an approximate TPD does not perform well. The approximate TPD is not well suited for this problem, and may not be used in

the further calculations.

One huge advantage using an exact TPD, is that the time-step $\tau > 0$ may be chosen freely. However, numerically we run into problems evaluating values of the modified Bessel function. The evaluation of the function are based on different series expansions depending on the input value, and may be found in e.g. Abramowitz and Stegun (1972). However, inputs above 1300 are not possible to calculate numerically.

Studying the theoretical solution from equation (2.31), it is obvious that R and R' may be chosen less than 7, since the PDF gives a probability around 10^{-10} and is low enough for most applications. Assuming $R \leq 7$, $R' \leq 7$, $\kappa = 1$, and the numerical boundary of the input in the modified Bessel function of equation (2.34) to be 1300, the equation

$$\frac{\exp(-a\tau)}{1-\exp(-2a\tau)}\frac{RR'}{\kappa} \leq 1300$$

leads to

$$\frac{\exp(-a\tau)}{1-\exp(-2a\tau)} \leq 26.53 = \gamma.$$

Now we get a restriction on τ,

$$\tau \geq \frac{1}{a}\ln\left(\frac{1+\sqrt{4\gamma^2+1}}{2\gamma}\right) \approx \frac{0.01885}{a}.$$

Choosing $a = 0.047$, -a number found in section 5.5, $\tau \geq 0.40$, which is a fairly large number. A large a-value gives the opportunity to choose a small τ, improving the time-stepping procedure, but at the cost of increase in CPU time.

5.4 Equation of motion, 3-D case

Combining the equations (5.1), (5.5) and (5.8), we now have 3 one-dimensional stochastic differential equations,

$$\begin{aligned}
\dot{x}_1(t) &= x_2(t) \\
\dot{x}_2(t) &= \frac{1}{M}\left(-g[x_1(t), x_2(t), x_3(t)] - h[x_1(t)] + \mu x_3^2(t) + \bar{\mu}\right) \\
\dot{x}_3(t) &= a\left(\frac{1}{x_3(t)} - x_3(t)\right) + \sqrt{2a}N(t),
\end{aligned} \tag{5.14}$$

where $[Z(t), \dot{Z}(t), R(t)]^\top = [x_1(t), x_2(t), x_3(t)]^\top$. The system of equations (5.14) may be written

$$\dot{x}(t) = m[x(t)] + \sqrt{2a}\bar{N}(t), \tag{5.15}$$

where

$$x(t) = [x_1(t), x_2(t), x_3(t)]^\top$$

$$m[x(t)] = \begin{bmatrix} m_1[x(t)] \\ m_2[x(t)] \\ m_3[x(t)] \end{bmatrix} = \begin{bmatrix} x_2(t) \\ \frac{1}{M}\left(-g[x_1(t), x_2(t), x_3(t)] - h[x_1(t)] + \mu x_3^2(t) + \bar{\mu}\right) \\ a\left(\frac{1}{x_3(t)} - x_3(t)\right) \end{bmatrix},$$

$$\bar{N}(t) = \begin{bmatrix} 0 \\ 0 \\ N(t) \end{bmatrix}.$$

We notice that equation (5.15) does not include time explicitly, indicating that this equation of motion may have a stationary PDF.

The theory for the Path Integration technique, presented in chapter 4, may now be applied on equation (5.15). As seen in section 5.3, an approximate TPD using the weak Runge-Kutta-Maruyama approximation of order $\beta = 1$ for the Rayleigh process, gives a wrong solution due to the singularity $R = 0$. And worse, the error close to $R = 0$ spreads into the numerical solution when propagating in time, -also in the 3D-case. So the exact TPD will be used in the rest of in this chapter. A further investigation in how to handle equation (5.15) using an approximate TPD, is found in chapter 6.

5.5 Numerical example

The example structure has the main particulars as listed in Table 5.1, where the natural period T_e should be construed as pertaining to small oscillations around the mean displacement position. The mass M includes added mass, and the wave drift damping is assumed constant corresponding to a damping ratio $\xi = 0.40$. A sketch of the deep floater is shown in Figure 5.3, while the mooring line arrangement is shown in Figure 5.4.

Table 5.1: The main particulars of the structure

Parameter	Value
M	$2.68 \cdot 10^8$ kg
D/M	0.0415 (s^{-1})
T_e	121 s

The wave condition used in the calculations is described by the following JONSWAP spectrum

$$S_X(\omega) = \alpha g^2 \omega^{-5} \exp\left\{-\frac{5}{4}\left(\frac{\omega_p}{\omega}\right)^4 + \ln\gamma \cdot \exp\left(-\frac{\left(\frac{\omega}{\omega_p} - 1\right)^2}{2\sigma^2}\right)\right\}$$

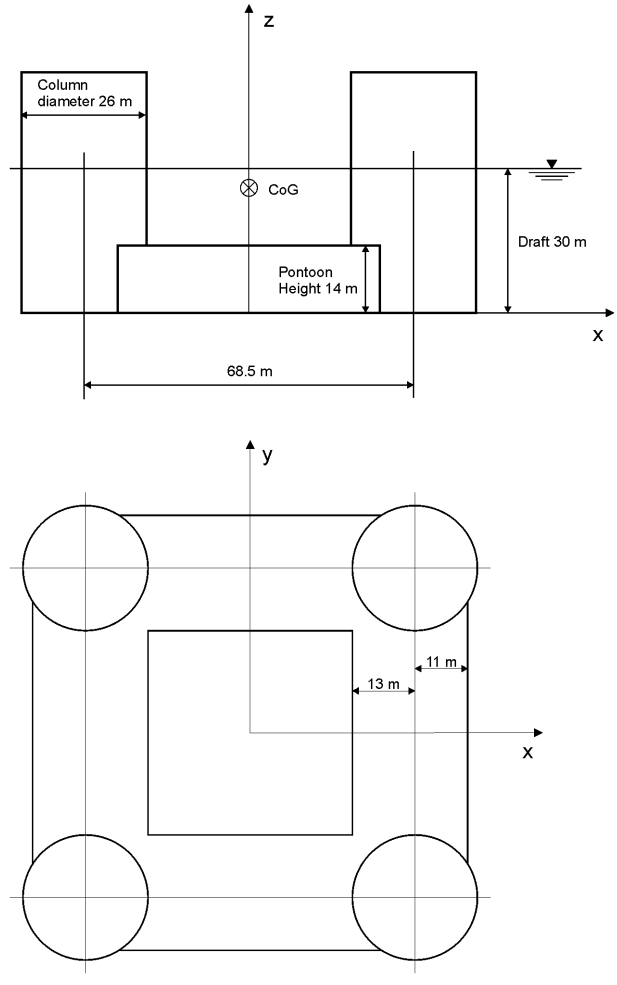

Figure 5.3: The deep floater (superstructure removed).

where

$$\alpha = 5.78 \left(\frac{H_s}{T_p^2}\right)^{2.036} (1 - 0.298 \ln \gamma)$$

$$\omega_p = \frac{2\pi}{T_p}$$

$$\sigma = \begin{cases} 0.07 & : \quad \omega \leq \omega_p \\ 0.09 & : \quad \omega > \omega_p \end{cases}$$

The specific parameter values chosen here are significant wave height $H_s = 14.8$ m, peak period $T_p = 14$ s and peakedness parameter $\gamma = 5.5$.

The quadratic transfer function for the slowly varying hydrodynamic forces are given by their diagonal values only, that is, only $\hat{K}_2(\omega_j, -\omega_j)$-values are available, which is typical

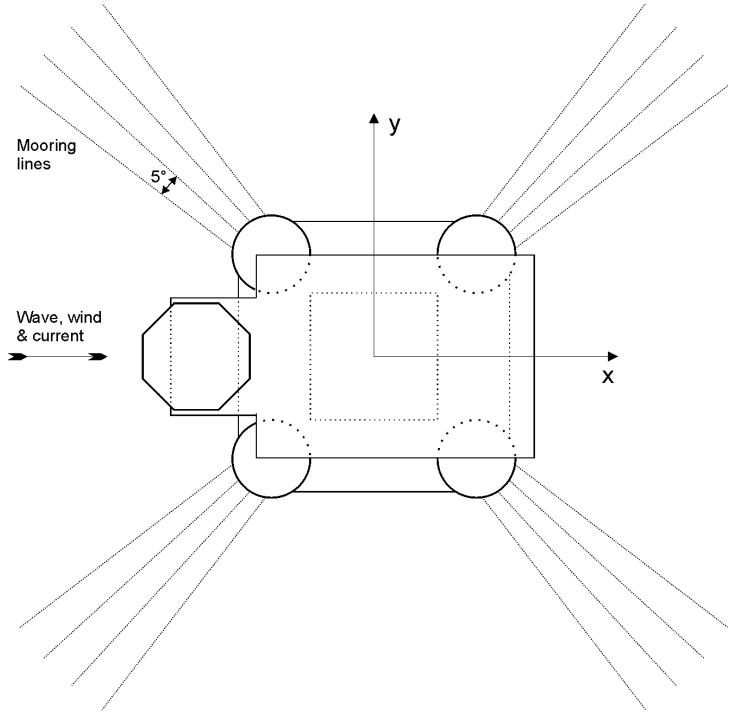

Figure 5.4: Sketch of the floater with mooring lines.

for most practical response calculations of this type. The reason for this is that the diagonal values of $\hat{K}_2$ can be calculated from the first order velocity potential of the wave field, which requires much less computational efforts than the off-diagonal terms, which involves the second order velocity potential. However, to calculate the eigenvalues and eigenvectors needed for our theory, it is necessary to populate the whole matrix $\hat{K}_2(\omega_j, -\omega_k)$. There are several possible ways of doing this. We shall adopt a version of what is known as the Newman approximation. Loosely speaking, the method chosen is such that the elements of the full matrix have the same value at positions along the orthogonals to the diagonal values. Originally, only 12 diagonal values for $\hat{K}_2(\omega_j, -\omega_j)$ were provided. This was augmented to 37 values by interpolation to get a better representation of the force process. The two quadratic transfer functions are shown in Figures 5.5 and 5.6.

A graphical representation of the G-matrix given by equation (5.4) is depicted in Figure 5.7.

It was mentioned earlier that the eigenvalues of the G-matrix usually showed a rapid decrease in absolute value. To demonstrate this for the present example structure, the first 5 eigenvalues are listed in Table 2.

Another element in the model building was the assumption that the spectral density $S_1(\omega_k) = |v_1(\omega_k)|^2$ of the eigen-process $W_1(t)$ was equal to the spectral density given by equation (5.6). To check this assumption, the result of fitting the last spectral density to the first is shown in Figure 5.8. The parameter values that gave the chosen fit were $a = 0.047$ and $\omega_q = 0.46$. The spectral density $|v_1(\omega_k)|^2$ has been plotted for both 12

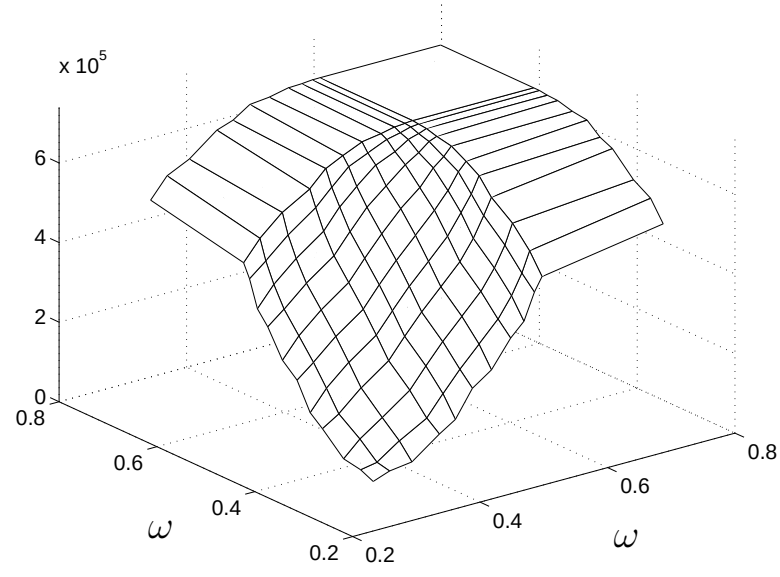

Figure 5.5: Quadratic transfer function $\hat{K}_2(\omega_j, -\omega_k)$ for 12 frequencies populated according to a Newman approximation.

Eigenvalue	Value	Relative value $\lvert\lambda_j\rvert/\lambda_1$
λ_1	2526035 N	1
λ_2	-510869 N	0.2022
λ_3	68455 N	0.0271
λ_4	-14661 N	0.0058
λ_5	11385 N	0.0045

Table 5.2: The first 5 eigenvalues of the G-matrix listed in decreasing absolute value

and 37 frequencies, and they are seen to be almost identical. The agreement obtained between $|v_1(\omega_k)|^2$ and the rhs of equation (5.6) is seen to be fairly good, especially since the important aspect of the fitting is to get the envelope process correct. Hence it is not crucial to have agreement across all frequencies, but rather at the most energetic portions of the spectral densities.

In the numerical calculations the effect of wind and current has been included as an added constant force term. According to this, the total force used in the calculations can be evaluated using equation (5.5) and written as

$$F(t) = 101.315 \cdot 10^5 + 25.782 \cdot 10^5 \, R(t)^2. \tag{5.16}$$

The effect of the nonlinear mooring system is taken into account by fitting the restoring force function $h[\cdot]$ to calculated values for the restoring force as a function of the platform displacement from the mean response position, which was calculated to be 27.5 m. The origin is at the equilibrium position when there is no external forcing. Figure 5.9 shows the calculated values for the restoring force together with the fitted curves. The calculation of

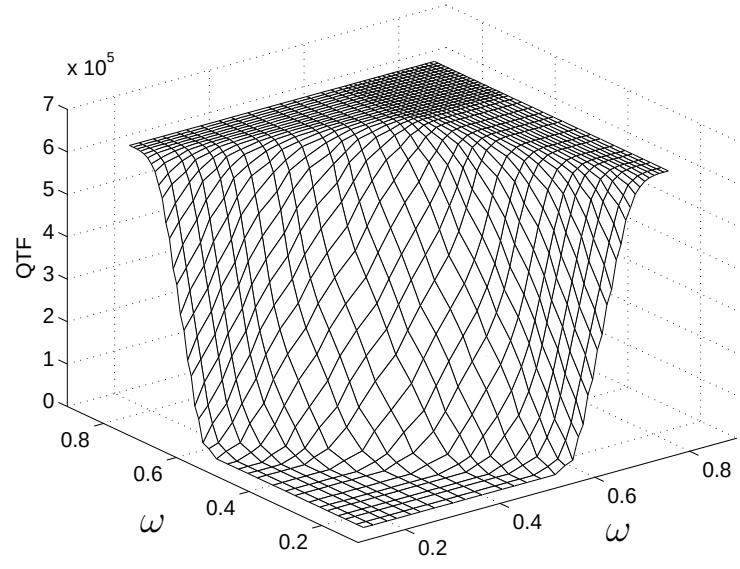

Figure 5.6: Quadratic transfer function $\hat{K}_2(\omega_j, -\omega_k)$ for 37 frequencies populated according to a Newman approximation.

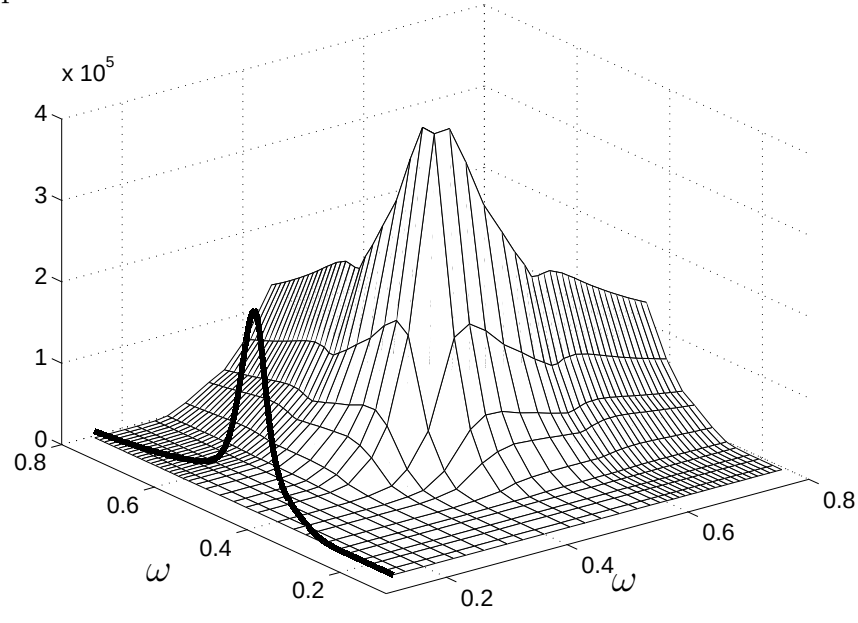

Figure 5.7: The G-matrix together with the corresponding JONSWAP wave spectrum.

the restoring forces was based on information about the mooring line characteristics and the mooring line configuration using a program (MIMOSA), and provided by Marintek. In Table 5.3 the fitted functions are presented.

The numerical input has then been fully specified, and the numerical PI procedures can now be applied. An exact TPD was used, and the interpolation in the 3 dimensional space was done by using cubic interpolation in the first two dimensions, and interpolating

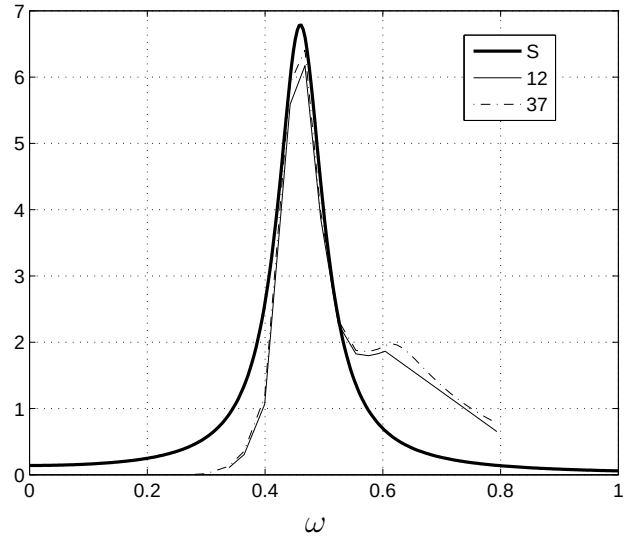

Figure 5.8: The spectral densities associated with the eigen-process $W_1(t)$.

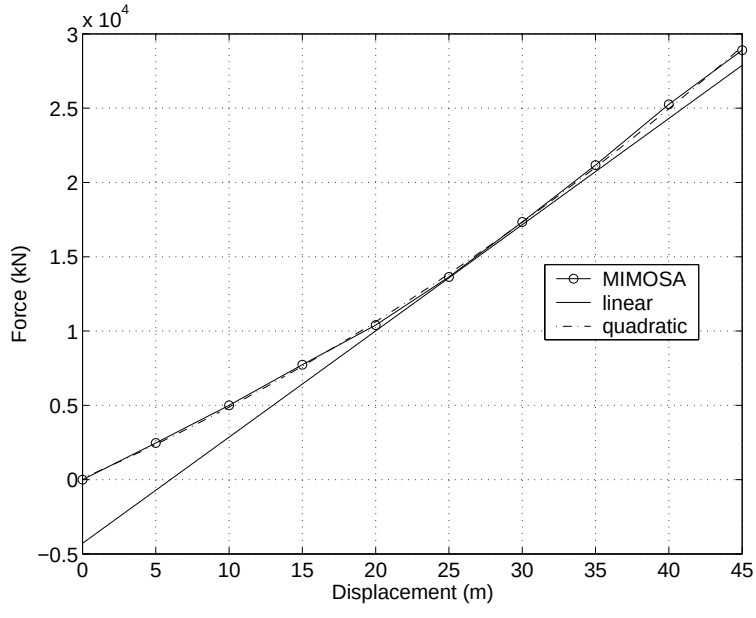

Figure 5.9: The static pull out characteristics of the mooring line system and fitted functions.

linearly in the last one. The grid was uniform in all directions.

Figures 5.10 – 5.13 shows the marginal PDF of the surge displacement response of the structure in head seas for the three fitted restoring force terms. In each figure is shown the effect of grid size in the calculation domain. It is seen that the number of grid points ($nx \times ny \times nz$) has significant influence on the results, especially for evaluating the top of the PDF. It is seen that in all three cases very good agreement with the Monte Carlo

Approx.	$h[z]$
Linear	$-1333091 + 64552z$
Quadratic	$90545 + 431970z + 4745z^2$

Table 5.3: The fitted restoring force term

results is obtained with $nx = ny = nz \geq 71$, although increasing the parameters to 101 gives almost perfect match. It may be noted that the tail behaviour of the marginal PDFs appears to be close to exponential, which reflects the fact that the nonlinearities in the equation of motion of the structure are quite weak. The effect of the nonlinear restoring force is seen by a smaller probability for the large excursions.

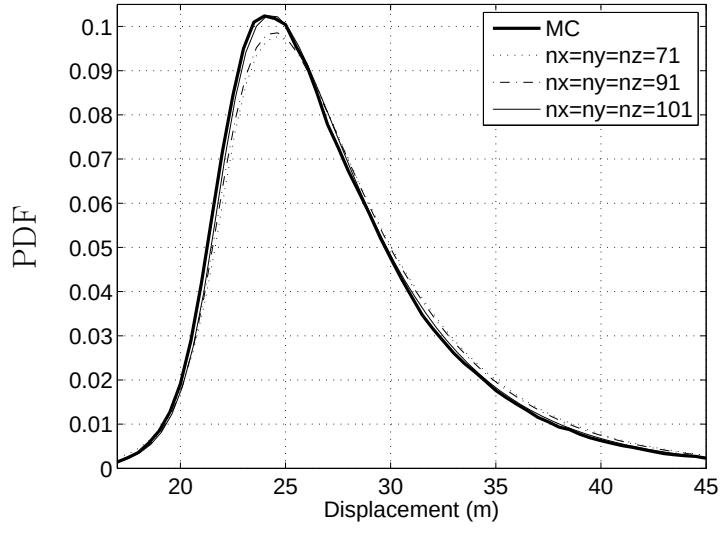

Figure 5.10: The marginal PDF of surge displacement for varying grid size for $h[z]$ linear compared with the results of Monte Carlo simulation.

In Figures 5.14 and 5.15 the marginal PDF of the surge velocity for $h[z]$ quadratic and the results of Monte Carlo simulation is plotted. It is seen that the PDF is almost symmetrical and exponential in the tails. This can again be explained by the weak nonlinearities. It is also worth noting that the sensitivity to the grid size is not as pronounced as for the displacement response.

The marginal PDF of the Rayleigh envelope process $R(t)$ is shown in Figures 5.16 and 5.17 for varying grid size, which is shown to have only a moderate effect on the results. The agreement with the exact solution is very good.

To check the sensitivity of the results to the value of the a-parameter, the results for the two values $a = 0.045$ and $a = 0.05$ were also calculated. The influence on the marginal PDF of surge displacement is shown in Figure 5.18. It is seen that there is negligible difference between the results.

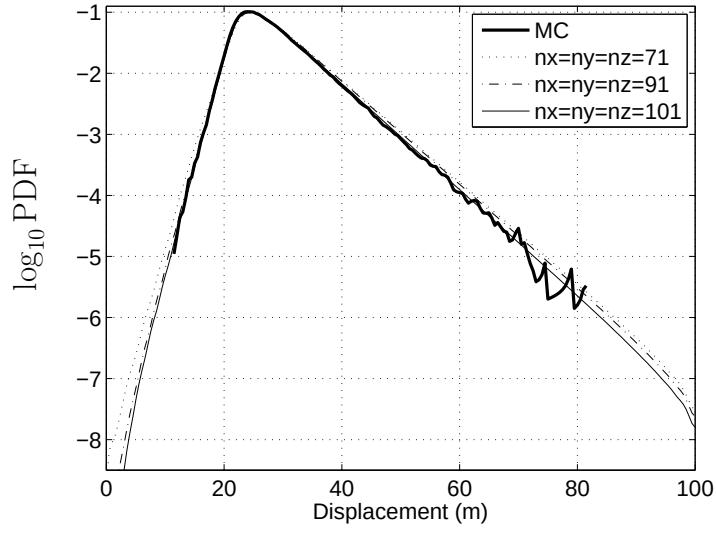

Figure 5.11: The marginal PDF of surge displacement for varying grid size for $h[z]$ linear compared with the results of Monte Carlo simulation, logarithmic scale.

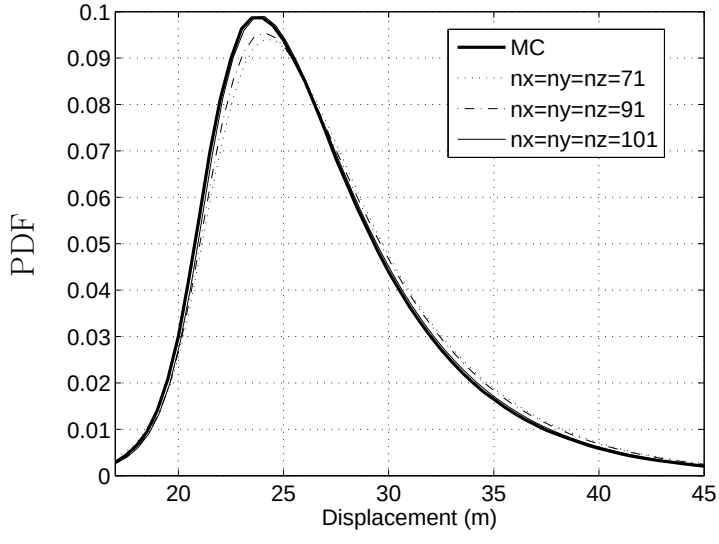

Figure 5.12: The marginal PDF of surge displacement for varying grid size for $h[z]$ quadratic compared with the results of Monte Carlo simulation.

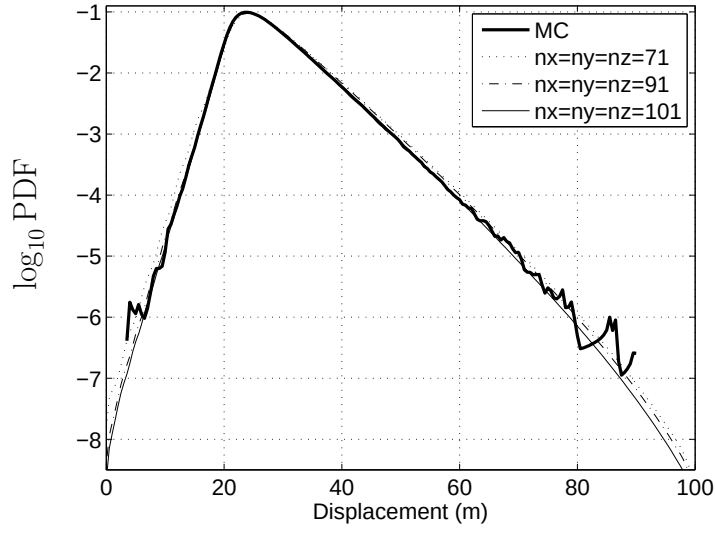

Figure 5.13: The marginal PDF of surge displacement for varying grid size for $h[z]$ quadratic compared with the results of Monte Carlo simulation, logarithmic scale.

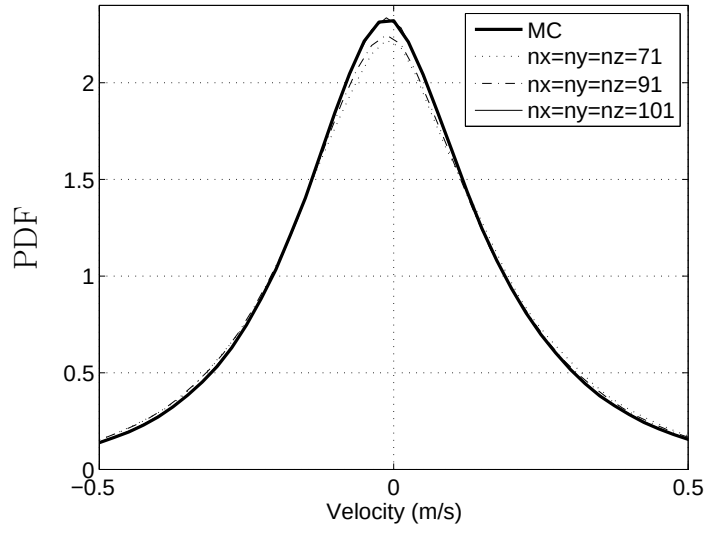

Figure 5.14: The marginal PDF of surge velocity for varying grid size for the quadratic approximation $h[z]$ compared with the results of Monte Carlo simulation.

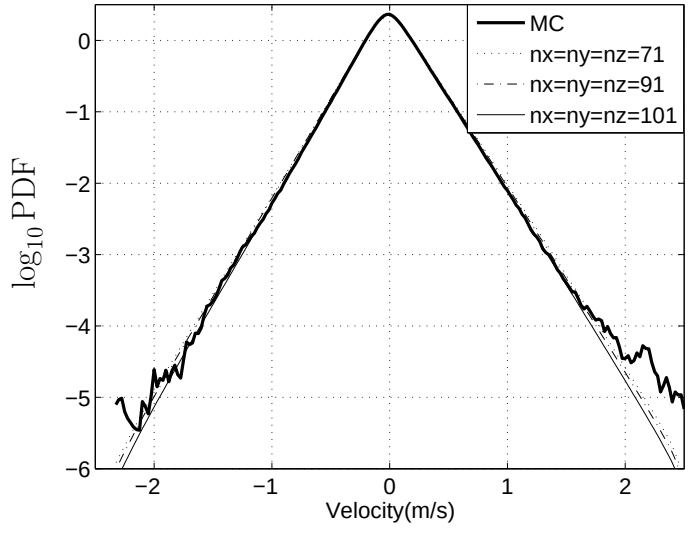

Figure 5.15: The marginal PDF of surge velocity for varying grid size for the quadratic approximation $h[z]$ compared with the results of Monte Carlo simulation, logarithmic scale.

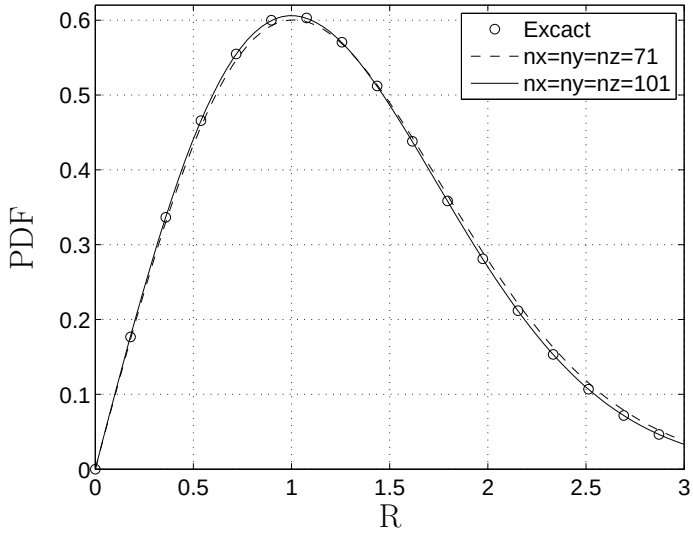

Figure 5.16: The marginal PDF of the Rayleigh process R(t) for varying grid size compared with the results of Monte Carlo simulation.

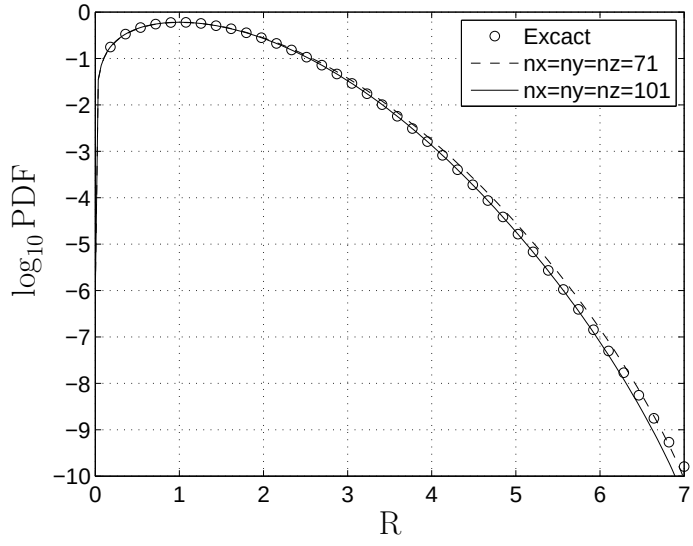

Figure 5.17: The marginal PDF of the Rayleigh process R(t) for varying grid size compared with the results of Monte Carlo simulation, logarithmic scale.

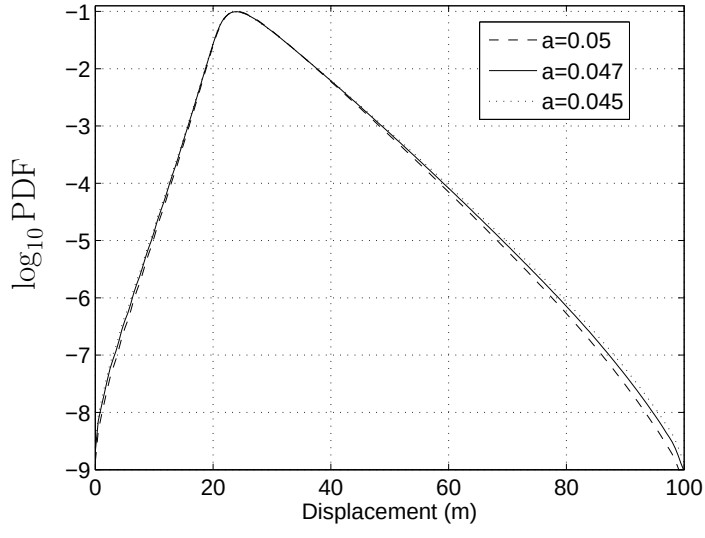

Figure 5.18: The marginal PDF of surge displacement for different values of the parameter a.

5.6 Mean upcrossing rate

A nice aspect of the PI is that the joint PDF of displacement and velocity $f_{Z\dot{Z}}(z,\dot{z})$ is available. This makes it possible to calculate the mean level upcrossing rate, which provides estimates of probabilities of exceedance for specified periods of time. Let $\nu_Z^+(\zeta)$ denote the mean rate of ζ-upcrossings by $Z(t)$. As mentioned in section 3.3, $\nu_Z^+(\zeta)$ is found by the Rice formula

$$\nu_Z^+(\zeta) = \int_0^\infty \dot{z} f_{Z\dot{Z}}(\zeta,\dot{z})\, d\dot{z}. \tag{5.17}$$

In Figure 5.19 the upcrossing frequency is plotted as a function of ζ. It is seen that a linear

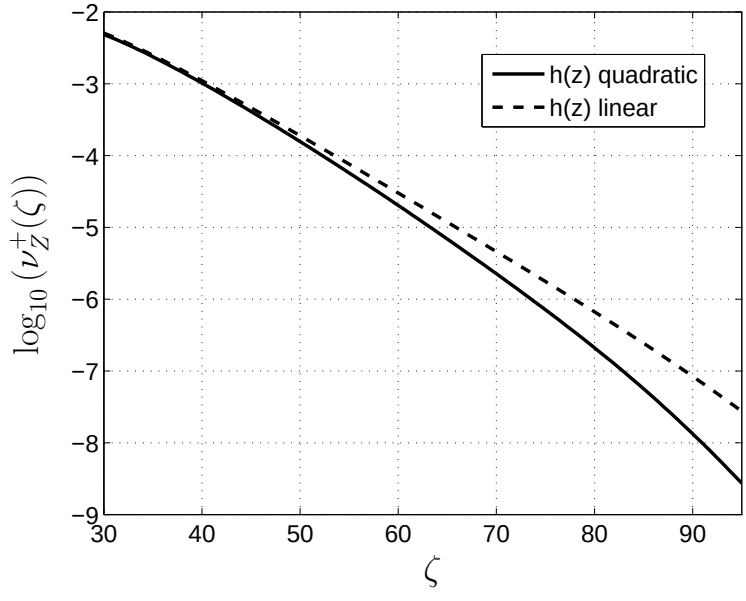

Figure 5.19: The upcrossing frequency for different approximations of the restoring force $h(z)$, logarithmic scale.

restoring force gives an exponential behaviour in the tail of the upcrossing frequency. It is also seen that introducing a non-linearity in the restoring force, the upcrossing frequency changes shape, and e.g. lower the upcrossing frequency by a factor 10 for $\zeta = 90$.

Let $\mathrm{P}_F(T) = \mathrm{P}_F(T;\zeta)$ denote the probability that $Z(t)$ exceeds the value ζ during a period of time of length T. Assuming that each upcrossing is independent of the previous one, and the process $Z(t)$ is not too narrow-banded, we may write

$$\mathrm{P}_F(T) = 1 - \exp(-\nu_Z^+(\zeta)T).$$

In Table 5.4 and 5.5 values of $\nu_Z^+(\zeta)$ and $\mathrm{P}_F(T)$ are listed for a set of levels ζ and for $T =$ 3, 6, 18 hours. In Figure 5.20 curves showing the exceedance probability $\mathrm{P}_F(T)$ for the case with the quadratic restoring force term are plotted.

ζ (m)	$\nu_Z^+(\zeta)$	$P_F(3)$	$P_F(6)$	$P_F(18)$
25.0	6.780E-03	1.0	1.0	1.0
30.0	5.062E-03	1.0	1.0	1.0
35.0	2.495E-03	1.0	1.0	1.0
40.0	1.100E-03	1.0	1.0	1.0
45.0	4.621E-04	0.9932	1.0	1.0
50.0	1.889E-04	0.8699	0.9831	1.0
55.0	7.582E-05	0.5590	0.8056	0.9926
60.0	3.005E-05	0.2771	0.4775	0.8573
65.0	1.179E-05	0.1195	0.2248	0.5342

Table 5.4: Upcrossing rates and exceedance probabilities for linear restoring force.

ζ (m)	$\nu_Z^+(\zeta)$	$P_F(3)$	$P_F(6)$	$P_F(18)$
25.0	6.725E-03	1.0	1.0	1.0
30.0	4.839E-03	1.0	1.0	1.0
35.0	2.371E-03	1.0	1.0	1.0
40.0	1.022E-03	1.0	1.0	1.0
45.0	4.102E-04	0.9881	0.9999	1.0
50.0	1.565E-04	0.8155	0.9660	1.0
55.0	5.726E-05	0.4612	0.7097	0.9755
60.0	2.018E-05	0.1958	0.3533	0.7296
65.0	6.870E-06	0.07151	0.1379	0.3593

Table 5.5: Upcrossing rates and exceedance probabilities for quadratic restoring force.

Let $M_Z(T)$ denote the maximum displacement, as done in section 3.8. The expected maximum displacement may be found using the formula

$$\mathrm{E}(M_Z(T)) = \int \mathrm{P}_F(T;\zeta)d\zeta = \int \left(1 - \exp\left(-\nu_Z^+ T\right)\right) d\zeta \,. \tag{5.18}$$

In our case the integration range is $[0, 100]$. Figure 5.21 presents curves showing the expected maximum displacement as a function of time for both linear and quadratic restoring forces. It is seen that using a linear approximation gives a significant larger expected maximum displacement than using a quadratic approximation, and the gap between the two graphs grows as time passes. This is due to the fact that non-linear restoring force becomes more vital as the displacement increase.

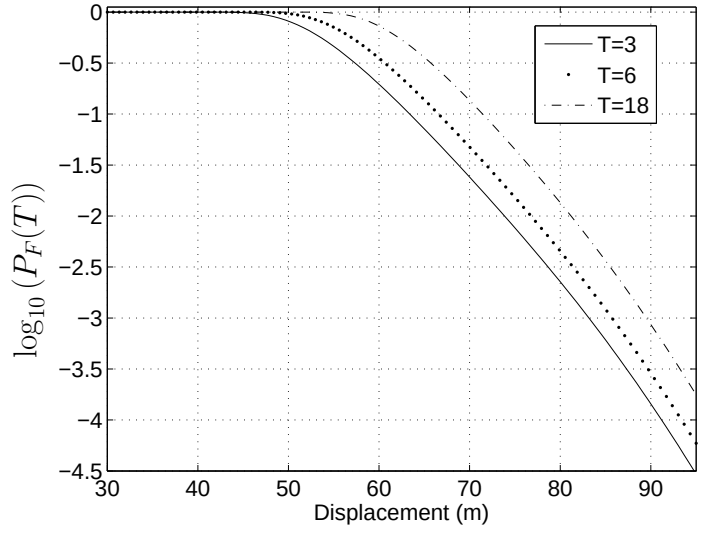

Figure 5.20: The exceedance probability as a function of the displacement response level for $T = 3$, 6, 18 hours, logarithmic scale.

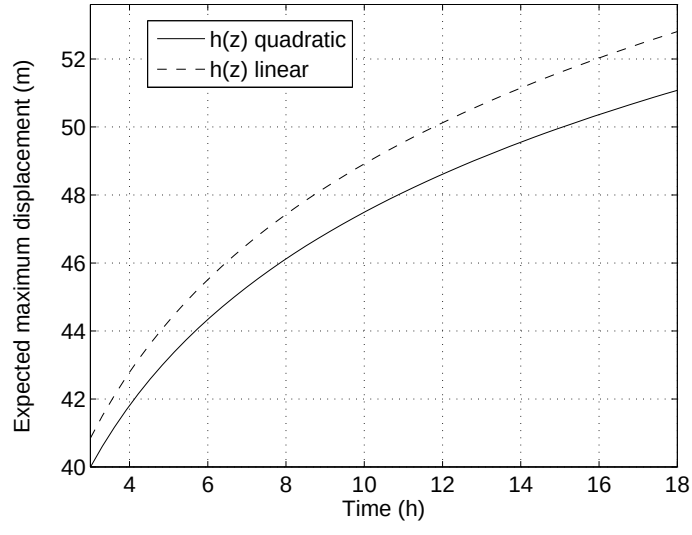

Figure 5.21: Expected maximum displacement as a function of time.

5.7 Comparing results from different techniques

Data used in the previous section were provided by Marintek, Trondheim. Marintek has made some calculations themselves, based on linearization techniques (MIMOSA), measurements from a basin, and time series. As seen in Table 5.6, our results using PI with a quadratic and linear restoring force, assuming an 18 hour storm, is compared with Mar-

	Marintek	PI Quadratic	PI Linear
Expected displacement	27.97	26.94	27.45
Standard deviation	4.93	5.45	5.49
Maximum displacement	54.49	51.08	52.80

Table 5.6: Comparing results from different techniques.

intek's achievements. Note that the maximum displacement using the PI technique is the expected maximum displacement based on equation (5.18). We observe that the results from PI using a linear restoring force provide good match with the time series from Marintek. The reason might be that Marintek base its calculations on a linear model. Figure 5.3 shows that a quadratic model is more likely to be a realistic representation of the restoring force than a linear one, suggesting that a linear approximation might over estimate the extreme values of the system.

The expected velocity, for both a quadratic or linear approximation of the restoring force, is of the order 10^{-4}. This indicates that the expected velocity is zero, giving the structure no off-drift. This is in agreement with the actual situation, -the platform is held by 16 mooring lines with anchors.

5.8 Empirical estimation of the upcrossing frequency

There are two alternative approaches of estimating the upcrossing frequency in addition to the PI technique described in the previous sections. One approach is to estimate the joint PDF $f_{X\dot{X}}(\cdot,\cdot)$ empirically from the time histories, and then use the Rice formula from equation (5.17) to calculate upcrossing frequencies. However, assuming the requisite ergodic properties of the response process, the upcrossing frequencies are more easily estimated from the ergodic mean value. That is, with probability one,

$$\nu_Z^+(\zeta) = \lim_{t\to\infty} \frac{1}{t}\, n^+(\zeta;t),$$

where $n^+(\zeta;t)$ denotes a realization of $N^+(\zeta;t)$, the rate of upcrossings of the level ζ by the random variable X. $n^+(\zeta;t)$ denotes the counted number of upcrossings of the level ζ during time t from a particular simulated time history. In practice, m time histories of a suitable, specified length, T say, are simulated. The appropriate ergodic mean value estimate of $\nu_Z^+(\zeta)$ is then

$$\hat{\nu}_Z^+(\zeta) = \frac{1}{mT}\sum_{j=1}^{m} n_j^+(\zeta;T),$$

where $n_j^+(\zeta;T)$ denotes the counted number of upcrossings of the level ζ by time history number j.

For a suitable number $m \geq 30$, and provided that T is sufficiently large, a good approximation of the 95% confidence interval for the value $\nu_Z^+(\zeta)$ can be obtained as

$\hat{\nu}_Z^+(\zeta) \pm 1.96\,\hat{s}(\zeta)/\sqrt{m}$, where the empirical standard deviation $\hat{s}(\zeta)$ is given as the positive root of the empirical variance,

$$\hat{s}(\zeta)^2 = \frac{1}{m-1}\sum_{j=1}^{m}\left(\frac{n_j^+(\zeta;T)}{T} - \hat{\nu}_Z^+(\zeta)\right)^2,$$

as described in most books regarding basic statistics, e.g. Walpole et al. (2002).

The forward time-stepping procedure was done using a 4th order Runge-Kutta scheme. Choosing a suitable time-step τ for the numerical scheme is always a challenge. If one choose τ too large, one may experience a too large value for the upcrossing frequency. Since the number of iterations $N = T/\tau$ for each time history, small values on τ gives longer CPU-time. In Figures 5.22 and 5.23 the empirical estimation of the upcrossing

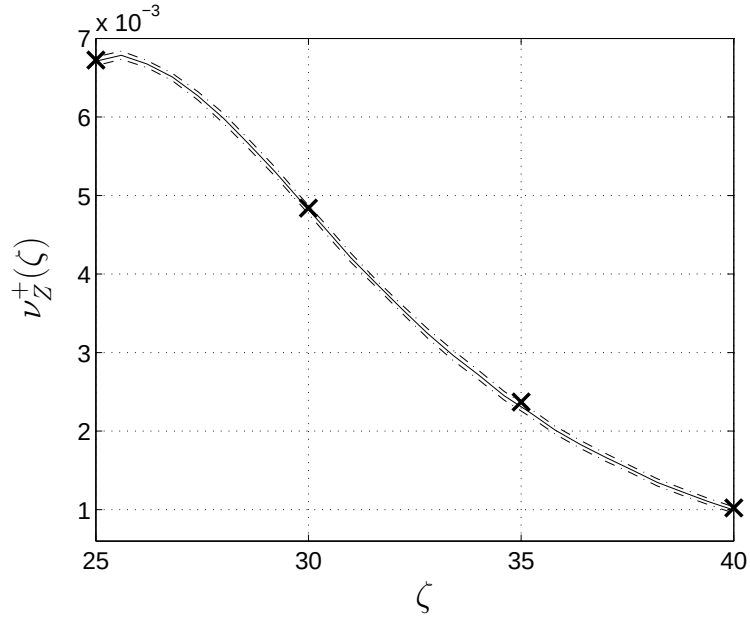

Figure 5.22: Empirically estimated values of the upcrossing frequency $\hat{\nu}_Z^+(\zeta)$(-), confidence interval $(-\cdot)$, and values found by a PI technique $(\times)$.

frequency $\hat{\nu}_Z^+(\zeta)$ as well as the 95% confidence interval, and the upcrossing frequency from a the PI technique, $\nu_Z^+(\zeta)$, are plotted. The main model from section 5.5 with a quadratic restoring force was used, as well as the values $T = 18\,\text{h}$ and $m = 30$. As seen, $\hat{\nu}_Z^+(\zeta)$ and $\nu_Z^+(\zeta)$ are almost identical for $\zeta \leq 60$. The strength of PI are seen for large values of ζ. The empirical estimation fails to get reasonable values, and the variance is seen to explode. However, as seen in Figure 5.19, the PI technique shows its strength, giving precise results for also large values of ζ.

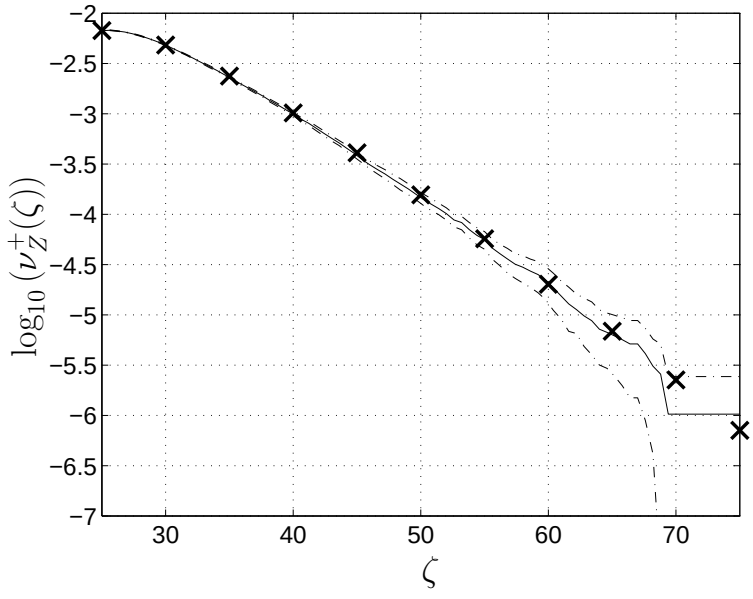

Figure 5.23: Empirically estimated values of the upcrossing frequency $\hat{\nu}_Z^+(\zeta)$(-), confidence interval $(-\cdot)$, and values found by a PI technique $(\times)$, logarithmic scale.

5.9 Case study: Strong non-linear restoring force and damping

In this section, an example of the robustness of the PI technique is demonstrated.

Again we study the dynamic model of equation (5.1). The damping term is a function of the velocity $\dot{Z}(t)$,

$$g\left[D(t), \dot{Z}(t)\right] \cdot M^{-1} = \beta\omega_0\zeta\dot{Z} + \kappa\dot{Z}|\dot{Z}|\,, \tag{5.19}$$

and the restoring force is a cubic polynomial of the displacement $Z(t)$,

$$h(Z) = 129706 + 417641Z + 558Z|Z| + 40Z^3.$$

Here M is the mass of the structure, ω_0 is the natural frequency, ζ is the damping ratio, $\beta \in [0, 2]$, and κ is a suitable constant. The cubic term in the restoring force is deliberately set large, and is not fully comparable with the original example structure presented in section 5.5. The damping term has been split up in a linear and a quadratic part, where the expectancy and variance are the same as in the linear case, providing us with a value of κ. The force is still approximated with the Rayleigh process of equation (5.16).

5.9.1 Linear damping term and strong restoring force

As a first case study, the variable β from equation (5.19) has been chosen equal to 2, so the system has linear damping. The restoring force is modelled as a cubic polynomial. As seen in Figures 5.24 – 5.29 the PI technique works superb, and provides estimates of the marginal PDFs very close to a Monte Carlo simulation. It also provides nice results for low probabilities, where the Monte Carlo simulation fails.

Compared with earlier results, we observe that the mean response position as well as the probability for large excursions from the mean response position, is lowered. This is in agreement with what one should expect. The strong restoring force now pulls the structure back harder when the displacement is large, compared to previous results using a linear or quadratic approximation of the restoring force. The marginal PDF of the velocity is almost similar to previous calculations, having an exponential behaviour.

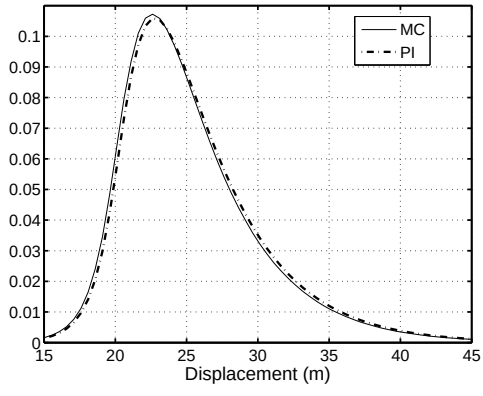

Figure 5.24: The marginal PDF of surge displacement for strong non-linear restoring force using a PI technique compared with the results of Monte Carlo simulation.

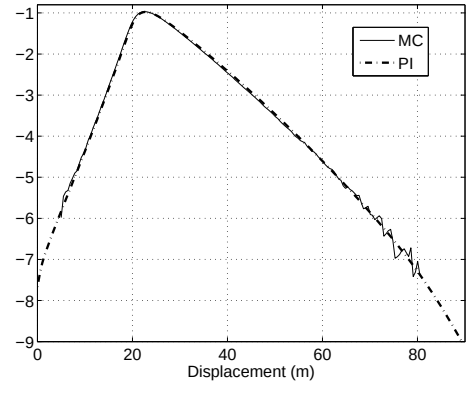

Figure 5.25: The marginal PDF of surge displacement for strong non-linear restoring force using a PI technique compared with the results of Monte Carlo simulation, logarithmic scale.

5.9.2 Non-linear damping term and strong restoring force

As a second case study, the variable β from equation (5.19) has been chosen equal to 1, balancing the damping on the linear and the non-linear term in some way. As seen in Figures 5.30 – 5.35 again the PI technique works superb, and provides estimates of the marginal PDFs very close to a Monte Carlo simulation. It also provides nice results for low probabilities, where the Monte Carlo simulation fails.

Compared to earlier results, we see that the non-linearities lower the probability for large deviations from the mean value both in the displacement and the velocity. This is in agreement with what one should expect. As seen in section 5.9.1, the cubic term of the restoring force pulls the structure back when the displacement is large. In addition, the

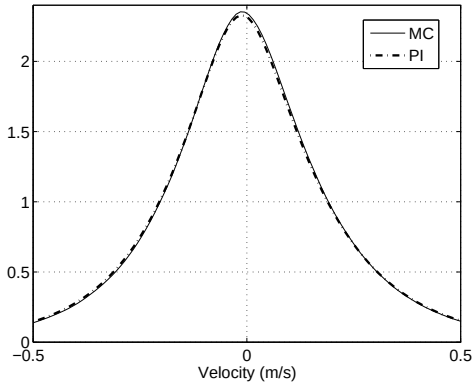

Figure 5.26: The marginal PDF of surge velocity for a strong restoring force using a PI technique compared with the results of Monte Carlo simulation.

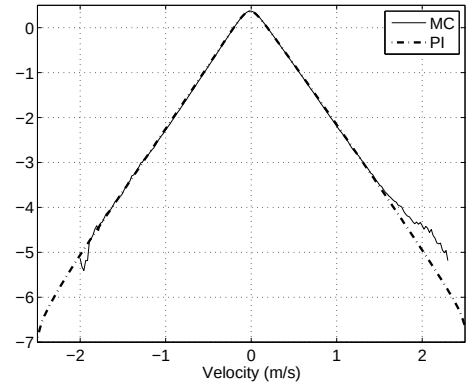

Figure 5.27: The marginal PDF of surge velocity for a strong restoring force using a PI technique compared with the results of Monte Carlo simulation, logarithmic scale.

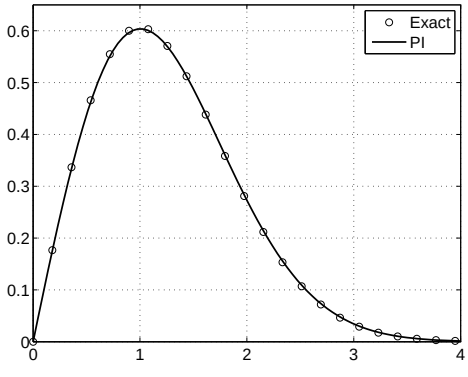

Figure 5.28: The marginal PDF of the Rayleigh process for a strong restoring force using a PI technique compared with the exact solution.

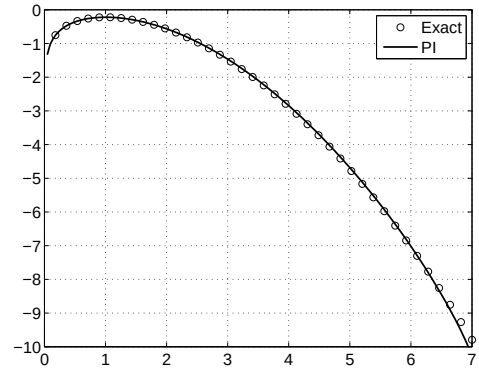

Figure 5.29: The marginal PDF of the Rayleigh process for a strong restoring force using a PI technique compared with the exact solution, logarithmic scale.

non-linear damping term slows the structure down when the speed is large. Compared to earlier results, the marginal PDF of the velocity of the structure now has a more Gaussian behaviour, with a large amount of probability mass centered around the origin.

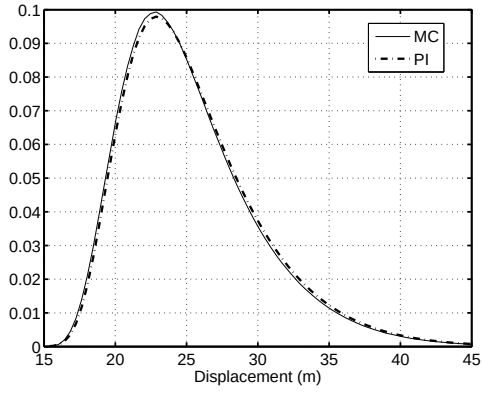

Figure 5.30: The marginal PDF of surge displacement for non-linear damping and strong restoring force using a PI technique compared with the results of Monte Carlo simulation.

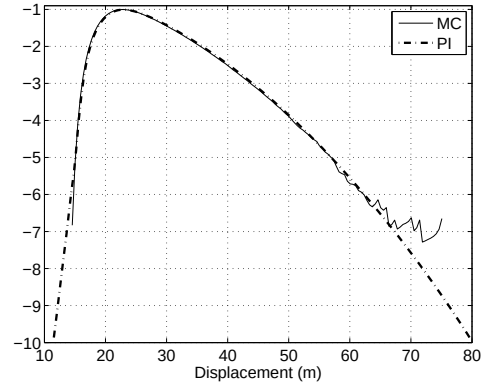

Figure 5.31: The marginal PDF of surge displacement for non-linear damping and strong restoring force using a PI technique compared with the results of Monte Carlo simulation, logarithmic scale.

5.9.3 Conclusion

The main objection in this section was to show that the PI technique works well also when strong non-linearities are introduced. This is a property highly appreciated, and the results presented shows that the PI technique provides good estimations of the PDF, also down to very low probabilities.

5.10 Numerical considerations and difficulties

Given a 3 dimensional SDE as in equation (5.15) and the theory for the PI technique, one have to decide 5 parameters when starting a numerical calculation; -the number of grid points nx, ny and nz in each dimension, how many integration points p needed for the integral from equation (4.24), and τ, the time-length we step forward. As mentioned in section 5.3, τ has to be chosen larger than 0.40, and although the TPD is exact, a large value on τ should give a poorer result than smaller ones. The cause of this is the back-stepping procedure, which is more precise for small time-steps than large ones. Choosing $\tau = 0.4$ gives 4 parameters to vary.

The size of the grid resolution and the number of integrating points clearly influence the CPU time for the program, so keeping them as small as possible is an advantage. However,

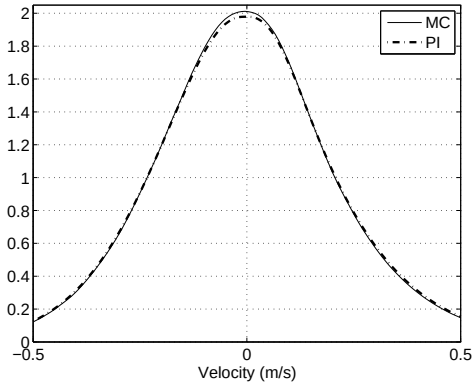

Figure 5.32: The marginal PDF of surge velocity for non-linear damping and strong non-linear restoring force using a PI technique compared with the results of Monte Carlo simulation.

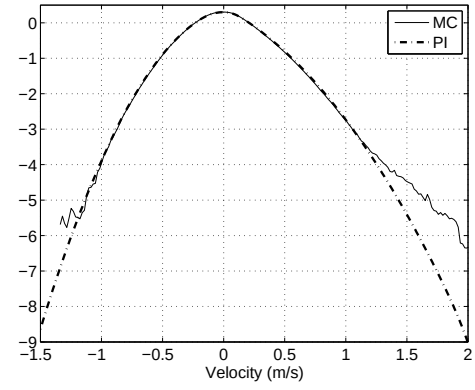

Figure 5.33: The marginal PDF of surge velocity for non-linear damping and strong non-linear restoring force using a PI technique compared with the results of Monte Carlo simulation, logarithmic scale.

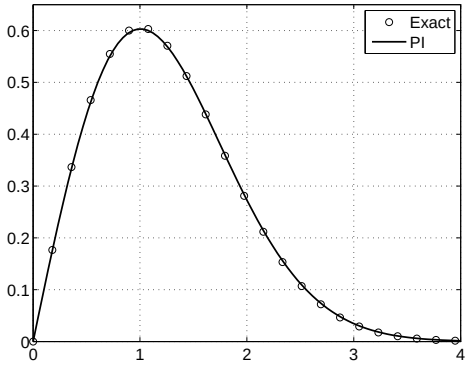

Figure 5.34: The marginal PDF of the Rayleigh process for non-linear damping and strong restoring force using a PI technique compared with the exact solution.

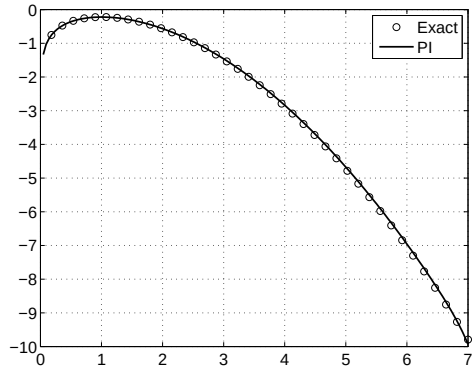

Figure 5.35: The marginal PDF of the Rayleigh process for non-linear damping and strong restoring force using a PI technique compared with the exact solution, logarithmic scale.

small values for the 4 parameters gives poorer results than large ones, so there is a fine line between CPU time and accuracy.

The most obvious way to keep the numerical costs down, and keeping the parameters fixed, is to start as close to the solution as possible. The starting probability can be a previously found PDF, either by a Monte Carlo method or an interpolated PDF found earlier with fewer grid points, or it could be a normal distribution with the expectation and covariance matrix found by a good guess (or a Monte Carlo method). A second strategy is keeping the parameters nx, ny, nz and p as small as possible, giving the optimal CPU time. This, of course, is a matter of testing, getting optimal parameters, and is highly dependent on the problem one study. A third strategy is to improve the integrating process, choosing e.g. a Simpson approximation instead of a midpoint approximation as described in section 4.6.8. This may both improve the result and keeping the value of p low. And last, but not least, making a fast program helps a lot. A lot of calculations may be done only once and stored for later use. The program may also be rewritten and run on parallel computers. This however, has not been studied.

5.11 Errors

Using a PI technique, 4 main types of errors occur,

1. Integration errors.
2. Interpolation errors.
3. Errors in handling the deterministic term of the SDE.
4. Errors in handling the stochastic term of the SDE.

Intergration errors occur when the integral of equation (4.10) has to be calculated, as discussed in section 4.6.8. An efficient integration technique as well as small partitions reduce this error.

Interpolation errors occur when we try to find the interpolated value $p(x', t'|x_0, t_0)$ of equation (4.7). In section 4.6.2, 4.6.3 and 4.6.4, different interpolation techniques have been discussed, and B-splines were chosen for their nice properties. High resolution of grid points also reduce this error.

Different ways of handling the deterministic term of the SDE have been discussed in section 4.6.7. The idea is to follow the dynamic in an efficient way. Clever numerical schemes includes the Runge-Kutta 4th order, and reduce the error compared to the basic Euler scheme. Small time-steps also provides better results.

In section 4.6.5, the stochastic term has been subjected to a closer scrutiny. Different numerical schemes handle the stochasticity better than other, reducing the numerical errors. Exact TPDs are optimal.

5.12 Equation of motion, 4-D case

As mentioned in section 5.2.2, strong coupling between the force and the damping has been observed. We now assume also the damping $g(\cdot)$ in equation (5.1) to be described as a Markov-Rayleigh process. We combine equations (5.1), (5.8), (5.11), and (5.12) as 4 one-dimensional stochastic differential equations, and write it as a system of equations,

$$x(t) = m[x(t)] + Q\bar{N}(t), \tag{5.20}$$

where

$$\begin{aligned}
x(t) &= [Z(t), \dot{Z}(t), R(t), S(t)]^\top = [x_1(t), x_2(t), x_3(t), x_4(t)]^\top \\
m[x(t)] &= \begin{bmatrix} m_1[x(t)] \\ m_2[x(t)] \\ m_3[x(t)] \\ m_4[x(t)] \end{bmatrix} = \begin{bmatrix} x_2(t) \\ \frac{1}{M}\left(-\eta x_4^2(t) - h[x_1(t)] + \mu x_3^2(t)\right) \\ a\left(x_3(t) - \frac{1}{x_3(t)}\right) \\ b\left(x_4(t) - \frac{1}{x_4(t)}\right) \end{bmatrix} \\
\bar{N}(t) &= \begin{bmatrix} N(t) \\ \tilde{N}(t) \end{bmatrix} \\
Q &= \begin{bmatrix} 0 & 0 \\ 0 & 0 \\ \sqrt{2a} & 0 \\ \sqrt{2b}\beta & \sqrt{2b}\sqrt{1-\beta^2} \end{bmatrix}.
\end{aligned}$$

Varying degree of statistical dependence between damping and force result as β increases from 0 to 1.

Following the approach used in section 5.4, we are interested in finding the TPD for this system, similar to equation (4.5), i.e.

$$p(x, t|x', t') = \prod_{i=2}^{2} \delta\left\{x_i - (x_i' + r_i(x'))\right\} \cdot p_R(x_3, x_4, t|x_3', x_4', t'),$$

where $p_R(\cdot)$ is the exact TPD for the system.

The 2-dimensional coupled Rayleigh case may be written as

$$\begin{aligned}
\dot{x_1} &= -\frac{\epsilon_1}{2}\left(x_1 - \frac{\kappa_1}{x_1}\right) + \sqrt{\epsilon_1}\,\eta_1 \\
\dot{x_2} &= -\frac{\epsilon_2}{2}\left(x_2 - \frac{\kappa_2}{x_2}\right) + \sqrt{\epsilon_2}\left(\beta\,\eta_1 + \sqrt{1-\beta^2}\,\eta_2\right),
\end{aligned} \tag{5.21}$$

where $\epsilon_1, \epsilon_2, \kappa_1, \kappa_2$ are some positive constants, and $0 \le \beta \le 1$. Rewriting equation (5.21), we get the 2-dimensional stochastic equation

$$\dot{x} = m(x) + Q\,N_t$$

where

$$\begin{aligned} x &= [x_1, x_2]^\top \\ m(x) &= \begin{bmatrix} m_1[x(t)] \\ m_2[x(t)] \end{bmatrix} = \begin{bmatrix} -\frac{\epsilon_1}{2}\left(x_1(t) - \frac{\kappa_1}{x_1(t)}\right) \\ -\frac{\epsilon_2}{2}\left(x_2(t) - \frac{\kappa_2}{x_2(t)}\right) \end{bmatrix} \\ Q &= \begin{bmatrix} \sqrt{\epsilon_1} & 0 \\ \sqrt{\epsilon_2}\,\beta & \sqrt{\epsilon_2}\sqrt{1-\beta^2} \end{bmatrix} \\ N_t &= [\eta_1, \eta_2]^\top \end{aligned} \tag{5.22}$$

As described in section 2.15, there is a close connection between the FP equation and a SDE. The Fokker-Planck equation for system (5.21) is

$$\begin{aligned} \frac{\partial f}{\partial t}(x_1, x_2) = &-\sum_{\alpha=1}^{2} \frac{\partial}{\partial x_\alpha}[m_\alpha(x_1, x_2) f(x_1, x_2)] \\ &+ \frac{1}{2}\sum_{\alpha=1}^{2}\sum_{\gamma=1}^{2} \frac{\partial^2}{\partial x_\alpha \partial x_\gamma}[K_{\alpha\gamma}(x_1, x_2) f(x_1, x_2)], \end{aligned} \tag{5.23}$$

where

$$K_{\alpha\gamma}(x_1, x_2) = \begin{pmatrix} \epsilon_1 & \sqrt{\epsilon_1\epsilon_2}\,\beta \\ \sqrt{\epsilon_1\epsilon_2}\,\beta & \epsilon_2 \end{pmatrix},$$

and m is as described in equation (5.22). In order for the system in equation (5.23) to have a stationary solution and an exact TPD to be found by the earlier described method in section 2.14, the conditions in equation (2.38) has to be fulfilled. Because the matrix $K_{\alpha\gamma}(x_1, x_2)$ is a constant matrix; $\partial K_{\alpha\gamma}(x_1, x_2)/\partial x_i = 0$ for $i \in \{1, 2\}$, equation (2.38) simplifies to

$$\frac{\partial}{\partial x_\delta}\sum_{\alpha=1}^{2} A_{\gamma\alpha} K_\alpha = \frac{\partial}{\partial x_\gamma}\sum_{\alpha=1}^{2} A_{\delta\alpha} K_\alpha \ , \tag{5.24}$$

where $\delta = 1$ and $\gamma = 2$ for example. Now, our inverse,

$$A = \frac{1}{\epsilon_1\epsilon_2(1-\beta^2)} \begin{pmatrix} \epsilon_2 & -\sqrt{\epsilon_1\epsilon_2}\,\beta \\ -\sqrt{\epsilon_1\epsilon_2}\,\beta & \epsilon_1 \end{pmatrix},$$

in addition to equation (5.24), provides us with the condition

$$\begin{aligned} \frac{\partial}{\partial x_1}\left[\frac{\sqrt{\epsilon_1^3\epsilon_2}}{2}\,\beta\left(x_1 - \frac{\kappa_1}{x_1}\right) - \frac{\epsilon_1\epsilon_2}{2}\left(x_2 - \frac{\kappa_2}{x_2}\right)\right] = \\ \frac{\partial}{\partial x_2}\left[-\frac{\epsilon_1\epsilon_2}{2}\left(x_1 - \frac{\kappa_1}{x_1}\right) + \frac{\sqrt{\epsilon_1\epsilon_2^3}}{2}\,\beta\left(x_2 - \frac{\kappa_2}{x_2}\right)\right] \end{aligned} \tag{5.25}$$

to be true as long as $\beta \neq 1$. Of course, equation (5.25) is only true if $\beta \equiv 0$. But $\beta = 0$ means stochastic *independence* between the force and the damping, -the very effect we were to study. So finding an exact analytical expression when $\beta \neq 0$ for the stationary PDF, -and also a TPD, seems impossible with this method. An approximate TPD is therefore needed, and is studied in the next chapter.

Chapter 6

TPDs using improved techniques

Bearing in mind the numerical problems from chapter 5 and the fact that an exact TPD for the 4-dimensional stochastic system in equation (5.20) is not available, we head for ways to use the approximate TPD in a PI scheme, to find a stable numerical solution to systems of equations including the Rayleigh process (5.8). The tools used in this chapter are a general grid, the not-a-knot condition, and handling the noise-term in a better way.

Different approaches to place the grid have been studied. Crucial is the integrating area close to zero, as described in section 4.6.8. The grid for the Rayleigh process is made so that the PDF has a fixed value of zero for our first point, and the next point has to be placed so that the back-stepping procedure may be used without large numerical errors. This is important in order to get the right solution as the number of interpolation points increase, and to keep the CPU time of the program to a minimum. The rest of the points are placed uniformly. Optionally we could use a uniform grid, and choose a small enough τ so that the back-stepping procedure goes smoothly.

The not-a-knot condition replaces the method of explicitly setting spline coefficients for basis functions with support outside the interval to zero, -as described in section 4.6.3.

But most important, the noise term has now been handled with a modified *Order 2.0 Weak Taylor Scheme*. The corresponding TPD is found in equation (4.22).

6.1 The Rayleigh process, 1-D case

Studying the 1-D case is always interesting, giving us hints and clues of what is possible numerical approaches to the problem. We first study the 1-D Rayleigh process

$$\dot{R}(t) = a\left(\frac{1}{R(t)} - R(t)\right) + \sqrt{2a}N(t), \tag{6.1}$$

where $a = 0.047$ and $N(t)$ denotes standard Gaussian white noise with $E[N(t)N(t+\tau)] = \delta(\tau)$. We may easily rewrite this as a discretized system and construct a fast and efficient program finding the stationary PDF in a short time.

The stationary solution is found in Figure 6.1 and Figure 6.2, together with the theoretical solution from equation (2.31). The calculation was done with parameters $p = 21$,

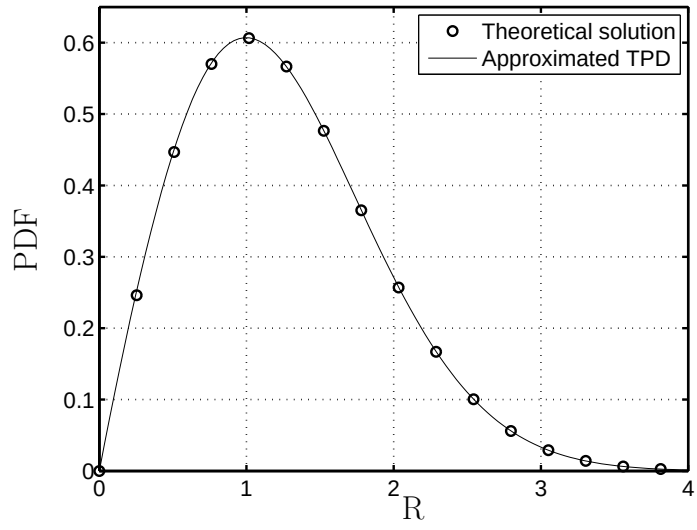

Figure 6.1: Comparing the theoretical solution and the solution using an approximate TPD of equation (6.1).

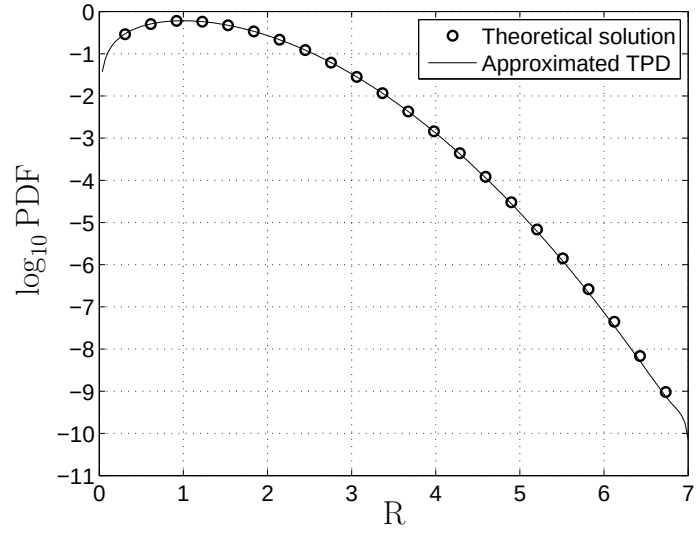

Figure 6.2: Comparing the theoretical solution and the solution using an approximate TPD of equation (6.1), logarithmic scale.

$n = 35$, and $\tau = 0.03$. It is seen that the numerical results are very good, both on the top of the distribution and in the tail. Compared with the results from using an exact TPD from chapter 5, the results from using an approximate TPD is as good. The number of calculations before reaching a stationary PDF, is however larger by a factor of 100. In a

1-D case this is barely noticeable, but in the 3-D case it becomes a factor to consider.

6.2 Different approaches in trying to study the Rayleigh process

We know the Rayleigh process from equation (2.29),

$$\frac{dR(t)}{dt} = -\frac{\epsilon}{2}\left(R(t) - \frac{\kappa}{R(t)}\right) + \sqrt{\epsilon}\, N_t, \tag{6.2}$$

studied in chapter 5 and section 6.1 with $\kappa = 1$ and $\epsilon = 2a$, is hard to deal with numerically. In order to get an easier equation, the following transformations have been done.

6.2.1 Variable transformation by squares

Attacking the Rayleigh process, we multiply equation (6.2) with R, obtaining the equation

$$R\dot{R} = -\frac{\epsilon}{2}\left(R^2 - \kappa\right) + R\sqrt{\epsilon}\, N_t. \tag{6.3}$$

The lhs may be written as the derivative of R squared, providing us with the equation

$$\frac{1}{2}\frac{\partial}{\partial t}\left(R^2\right) = -\frac{\epsilon}{2}\left(R^2 - \kappa\right) + R\sqrt{\epsilon}\, N_t.$$

Introducing a new variable, $B = R^2$, the Rayleigh process may now be written as

$$\dot{B} = -\epsilon(B - \kappa) + 2\sqrt{B\epsilon}\, N_t. \tag{6.4}$$

Now, the drift term does not have any singularities, but the diffusion term now depends on B.

Equation (6.4) may now be written as a FP-equation, and the stationary PDF of the corresponding FP-equation may be found using equation (2.28),

$$\bar{f}(B) = \frac{1}{\sqrt{2\,\kappa\pi}}\, B^{-\frac{1}{2}} \exp\left(-\frac{B}{2\kappa}\right),\ B > 0\,.$$

The new problem lies in evaluating the approximated PDF close to $B = 0$, since the value of $\bar{f}$ goes to infinity as B approaches zero. Although using a general grid with lots of grid-points close to zero, the numerical result is not good enough compared to the theoretical solution. This is because the interpolation method in some way has to be told what to expect near $B = 0$, and since B goes to infinity here, trying to rewrite equation (6.2) into equation (6.3) seems impractical.

6.2.2 Scaling

Using a transformation

$$R = \gamma\, B\,,$$

and writing $\epsilon = 2a$, equation (6.2) becomes

$$\dot{B} = a\left(\frac{\kappa}{\gamma^2 B} - B\right) + \frac{\sqrt{2a}}{\gamma}\, N_t.$$

Although this seems simpler since $\gamma \neq 0$ may be chosen freely, it is numerically in fact the same equation as equation (6.2) with its properties and difficulties regarding back-stepping and number of grid and integrating points. So unfortunately, there is nothing to gain by this rewriting.

6.2.3 Logarithmic variable transformation

Using a transformation

$$U = \ln R\,,$$

and writing $\epsilon = 2a$, equation (6.2) becomes

$$\dot{U} = a\left(\exp(-2U) - \kappa\right) + \sqrt{2a}\exp(-U)\, N_t. \tag{6.5}$$

The theoretical stationary solution to equation (6.5) is found to be

$$\bar{f}(U) \propto \exp\left((2+\kappa)U - \frac{1}{2}\exp(2U)\right), \tag{6.6}$$

and is shown in Figure 6.3 for $\kappa = 1$. Although this PDF seems simple in its form, it is nearly impossible to use the PI technique on this problem. This is due to the back-stepping procedure. As seen in Figure 6.3, we should expect to place our integrating points from -8 to 2. With a time-stepping procedure on the deterministic term in equation 6.5, -where we use a Runge-Kutta 4th order backwards, this will include a number $\exp(2 \cdot 8)$, which is a large number. Of course, a time-step τ as small as 10^{-9} has to be used, and far too impractical.

In addition, using negative numbers in the noise-term in the same equation shows that we would have to integrate over a large area, giving a poor numerical result.

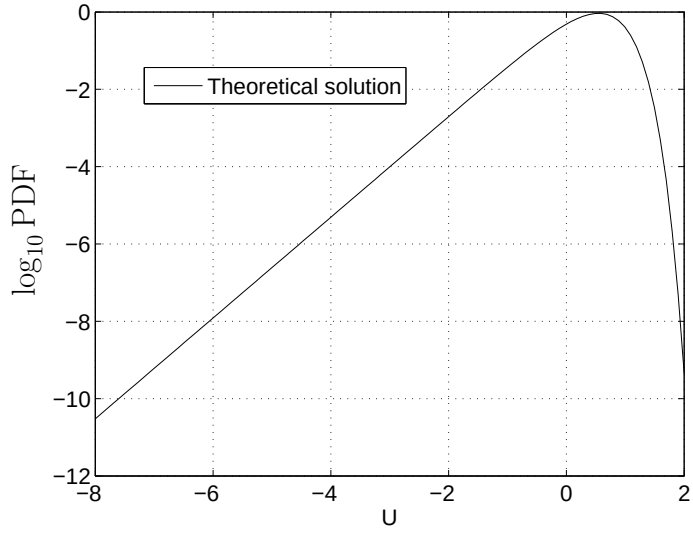

Figure 6.3: Theoretical stationary solution described by equation (6.6).

6.3 The Rayleigh process, 2-D case

In lack of a real physical 2-dimensional case study, the following system of equations

$$\begin{aligned} \dot{x}(t) &= 0.02\,x(t) - 0.05\,x(t)^2 + 0.01\,y^2(t) \\ \dot{y}(t) &= a\left(\frac{1}{y(t)} - y(t)\right) + \sqrt{2a}N(t), \end{aligned} \tag{6.7}$$

has been studied. The Rayleigh equation (the latter one) is as described in section 6.1 with $a = 0.047$. Here we experience an interpolation problem. Using cubic B-splines in both directions gives some negative spline-coefficients in the calculation, introducing numerical errors that spreads through the solution. The remedy is to interpolate linearly in these regions and using cubic splines everywhere else. This, however, increase the CPU time of the program. The accuracy in the solution also decrease.

The results may be found in Figures 6.4 - 6.7, where the variables $nx = 111$, $ny = 111$ and $\tau = 0.001$. As seen, the results are very good, but good results comes at a cost. The number of grid points has increased dramatically compared with the 1-D case. More points are needed in each direction, and this also leads to a small τ, in order to get grid points close to zero in the y-dimension. It is also worth mentioning that a general grid has been used here.

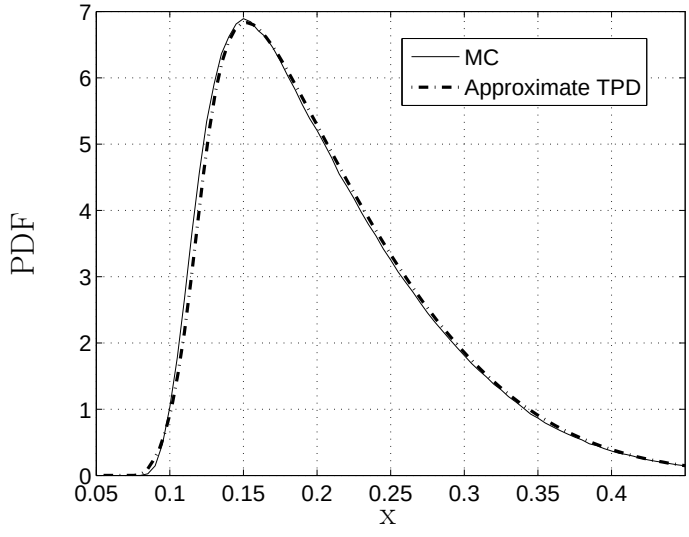

Figure 6.4: Comparing the Monte Carlo simulation and the solution using an approximate TPD of system (6.7), x-direction.

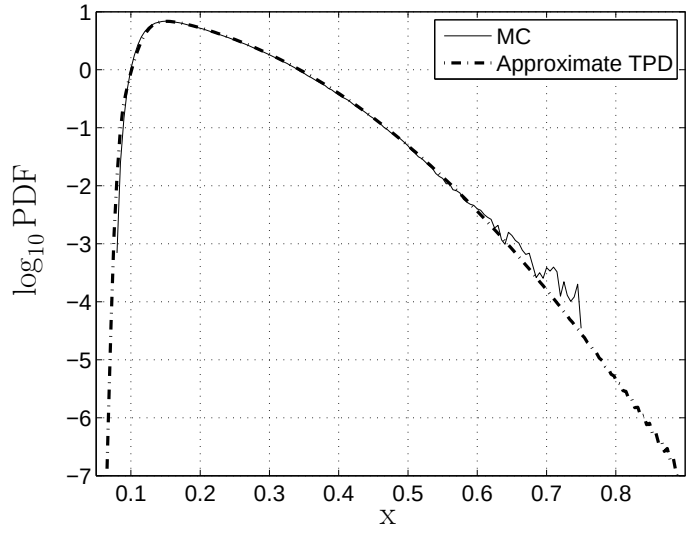

Figure 6.5: Comparing the Monte Carlo simulation and the solution using an approximate TPD of system (6.7), x-direction, logarithmic scale.

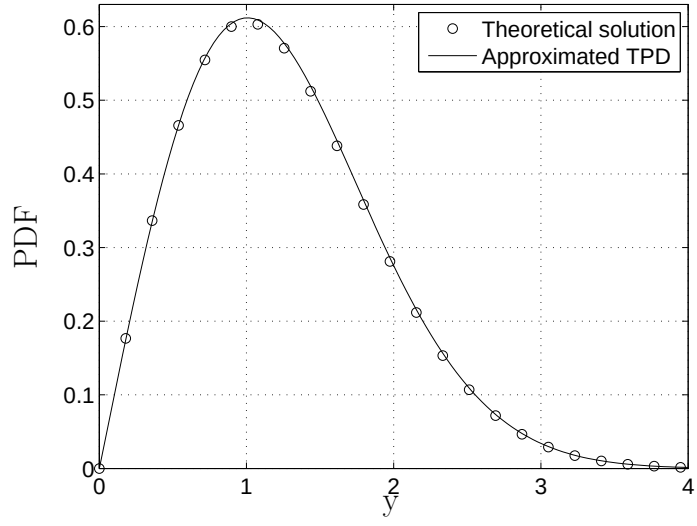

Figure 6.6: Comparing the exact solution and the solution using an approximate TPD of system (6.7), y-direction.

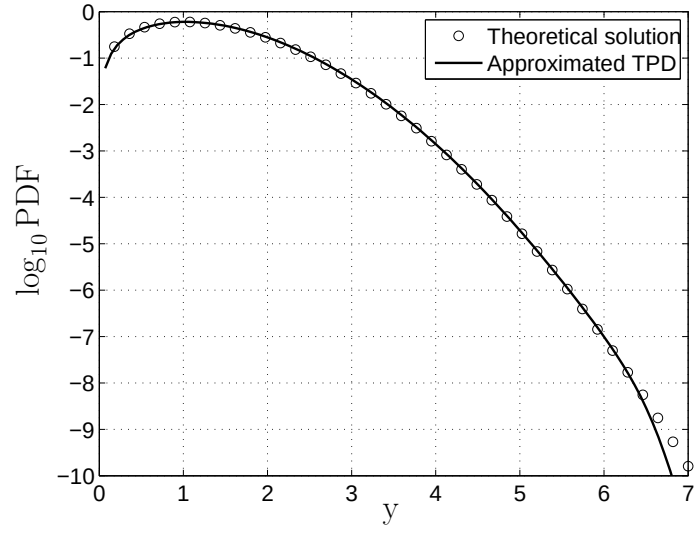

Figure 6.7: Comparing the exact solution and the solution using an approximate TPD of system (6.7), y-direction, logarithmic scale.

6.4 The Rayleigh process, 3-D case

Returning to the system of equations (5.14), for which we are interested in finding the stationary solution, we use the numerical information gathered from the previous sections. The same problems as in section 6.3 occur here, and we have to use linear interpolation where the spline coefficients are negative. A general grid has been applied.

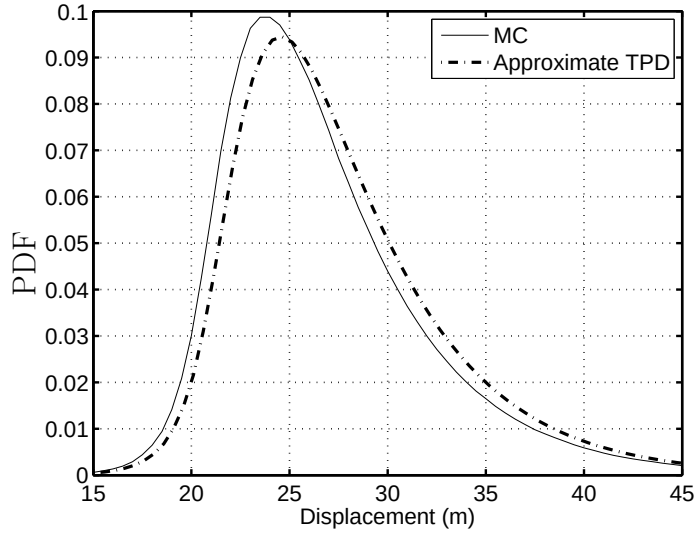

Figure 6.8: The marginal PDF of surge displacement for the approximate TPD compared with the results of a Monte Carlo simulation.

As described in section 6.3 and 4.6.2, linear approximation are neither smooth nor efficient approximators, and provide small errors in the density function. The system responds by pushing probability mass into (or out of) troublesome areas, thereby inducing errors in other parts of the PDF. The combination of an approximate TPD and a vast amount of linear approximations, 18-22 % of the total number of interpolations ($nx = ny = nz = 101$, $p = 31$, $\tau = 0.01$), makes the system unstable. The system never reach a stable solution, but oscillates between different solutions. The remedy, one should assume, is to rise the number of grid and interpolation points and/or decrease the time step τ. The drawback is the increase of CPU time.

By increasing the number of grid points to 151 in each direction, more interpolations are done by cubic splines. But still a vast amount of interpolations, 11-13 %, are done linearly, predominated at the edge of the grid. The PDF now reach a stationary solution, but the solution is not equal to the PDF found in chapter 5, using an exact TPD. The marginal densities is found in Figures 6.8 - 6.13, where $nx = ny = nz = 151$, $p = 31$, and $\tau = 0.01$.

Using an approximated TPD produce a different stationary solution than using an exact TPD. They both describe the same system, but converges to different solutions. Increasing

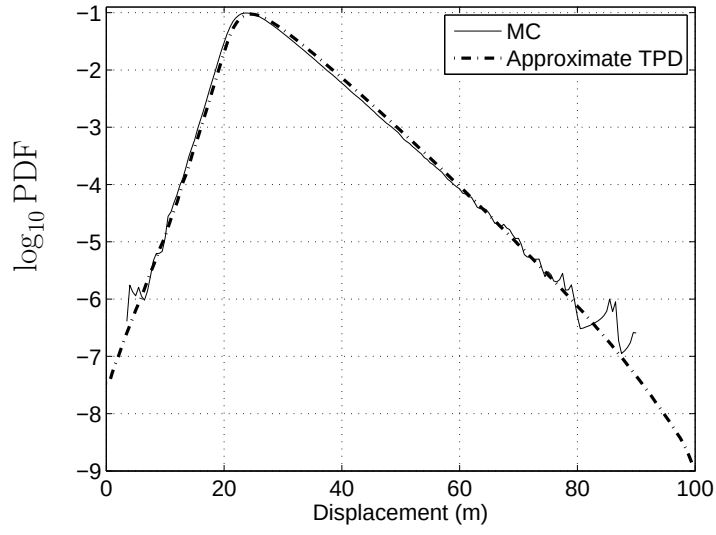

Figure 6.9: The marginal PDF of surge displacement for the approximate TPD compared with the results of a Monte Carlo simulation, logarithmic scale.

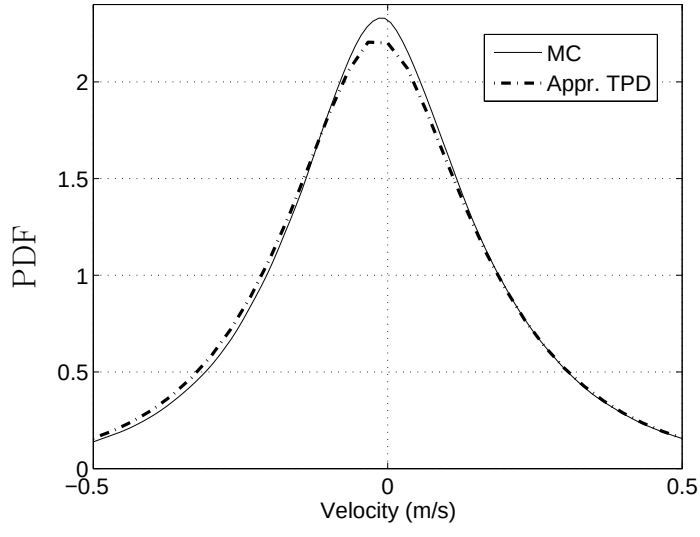

Figure 6.10: The marginal PDF of surge velocity for the approximate TPD compared with the results of a Monte Carlo simulation.

the number of grid and integrating points or decreasing the time step τ, have no influence on the stationary solution. The only change is the CPU time. This indicates that it is not interpolation errors that causes the difference between the stationary solutions, -it is the approximative TPD that is not good enough. A discretized system based on a more accurate Taylor scheme of order 3 or higher, as mentioned in section 4.6.6, providing us

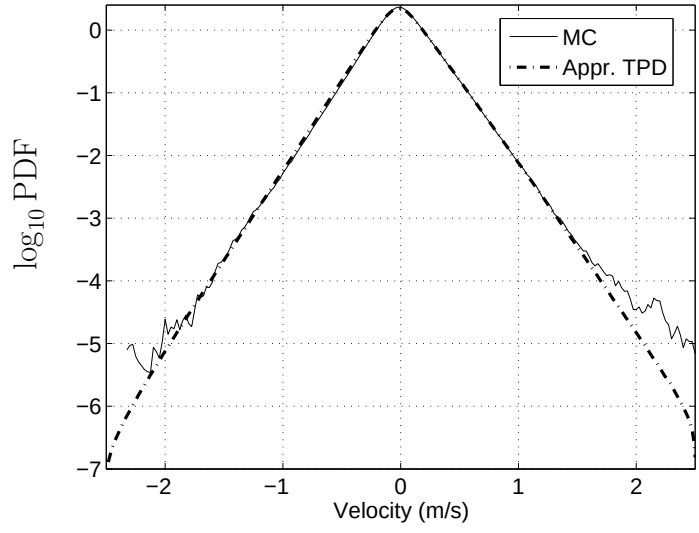

Figure 6.11: The marginal PDF of surge velocity for the approximate TPD compared with the results of a Monte Carlo simulation, logarithmic scale.

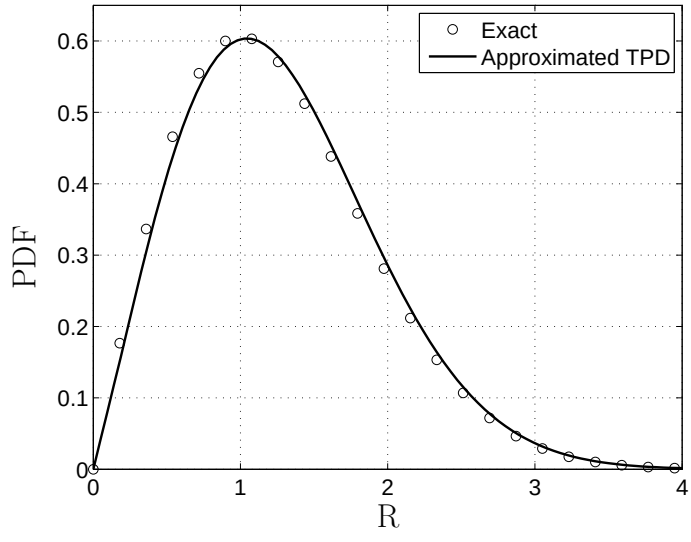

Figure 6.12: The marginal PDF of Rayleigh process for the approximate TPD compared with the results of a Monte Carlo simulation.

with an even better TPD, might improve the results. This, however, has not been studied.

Our main object is calculating the upcrossing frequency $\nu_Z^+(\zeta)$. The impact of this difference in TPDs is described in Figures 6.14 and 6.15, where the upcrossing frequency and exceedance probability $\mathrm{P}_F(T)$ using an exact and an approximate TPD are presented. One can hardly see any difference at all between the two different techniques. This indicates

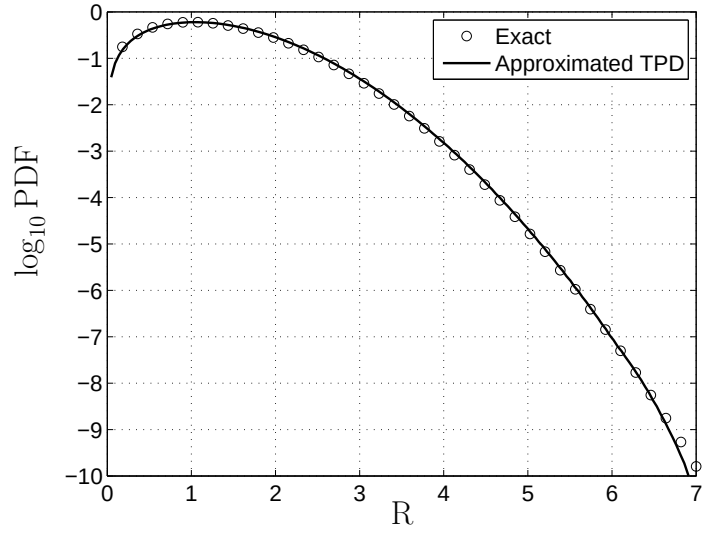

Figure 6.13: The marginal PDF of Rayleigh process for the approximate TPD compared with the results of a Monte Carlo simulation, logarithmic scale.

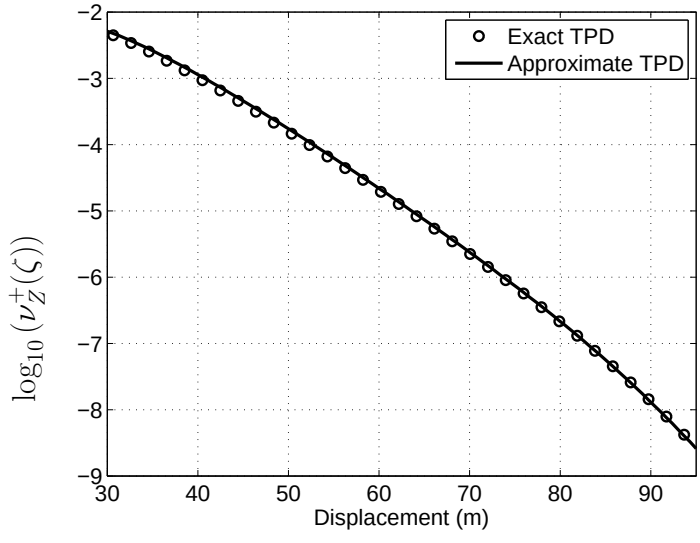

Figure 6.14: The upcrossing frequency using an exact and an approximate TPD, logarithmic scale.

that in order to find the upcrossing frequency and the exceedance probability, one need not necessarily use an exact TPD. In our case, an approximate TPD seems to be sufficient.

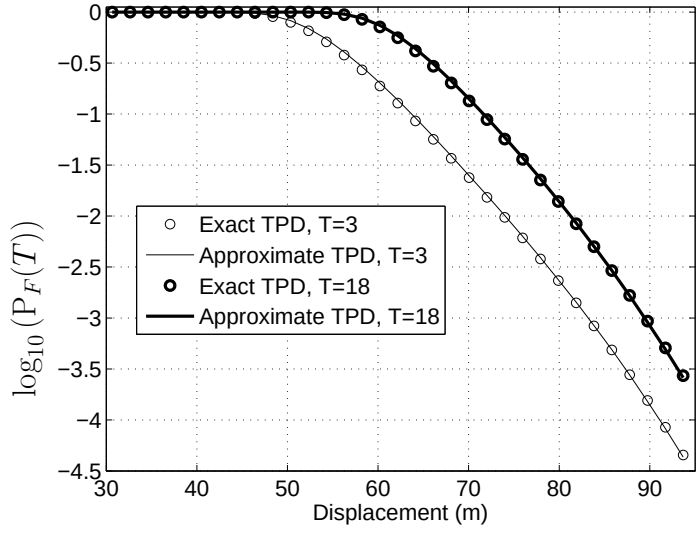

Figure 6.15: The exceedance probability as a function of the displacement response level for $T = 3, 18$ hours, using different TPDs, logarithmic scale.

6.5 Numerical considerations

The choice of an interpolation routine is important in path integration. Cubic spline interpolation was chosen because it seemed to work well when the distribution is sufficiently smooth and the borders of the computational domain does not have a large impact on the global dynamics of the system. However, some problems occur in areas close to a large jump in the interpolated values. Here, the interpolating spline often will have unreasonable oscillations, in form of negative spline coefficients and negative values of the PDF. The methods investigated were parabolic splines, bezier splines, and tension splines. Unfortunately, these methods did not improve the results.

In Naess and Mo (2004), a conditional path integration method was suggested. Here, a 4 dimensional PDF is pointwise divided by the marginal density for 2 variables. This way, a more flat density is obtained, which should be more suitable for integration procedures, -possible with high accuracy even for linear approximation and for a very coarse grid. The interpolated value of the PDF is obtained by multiplying the interpolated values in the conditional density with the given marginal density (or for example a Gaussian). As stated in the article, the method has some serious drawbacks. In many cases it turns out that the conditional density is in fact less flat than the original PDF. In addition, when the marginal density is unknown, and one instead uses a Gaussian, some non-Gaussian problems seem to converge more to a Gaussian solution rather than a correct stationary distribution. This method was tested on the system of equations (5.14). Here, the marginal PDF in z-direction was known, but unfortunately, this did not improve the result.

Chapter A

The impulse function

The *unit impulse function* $\delta(x - x_0)$, also called the Dirac delta function, is defined to be infinite when its argument is zero, to be zero when its argument is nonzero, and to have a unit area,

$$\delta(x - x_0) = \begin{cases} \infty & \text{when } x = x_0 \\ 0 & \text{when } x \neq x_0 \end{cases}$$

$$\int_{-\infty}^{\infty} \delta(x - x_0)dx = 1\,.$$

Of course, the fact that $\delta(\cdot)$ is infinite at one point, tells us that it is not a function. Instead we define (Haberman, 1987) it as an operator with the property that for any continuous $f(x)$ at $x = x_0$,

$$f(x_0) = \int_{-\infty}^{\infty} f(x)\delta(x - x_0)dx. \tag{A.1}$$

The impulse function is so concentrated that in integrating it with any continuous function $f(x)$, it *sifts* out only the value at $x = x_0$, and the integral in equation (A.1) are often referred to as the *sifting integral*. Further, it is often desirable to define the impulse function to be an even function.

The Fourier transform $\hat{F}$ of the unit impulse function is defined

$$\hat{F}(u, x_0) = \int_{-\infty}^{\infty} \delta(x - x_0)\exp(-iux)dx = \exp(-iux_0),$$

and hence

$$\hat{F}(u, 0) = 1.$$

Formal application of the Fourier inversion integral then gives

$$\frac{1}{2\pi}\int_{-\infty}^{\infty} \exp(-iux_0)\exp(-iux)du = \delta(x - x_0)$$

$$\frac{1}{2\pi}\int_{-\infty}^{\infty} \exp(-iux)du = \delta(x). \tag{A.2}$$

An integral is defined

$$I = \int_{-\infty}^{\infty} \delta(x - f(y))\, g(y)\, dy, \tag{A.3}$$

and by introducing a transformation of variables,

$$\zeta = f(y) \Rightarrow y = f^{-1}(\zeta)\,,$$

we may rewrite equation (A.3) as

$$\begin{aligned} I &= \int_{-\infty}^{\infty} \delta(x - \zeta)\, g(f^{-1}(\zeta)) \frac{\partial f^{-1}(\zeta)}{\partial \zeta}\, d\zeta \\ &= g(f^{-1}(x)) \left| \frac{\partial f^{-1}(x)}{\partial x} \right|. \end{aligned}$$

The last term, a Jacobi determinant, corresponds to the change of integral measure due to the non-linearity, and normally has to be approximated from the system equations.

Chapter B

Simplified Integral

From section 3.3, we know that the up-crossing frequency may be written

$$\nu_Z^+(\zeta) = -\frac{1}{(2\,\pi)^2} \fint_{-\infty}^{\infty} \frac{1}{v^2} \int_{-\infty}^{\infty} M(u,v)\, e^{-\,\mathrm{i}u\zeta}\, du\, dv \tag{B.1}$$

where the outer integral wrt v is interpreted as a principal value integral in the following sense: $\fint_{-\infty}^{\infty} = \lim_{\epsilon\to 0+} \left\{ \int_{-\infty}^{-\epsilon} + \int_{\epsilon}^{\infty} \right\}$ and $M(u,v)$ is given by

$$M(u,v) = \mathrm{E}\left[\exp\left(\mathrm{i}uZ + \mathrm{i}v\dot{Z} \right) \right] = \int_{-\infty}^{\infty} \int_{-\infty}^{\infty} e^{\mathrm{i}(u\,z + v\,\dot{z})}\, f_{Z\,\dot{Z}}\,(z,\dot{z})\, dz d\dot{z}. \tag{B.2}$$

Rewriting equation (B.1), we find

$$\nu_Z^+(\zeta) = -\frac{1}{(2\,\pi)^2} \lim_{\epsilon\to 0+} \left[I_1(\zeta) + I_2(\zeta) \right]$$

where

$$\begin{aligned} I_1(\zeta) &= \int_{\epsilon}^{\infty} \frac{1}{v^2} \int_{-\infty}^{\infty} M(u,v)\, e^{-\,\mathrm{i}u\zeta}\, du\, dv \\ I_2(\zeta) &= \int_{-\infty}^{-\epsilon} \frac{1}{v^2} \int_{-\infty}^{\infty} M(u,v)\, e^{-\,\mathrm{i}u\zeta}\, du\, dv \\ &= \int_{\epsilon}^{\infty} \frac{1}{v^2} \int_{-\infty}^{\infty} M(u,-v)\, e^{-\,\mathrm{i}u\zeta}\, du\, dv. \end{aligned}$$

Now

$$\nu_Z^+(\zeta) = -\frac{1}{(2\,\pi)^2} \lim_{\epsilon\to 0+} \int_{\epsilon}^{\infty} \frac{1}{v^2} \int_{-\infty}^{\infty} \left[M(u,v) + M(u,-v) \right] e^{-\,\mathrm{i}u\zeta}\, du\, dv \tag{B.3}$$

reducing the numerical effort in finding the up-crossing frequency almost in half.

A further simplification of equation (B.3) may be done in this manner

$$\nu_Z^+(\zeta) = -\frac{1}{(2\,\pi)^2} \lim_{\epsilon\to 0+} \int_{\epsilon}^{\infty} \frac{1}{v^2} I(v,\zeta) dv\,,$$

where

$$\begin{aligned}
I(v,\zeta) &= \int_{-\infty}^{\infty} \left[M(u,v) + M(u,-v)\right]\, e^{-\,\mathrm{i}u\zeta}\, du \\
&= \int_{-\infty}^{0} \left[M(u,v) + M(u,-v)\right]\, e^{-\,\mathrm{i}u\zeta}\, du + \int_{0}^{\infty} \left[M(u,v) + M(u,-v)\right]\, e^{-\,\mathrm{i}u\zeta}\, du \\
&= \int_{0}^{\infty} \left[M(-u,v) + M(-u,-v)\right]\, e^{\mathrm{i}u\zeta}\, du + \int_{0}^{\infty} \left[M(u,v) + M(u,-v)\right]\, e^{-\,\mathrm{i}u\zeta}\, du \\
&= \int_{0}^{\infty} \Big\{ M(u,v)\, e^{-\,\mathrm{i}u\zeta} + M(-u,-v)\, e^{\mathrm{i}u\zeta} \\
&\qquad + M(u,-v)\, e^{-\,\mathrm{i}u\zeta} + M(-u,v)\, e^{\mathrm{i}u\zeta} \Big\}\, du \qquad \text{(B.4)} \\
&= 2 \int_{0}^{\infty} \Re\left[M(u,v)\, e^{-\,\mathrm{i}u\zeta} + M(u,-v)\, e^{-\,\mathrm{i}u\zeta} \right]\, du \qquad \text{(B.5)} \\
&= 2\,\Re\left\{ \int_{0}^{\infty} \left[M(u,v) + M(u,-v)\right]\, e^{-\,\mathrm{i}u\zeta}\, du \right\}.
\end{aligned}$$

The step between equation (B.4) and equation (B.5) is found by inspection of equation (B.2), where the relations

$$\begin{aligned}
M(-u,v) &= M(u,-v)^*, \\
M(-u,-v) &= M(u,v)^*,
\end{aligned}$$

are easily seen. In addition, the fact that

$$A + A^* = 2\,\Re\,(A)$$

for any complex number A, is used.

Finally equation (B.1) may be written

$$\nu_Z^+(\zeta) = -\,\frac{1}{2\,\pi^2} \Re\left\{ \lim_{\epsilon \to 0+} \int_{\epsilon}^{\infty} \frac{1}{v^2} \int_{0}^{\infty} \left[M(u,v) + M(u,-v)\right]\, e^{-\,\mathrm{i}u\zeta}\, du\, dv \right\}. \qquad \text{(B.6)}$$

Bibliography

V. Aanesland, O. Faltinsen, and R. Shao. Wave-drift damping of a tlp. In *Environmental forces on offshore structures and their prediction*, volume 26, pages 383–400. Kluwer Academic Publishers, 1990.

Milton Abramowitz and Irene A. Stegun. *Handbook of mathematical functions with formulas, graphs, and mathematical tables*. Dower Publications, INC., New York, 1972.

A. T. Bharucha-Reid. *Elements of the Theory of Markov Processes and Their Applications*. McGraw-Hill Book Co., Inc., New York, 1960.

T.K. Caughey. Equivalent linearization techniques. In *Journal of the Acoustical Society of America*, volume 35, pages 1706–1711, 1963.

H. Cramer and M. R. Leadbetter. *Stationary and related stochastic processes*. John Wiley & Sons Inc., 1968.

W. B. Davenport and W. L. Root. *An introduction to the Theory of Random Signals and Noise*. John Wiley & sons., Inc., Publication, New York, 1987.

C. de Boor. *A practical Guide to Splines*. Springer, 2001.

M. G. Donley and P. D. Spanos. *Dynamic Analysis of Non-Linear Structures by the Method of Statistical Quadratization*, volume 57 of *Lecture Notes in Engineering*. Springer-Verlag, Berlin, 1990.

O. M. Faltinsen and A. E. Løken. Slow drift oscillations of a ship in irregular waves. *Journal of Applied Ocean Research*, 1979.

M. Grigoriu. *Stochastic processes*. Birkhäuser, 2002.

A. J. Grime and R. S. Langley. On the efficiency of crossing rate prediction methods used to determine extreme motions of moored offshore structures. *Applied Ocean Research*, 25(3):127–135, 2003.

R. Haberman. *Elementary applied partial differential equations*. Prentice Hall, Englewood Cliffs, New Jersey, 1987.

S. Haver and K. A. Nyhus. A wave climate description for long term response calculations. In *Proceedings 9th International Conference on Offshore Mechanics and Arctic Engineering*. New York, ASME, 1986.

P. Henrici. *Applied and computational complex analysis*, volume II. Wiley, New York, 1977.

D.V. Iourtchenko, E. Mo, and A. Naess. Response probability density functions of strongly nonlinear systems by the path integration method. Int. J. Non-linear Mechanics, In Print, 2006.

J. M. Johnsen. *Response statistics of nonlinear dynamic systems*. PhD thesis, NTH, University of Trondheim, 1992.

M. Kac and A. J. F. Siegert. On the theory of noise in radio receivers with square law detectors. *Journal of Applied Physics*, 18:383–397, 1947.

H. C. Karlsen and A. Næss. Statistical response predictions for a nonlinearly moored large volume structure in random seas. In *Sixth European Conference on Structural Dynamics*, 2005.

P.E. Kloeden and E. Platen. *Numerical Solutions to Stochastic Differential Equations*. Springer-Verlag, 1992.

E. Kreyszig. *Advanced engineering mathematics, 6th edition*. Wiley, New York, 1988.

R. S. Langley and S. McWilliam. A statistical analysis of first and second order vessel motions induced by waves and wind gusts. *Applied Ocean Research*, 15(3):13–23, 1993.

R. M. Leadbetter, G. Lindgren, and H. Rootzen. *Extremes and Related Properties of Random Sequences and Processes*. Springer-Verlag, New York, 1983.

H. Lin and S.C.S. Yim. Stochastic analysis of a single-degree-of-freedom nonlinear experimental moored system using an independent-flow-field-model. *Journal of Engineering Mechanics*, 130(2):161–169, 2004.

U. E. B. Machado. *Statistical Analysis of Non-Gaussian Environmental Lodads and Responses*. PhD thesis, Lund Institute of Technology, Lund University, Sweeden, 2002.

M. B. Marcus. Level crossings of a stochastic process with absolutely continous sample paths. *The Annals of Probability*, 5:52–71, 1977.

T. Marthinsen. The statistics of slow-drift oscillations with nonlinear restoring forces. In *Proceedings of IUTAM Symposium on Nonlinear Water Waves, Tokyo*, pages 459–466. New York, Springer-Verlag, 1987.

S. McWilliam and R. S. Langley. Extreme values of first- and second-order waveinduced vessel motions. *Applied Ocean Research*, 15(3):169–181, 1993.

A. Naess. Extreme response of nonlinear structures with low damping subjected to stochastic loading. *Journal of Offshore Mechanics and Artic Engineering, ASME*, 121:255–260, 1999.

A. Næss. Crossing rate statistics of quadratic transformations of gaussian processes. *Probabilistic Engineering Mechanics*, 16(3):209–217, 2001.

A. Næss. The mean rate of level crossings of a stochastic process expressed in terms of a characteristic function. *Preprint Statistics*, 4, 2002.

A. Næss. On the long-term statistics of extremes. *Applied Ocean Research*, 6(4):227–228, 1984.

A. Næss. Statistical analysis of second-order response of marine structures. *Journal of Ship Research*, 29(4):270–284, Dec. 1985.

A. Næss. The statistical distribution of second-order slowly-varying forces and motions. *Applied Ocean Res*, 8(2):110–118, 1986.

A. Næss. The response statistics of non-linear second-order transformations to gaussian loads. *Journal of Sound Vibrations*, 115(1):103–129, 1987.

A. Næss. Statistical analysis of nonlinear, second-order forces and motions of offshore structures in short-crested random sea. *Probabilistic Engineering Mechanics*, 5(4):192–203, 1990.

A. Naess and J. M. Johnsen. Response statistics of nonlinear, compliant offshore structures by the path integral solution method. *Probabilistic Engineering Mechanics*, 8:91–106, 1993.

A. Naess and H. Chr. Karlsen. Numerical calculation of the level crossing rate of second order stochastic Volterra systems. *Probabilistic Engineering Mechanics*, 19(2):155–160, 2004.

A. Naess and U. Machado. Response statistics of linear dynamic systems subjected to quadratic transformations of gaussian processes. In M. di Paola, editor, *Proceedings Euromech 413 - Stochastic Dynamics of Nonlinear Mechanical Systems*. Italy, DISeG, University of Palermo, 2000.

A. Naess and E. Mo. A conditional path integration method and its use in nonlinear stochastic dynamics. In *Proceedings 9th ASCE Specialty Conference on Probabilistic Mechanics and Structural Reliability*, 2004.

A. Naess and V. Moe. Efficient path integration methods for nonlinear dynamic systems. *Probabilistic Engineering Mechanics*, 15(3):221–231, 2000.

A. Naess and G.M. Ness. Second-order sum frequency response statistics of tethered platforms in random waves. *Applied Ocean Research*, 14(1):23–32, 1992.

A. Naess, H. Chr. Karlsen, and P. Teigen. A general numerical method for calculating the extreem response of compliant offshore structures in random seas. *Applied Ocean Research*, 28(1):1–8, 2006.

E. Neal. Second order hydrodynamic forces due to stochastic excitation. In *Proceedings 10th ONR Symposium*, Cambridge, Mass., 1974.

B. Øksendal. *Stochastic Differential Equations*. Springer-Verlag, 1995.

A. Papoulis. *Probability, Random Variables, and Stochastic Processes, Second edidion*. McGraw-Hill International book compagny, 1984.

J. A. Pinkster. Low frequency second order wave exciting forces on floating structures. In *NSMB publication / Netherlands Ship Model Basin*, volume 650. Netherlands ship model basin, Wageningen, Netherlands, 1980.

S. O. Rice. Mathematical analysis of random noise. In Nelson Wax, editor, *Selected Papers on Noise and Stochastic Processes*, pages 133–294. Dover Publications, Inc., New York, 1954.

H. Risken. *The Fokker-Planck Equation, Methods of Solutions and Applications, Second Edition*. Springer, 1989.

J. B. Roberts. Nonlinear analysis of slow drift oscillations of moored vessels in random seas. *Journal of Ship Research*, 25(2):130–140, 1981.

J.B. Roberts. A markov energy method for nonlinear ship rolling in random waves. Technical Report 173, National Maritime Institute, March 1983.

J.B. Roberts and P.D. Spanos. *Random Vibrations and Statistical Linearization*. John Wiley, New York, 1990.

R.Y. Rubinstein. *Simulations and the Monte Carlo Method*. John Wiley, New York, 1981.

Larry L. Schumaker. *Spline functions, basic theory*. Wiley, New York, 1981.

Z. Schuss. *Theory and applications of stochastic differential equations*. John Wiley & Sons Inc., 1980.

C. Skaug. *Random Vibration and the Path Integral Method*. PhD thesis, NTNU, TRONDHEIM, 2000.

T.T Soong and M. Grigoriu. *Random vibration of mechanical and structural systems*. Englewood Cliffs, N.J., Prentice Hall, 1993.

R. G. Standing, J.A.B. Wills, and S. Singh. Wind loading and dynamic response of a floating production platform in waves. In *Environmental forces on offshore structures and their prediction*, volume 26, pages 351–382. Kluwer Academic Publishers, 1990.

R. L. Stratonovich. *Conditional Markov processes and their application to the theory of optimal control*. New York : American Elsevier Pub. Co., 1968.

R. L. Stratonovich. *Topics in the Theory of Random Noise*. Gordon and Breach, Science Publishers, New-York-London, 1963.

P. Teigen and A. Naess. Extreme response of floating structures in combined wind and waves. In *Journal of Offshore Mechanics and Artic Engineering*, pages 87–93. New York, ASME, 1999a.

P. Teigen and A. Naess. Stochastic response analysis of deepwater structures in short-crested random waves. In *Journal of Offshore Mechanics and Artic Engineering*, pages 181–186. New York, ASME, 1999b.

T. Vinje. Statistical distributions of hydrodynamic forces on objects in current and waves. *Norwegian Maritime Research*, 2:20–26, 1980.

T. Vinje. On the statistical distribution of second-order forces and motions. *International Shipbuilding Progress*, 30:58–68, 1983.

R.E. Walpole, R.H. Meyers, S.L. Myers, and L. Ye. *Probability & Statistics for Engineers & Scientists*. Prentice-Hall, Inc., Upper Saddle River, New Jersey, 2002.

D. Williams. *Probability with martingales*. Cambridge University Press, 1991.

Eugene Wong and Bruce Hajek. *Stochastic Processes in Engineering Systems*. Springer-Verlag, New York, 1985.

U. Zähle. A general rice formula, palm measure, and horizontal window conditioning for random fields. *Stochastic Process Applications*, 17:265–283, 1984.